

INTEGRATED GEOSPATIAL TECHNIQUES FOR MONITORING PLOT-LEVEL
CROP GROWTH IN SMALL FARMS AND COMMUNITY GARDENS

by

SHANNON DOROTHY HEALY

(Under the Direction of Marguerite Madden)

ABSTRACT

Small farms and community gardens play a unique and important cultural, economic and local food supply role. This study brings precision agriculture practices to fine scale farms and community gardens, by exploring integrated geospatial techniques, including sUAS imagery acquisition and Structure from Motion (SfM) 3D modeling. From the created 3D models, plant heights are measured and compared to field measurements for validation of accuracy. Multiple crop growth forms and maturation stages are observed in order to understand how different factors, such as height, canopy, density and growth form, influence accuracy.

INDEX WORDS: 3D Modeling, UAS, Remote Sensing, Agricultural Monitoring,
Intra-season Crop Height, Small Farm, Crop Growth, Structure from
Motion (SfM)

INTEGRATED GEOSPATIAL TECHNIQUES FOR MONITORING PLOT-LEVEL
CROP GROWTH IN SMALL FARMS AND COMMUNITY GARDENS

by

SHANNON DOROTHY HEALY

BS, University of Delaware, 2013

A Thesis Submitted to the Graduate Faculty of The University of Georgia in Partial
Fulfillment of the Requirements for the Degree

MASTER OF SCIENCE

ATHENS, GEORGIA

2020

© 2020

Shannon Dorothy Healy

All Rights Reserved

INTEGRATED GEOSPATIAL TECHNIQUES FOR MONITORING PLOT-LEVEL
CROP GROWTH IN SMALL FARMS AND COMMUNITY GARDENS

by

SHANNON DOROTHY HEALY

Major Professor:	Marguerite Madden
Committee:	David Cotten
	Deepak Mishra

Electronic Version Approved:

Ron Walcott
Interim Dean of the Graduate School
The University of Georgia
May 2020

ACKNOWLEDGEMENTS

There are many individuals who have helped guide me through my degree. Their knowledge, patience and willingness to discuss ideas has made this work possible - Dr. Thomas Jordan, Dr. Marguerite Madden and Dr. David Cotten. I would like to thank Sarah Ross, the director of the Center for Research and Education at Wormsloe (CREW) for her support and the Wormsloe Foundation and the University of Georgia Graduate School for the funding of this work.

TABLE OF CONTENTS

	Page
ACKNOWLEDGEMENTS	iv
LIST OF TABLES	vii
LIST OF FIGURES	ix
CHAPTER 1	1
INTRODUCTION	1
Scientific Contribution.....	4
Primary Goals, Research Questions and Objectives	5
CHAPTER 2	9
LITERATURE REVIEW	9
Importance of Small Farms and Community Gardens.....	9
Application of Remote Sensing in Precision Agriculture	12
Satellite Imagery and Aerial Image Acquisition and Processing.....	14
Photogrammetric Processing and Analysis of UAS Imagery	18
Software for Structure from Motion	24
SfM and Vegetation	25
Plant Height Monitoring for Estimating Crop Yield	27
SfM Compared to Other Crop Measuring Techniques	28
CHAPTER 3	31
STUDY AREA	31
UGarden.....	32
UGA Center for Research and Education at Wormsloe (CREW)	36
METHODOLOGY	42
sUAS Flights to Acquire Imagery.....	42
Ground Control Points	53
Field Measurement of Plant Heights.....	55
Aerial Image Processing and Structure from Motion to Create Orthoimages and 3D Models..	57
CHAPTER 4	65

RESULTS	65
3D Model Processing	65
Plant Structure Estimation and Validation	67
Results of Actual Field Measured Heights and Modeled CSM-DEM Plant Heights	72
Results of Modeled vs. Actual Plant Heights by Individual Flight Date for Collards	78
Results of Modeled vs. Actual Plant Heights by Individual Flight Date for Kale	83
Results of Modeled vs. Actual Plant Heights by Individual Flight Date for Cabbage	88
Results of Modeled vs. Actual Plant Heights for All Flight Dates Combined	92
Results of Modeled vs. Actual Plant Heights by Individual Flight Date for Peppers	95
Percent Error of Plant Heights for All Flight Dates Combined	95
Imagery Outputs	98
CHAPTER 5	104
DISCUSSION	104
Issues with Processing, Intermediary Steps and Georegistering	105
Comparison of Results to Similar Studies	107
Plant Height	109
Wind and Clouds	109
Crop Canopy Structure	110
Underestimation of Plant Heights	112
Limitations	114
CHAPTER 6	116
SUMMARY AND CONCLUSIONS	116
Further Research	119
REFERENCES	121
APPENDIX A	1

LIST OF TABLES

	Page
Table 1: Selected satellites comparing various attributes.	15
Table 2: UGArden sUAS flight dates and data sizes.	49
Table 3: Agisoft Metashape information for flights at UGArden.	59
Table 4: Wormsloe CREW imagery processing information in Agisoft Metashape.	59
Table 5: UGArden flight dates with processing time in Agisoft Metashape (time abbreviated as hour:minutes:seconds).	67
Table 6: Wormsloe garden imagery with processing time in Agisoft Metashape (time abbreviated as minutes:seconds).	67
Table 7: Ground Control Point coordinates and point number used to georegister models.	69
Table 8: Calculated RMSE and mean x, y, z from the 8 GCPs after georegistration in QTModeler.	69
Table 9: Collards - actual field measured heights (cm) and model measured heights (cm) according to flight date.	74
Table 10: Kale - actual field measured heights (cm) and model measured heights (cm) according to flight date.	74
Table 11: Cabbage - actual field measured heights (cm) and model measured heights (cm) according to flight date.	74

Table 12: Peppers - actual field measured heights (cm) and model measured heights (cm)	
according to flight date.	74

LIST OF FIGURES

	Page
Figure 1: Depiction of overlapping imagery acquired for a feature of interest that will be processed by SfM to create a 3D model of the feature. Image credited to Westoby et al. (2012).	20
Figure 2: Study sites overlaid on the State of Georgia.	32
Figure 3: Orthomosaic processed in Agisoft Metashape from sUAS flight imagery, georeferenced and overlaid on the study area of UGarden in ArcMap.	35
Figure 4: Map of Wormsloe and surrounding area. Garden sites are depicted by red squares. Data creation credited to Dr. Thomas Jordan, Center for Geospatial Research, University of Georgia, Athens, GA.	38
Figure 5: Aerial image of Wormsloe CREW garden outlined in red, adjacent to the Skidaway river marsh flats.....	39
Figure 6: Aerial image of Wormsloe CREW raised bed gardens taken Sept. 10, 2019. ..	39
Figure 7: Sequential sUAS acquired imagery. The red box highlights the different placement in the images of the same cabbage patch during flight progression.....	43
Figure 8 a-b: Map Pilot screenshots of UGarden flight plan (a) lengthwise flight lines and (b) widthwise flight lines of the field create a grid pattern when combined for multiple perspectives for optimal 3D models.	44
Figure 9: Map Pilot's flight plan information, including distance covered, estimated flight time and altitude.....	44

Figure 10: Aerial view of UGArden study site on March 19, 2019.	45
Figure 11: Aerial view of UGArden study site, with targeted bed outlined in red.	46
Figure 12 a-c: The three monitored varieties of crops as imaged from the ground on April 30, 2019 (a) collards (b) kale (c) cabbage.....	48
Figure 13 a-c: Images of pepper plants at Wormsloe (a) aerial overview of raised bed garden, pepper plants outlined in red (b) ground image of pepper plants (c) pepper fruit.	51
Figure 14 a-c: Images of Wormsloe CREW okra garden (a) aerial overview of garden plot (b) ground image of okra (c) okra fruit.	52
Figure 15: The locations of the 8 ground control points are marked with yellow circles and blue flags in this orthomosaic of the UGArden study area.	54
Figure 16: One of the ground control points at UGArden.	55
Figure 17 a-b: Measuring plant heights for validation at (a) UGArden and (b) Wormsloe CREW.	56
Figure 18: Visual diagram depicting how pepper plant model heights were calculated. .	57
Figure 19 a-c: Examples of SfM product: (a) DEM (b) orthomosaic of images (c) dense point cloud.	58
Figure 20: sUAS imagery to be input into Agisoft Metashape for processing.	61
Figure 21: Location of sUAS photos and their alignment along flight lines to cover the study area plot at UGArden.	61
Figure 22 a-d: 3D dense point cloud from furthest distance (a) to closest (d).....	62

Figure 23 a-d: Derived from the 4/16/2019 flight (a) Agisoft Metashape tiled model – images draped over the dense point cloud which creates CSM. Magnified view of (b) collards (c) kale (d) cabbage.	63
Figure 24: 3D model of raised bed gardens at Wormsloe CREW. Pepper plants are outlined in red.	64
Figure 25: Example of processing steps and parameters in Agisoft Metashape from April 16, 2019 flight imagery.....	66
Figure 26: Models prior to georegistration (presented in QTModeler), illustrating the variation in z values.	68
Figure 27: Example of profile analysis tool (in yellow) in QTModeler, over kale plant 1.	71
Figure 28: Example of profile analysis tool output, depicting sample heights in the UGArden datasets.	71
Figure 29 a-b: (a) Linear regression of modeled height to actual height of collards and (b) the respective residuals (3/19/2019).	78
Figure 30 a-b: (a) Linear regression of modeled height to actual height of collards and (b) the respective residuals (04/02/2019).	79
Figure 31 a-b: (a) Linear regression of modeled height to actual height of collards and (b) the respective residuals (4/16/2019).	80
Figure 32 a-b: (a) Linear regression of modeled height to actual height of collards and (b) the respective residuals (4/30/2019).	81
Figure 33 a-b: (a) Linear regression of modeled height to actual height of collards and (b) the respective residuals (5/14/2019).	82

Figure 34 a-b: (a) Linear regression of modeled height to actual height of kale and (b) the respective residuals (3/19/2019).	83
Figure 35 a-b: (a) Linear regression of modeled height to actual height of kale and (b) the respective residuals (04/02/2019).	84
Figure 36 a-b: (a) Linear regression of modeled height to actual height of kale and (b) the respective residuals (4/16/2019).	85
Figure 37 a-b: (a) Linear regression of modeled height to actual height of kale and (b) the respective residuals (4/30/2019).	86
Figure 38 a-b: (a) Linear regression of modeled height to actual height of kale and (b) the respective residuals (5/14/2019).	87
Figure 39 a-b: (a) Linear regression of modeled height to actual height of cabbage and (b) the respective residuals (3/19/2019).	88
Figure 40 a-b: (a) Linear regression of modeled height to actual height of cabbage and (b) the respective residuals (4/02/2019).	89
Figure 41 a-b: (a) Linear regression of modeled height to actual height of cabbage and (b) the respective residuals (4/16/2019).	90
Figure 42 a-b: (a) Linear regression of modeled height to actual height of cabbage and (b) the respective residuals (4/30/2019).	91
Figure 43 a-b: (a) Linear regression of modeled height to actual height of collards and (b) the respective residuals for all flight dates combined.	92
Figure 44 a-b: (a) Linear regression of modeled height to actual height of kale and (b) the respective residuals for all flight dates combined.	93

Figure 45 a-b: (a) Linear regression of modeled height to actual height of cabbage and (b) the respective residuals for all flight dates combined.	94
Figure 46 a-b: (a) Linear regression of modeled height to actual height of peppers and (b) the respective residuals (9/10/2019).	95
Figure 47: The percent error of the model as compared to actual plant height for all flight dates combined for collards.	96
Figure 48: The percent error of the model as compared to actual plant height for all flight dates combined for kale.	97
Figure 49: The percent error of the model as compared to actual plant height for all flight dates combined for cabbage.	97
Figure 50: The percent error of the model as compared to actual plant height for pepper plants.	98
Figure 51: Actual image, tiled model and dense point cloud for all crop types, (a) collards, (b) kale and (c) cabbage at UGArden arranged by flight date.	102
Figure 52: Created 3D model of Wormsloe CREW okra garden. Red circles denote approximate location of where okra should have been.	103
Figure 53: Crop height profile, depicting negative height values in QTModeler.	107

CHAPTER 1

INTRODUCTION

Small farms and community gardens are important sources of food and come with a plethora of important social, economic and educational benefits. The U.S. Department of Agriculture Economic Research Service categorizes farms as “small” based on their income (i.e., gross cash farm income less than \$350,000). Under this definition, 90 percent of U.S. family farms are categorized as small farms and operate nearly half of all farmland, yet they account for only 24 percent of production (USDA 2016). Community gardens, which can consist of several individuals sharing the workload and food produced on shared public or private land, are receiving renewed interest and importance in local food production within urban and suburban communities.

Community gardens in the United States have a long history - starting more than a century ago in cities such as Detroit, Philadelphia, San Francisco and Boston. Historically, these community gardens were an emergency response to food shortages brought on by economic recessions or wartime. For example, Vacant Lot gardens were started in the 1890s, due to an economic recession that left many people unemployed and hungry (Smithsonian Gardens 2019). The participating cities supplied the seeds, gardening tools and instructional pamphlets printed in multiple languages. The prevalence of these gardens declined as the economy improved, but saw a resurgence in popularity, as a necessity and patriotic act, during World War I. There was a second resurgence in community gardens in the 1930s during the Great Depression, then called Thrift Gardens. They reached their

most well-known point during World War II as the famous Victory Gardens, which produced 40% of all vegetables in the United States in 1944. The aftermath of World War II led to suburban sprawl and generational and cultural changes, which considered manual labor a lower-class activity and led to a decline in community gardens and an increase in large, industrial-scale farms. Genetic diversity was subsequently lost as crops were selected for homogeneity and shelf stability for broader-scale agriculture activities. The environmental movement of the 1960s and 1970s, reignited interest in community gardens (Smithsonian Gardens 2019). Currently, small farms and community gardens contribute to all the aforementioned roles of the last century, with other added benefits including supporting local economies and farm-to-table restaurants, providing local foods, preserving genetic diversity and fostering stronger relationships within communities.

Despite the recognized benefits of small farms and community gardens, they receive less attention in terms of using modern technologies to monitor crops and improve crop yield. Farmers who practice precision agriculture with fields as large as 20,000 ha (50,000 acres) in size, generally use tractors guided by GPS and output from remotely sensed images and GIS models for precisely applying fertilizers, pesticides and irrigation (NASA 2001, Schimmelpfennig 2016). New methods using low-cost equipment and integrated geospatial technologies, however, are needed to assist community gardeners and fine-scale farmers growing a variety of crops in plots of about 0.5 to four ha, or one to ten acres, in size. Establishment of best practice guidelines for efficient use of emerging geospatial technologies must be created for these individuals, agricultural extension agencies and geospatial firms offering crop monitoring services for the use of low-cost monitoring techniques to spread. The outreach of ways to monitor plot-level crop growth

and quantify crop damage due to disturbances such as pest infestation, herbivory and extreme weather events is expected to improve food security, increase small farm yields and enhance local community gardening experiences.

Small unmanned aerial systems (sUASs) are a low-cost remote sensing technology that have great potential for aiding in the monitoring of small farm plots and community gardens. Some research-quality sUASs such as a DJI Mavic Air, cost just over \$900 (DJI 2019), can be flown using an individual's smart phone and include a camera that is considered to be of professional quality. The majority of sUASs are relatively easy to learn to fly and accessible to individuals in the U.S. who follow Federal Aviation Administration (FAA) rules and regulations. However, not all individuals flying sUASs realize the possibility to process imagery captured by the mounted cameras to include more than just videos and still images of landscapes they fly over. The acquired images or videos can be processed through increasingly available photogrammetric software programs to create geospatial products such as 3D models and surfaces, orthoimages, orthomosaics, digital elevation models (DEMs) and digital surface models (DSMs). From these derived geospatial products, vegetation structure, height and biomass can be measured and recorded for monitoring small farm and community garden crop production.

Given the increasing importance of food production from small farms and community gardens, this study explores ways to efficiently combine accessible geospatial techniques that are appropriate for monitoring fine-scale agriculture in local communities. Here, a farm or community garden will be considered small according to its size of fewer than four hectares (ha) in production. Although not prohibited for use in small vegetable plots in an individual's yard that produce food intended for an individual household, the

sUAS-based monitoring systems examined here will focus on the acquisition and assessment of an intra-seasonal image time series for monitoring various row crops on small farms and community gardens. By combining sUAS-collected imagery and photogrammetric image processing known as Structure from Motion (SfM) to create 3D plant structure data from overlapping images, I will be able to make recommendations for fine-scale farmers and managers to effectively monitor small farm crops.

Scientific Contribution

Community gardens and small farms have significant cultural and social roles in our communities and provide a considerable portion of our food in rural, suburban and urban areas. Their contributions span over a century, showing they are not a fad, but an important and long-term asset to food security. As geospatial technologies decrease in cost and increase in ease-of-use, it is important to integrate and implement the techniques and technologies formerly reserved for industrial-scale farming in the daily practices of smaller farms. Small farms and community gardens can also benefit from advancements in geospatial techniques to efficiently monitor crops for pest pressure, climate change effects and animal predation with goals to increase volume and yield through the techniques of precision agriculture that were once beyond their reach. Identifying the best methods for integrating these techniques and making them freely accessible through web distribution to fine-scale famers, community garden managers, agricultural extension agencies and small businesses providing geospatial monitoring services is expected to benefit the agricultural community, our local food systems and society as a whole. This study will contribute to increasing food security, yield, production and knowledge of self-sustaining farming.

Primary Goals, Research Questions and Objectives

The primary goals of this study are the development of an integrated method using accessible geospatial techniques and image processing tools that allow fine-scale, small landholder farmers and managers to monitor plant growth, vigor and biomass. The study aims to establish best practices for monitoring small farm and community garden productivity, as well as assess damages due to a variety of potential disturbances. Objectives of this study and research questions that underlie specific objectives include the following.

Objective 1. Assess integrated geospatial techniques appropriate for small landholder farmers to examine crop growth and volume over time through the use of sUAS imagery & Structure from Motion photogrammetry.

Research Question 1: How can fine-scale farmers improve crop monitoring, yield prediction and damage assessment using readily accessible and relatively low-cost sUAS-acquired imagery and image processing/analysis software?

By combining and exploring various geospatial techniques for monitoring vegetation, it is possible to develop a low-cost solution to the quantification of a bare earth model, crop growth rates, maximum biomass or yield at the peak of the growing season and the loss of biomass at the time of harvest or impact by damaging factors such as extreme weather or herbivory. Imagery of high spatial and temporal resolution required for these tasks can be acquired by small landowner farmers using off-the-shelf sUAS equipment. A time series of sUAS imagery will document crop growth over a growing season and will focus on obtaining highly overlapping images at relatively low flying heights and optimal lighting conditions. Readily available software also can be used to

perform photogrammetric processes such as image matching and Structure-from-Motion (SfM) to create digital 3D point clouds, derived bare earth DEMs, crop-specific surface models (CSMs), image-draped 3D models of crops and geo-corrected image mosaics (i.e., georectified orthomosaics). From these products, crop volumes, plant heights and other measurements of crop plant structure and condition may be achieved.

Protocols for optimal sUAS image acquisition, data management and data processing can be developed for a local community garden at the University of Georgia (UGA) known as the UGArden, located near the main campus in Athens, Georgia and representative of the Georgia Piedmont physiographic region. Close proximity of the UGArden study site allows rapid access to monitor stages of plant growth and refinement of protocols and best practices. A time-series of imagery also provides documentation of several stages of plant growth beginning with widely spaced seedlings through maximum growth and final harvest during a single growing season.

Objective 2. Apply best practices and refined techniques for a crop monitoring system for small landowner farmers to low-country coastal Georgia small farms.

Research Question 2: How can the techniques and protocols developed in Objective 1 at the UGArden within the Piedmont physiographic region of Georgia be applied to small farm plots on the Georgia coast that are representative of small landowner farmers in the Coastal Plain physiographic region?

In order for the robustness of the geospatial techniques practiced and refined in Piedmont Georgia at UGArden to be determined, protocols such as recommended sUAS flying heights and flight patterns for different crop types, optimal weather conditions and time of day, data management practices and the production of 3D models and orthoimages,

need to be applied in a second physiographic region of Georgia. Objective 2 of this study is an application of best practices of the small farm monitoring techniques to small-plot gardens grown at the UGA Center for Research and Education on Wormsloe (CREW) located on the Isle of Hope and within low-country coastal Georgia and the Coastal Plain physiographic region. This area is representative of the coastal low-country region ranging from South Carolina to Florida due to its historical agricultural usage, sandy soil and warm temperatures. Image data collection timed towards the end of the growing season when plants have reached maturity allows a maximum height CSM to be created and crop biomass calculated to estimate yield of small farm plots.

Objective 3. Examine a variety of crop shapes to determine if vegetation structure parameters, such as plant form, leaf size and shape or plant height, influence the accuracy of photogrammetric products (i.e., 3D surface models and orthoimages) and, therefore, the accuracy of measurements derived from these products.

Crops take on a variety of shapes or growth forms, from low-growing and compact to tall and thin, with a high diversity of leaf size, shape and number, along with sturdiness of stem and leaf blade. These characteristics are expected to influence the relative success of image processing functions, such as multi-image point matching and 3D point derivation, because any movement of the stalk, leaves, flowers, fruits or leaf stems will change the position of that plant or plant part on successively overlapping images. In other words, feature identification on multiple images is not possible if the feature moves significantly while the sUAS is passing overhead and acquiring images. Objective 3 aims to apply the developed small farm crop monitoring methodology to crops representing a range of structure types in order to assess its utility for some commonly grown row crops

in small farms and community gardens in Georgia. For example, cabbages are almost spheroid in shape and their compact growth form and large sturdy leaves are expected to experience minimal movement between successive frames of the sUAS imagery. In addition, since the majority of the plant is harvested for consumption, a CSM created at the stage of maximum cabbage growth is expected to most accurately estimate profitable crop yield. Leafy greens such as lettuces, kale and collards, are also harvested and consumed in almost their entirety, but their more loose growth form and variety of leaf shapes, sizes and firmness may reduce the success of photogrammetric feature matching and thus the accuracy of derivative 3D products for estimating yield. Finally, plants such as peppers or okra are expected to introduce some uncertainty in photogrammetric processing and success of 3D modeling because these plants are tall and thin with more finely dissected and somewhat flimsy leaves. Additionally, only the fruit of the plant is harvested for consumption. Leaves may obscure the fruit from view at certain angles and farmers would need to determine a quantitative relationship between plant and harvestable crop volume in terms of total plant and the volume or weight of harvested fruits.

Another aspect of Objective 3 is understanding the growth stages and characteristics of different crop types because growth form may change during the life cycle. A juvenile crop will have a shorter overall height with fewer and smaller leaves. If the crop grows fruit, the harvestable fruit will not be present in the early stages or may be obscured by leaves in later stages. For this reason, what is learned in Objective 1 will be applied to Objectives 2 and 3, and the results of Objective 3 will ultimately improve the geographic robustness and identify limitations in the methodology and protocols for small farm and community garden monitoring.

CHAPTER 2

LITERATURE REVIEW

Importance of Small Farms and Community Gardens

Small farms and community gardens are important sources for local food; they enhance rural livelihoods, support farm-to-table restaurants and create employment opportunities. They also strengthen relationships within local communities and enhance local economies (Henneberry et al. 2009, King et al. 2010, Boys & Hughes 2013, Olson 2018). Farming at a fine scale (i.e., physically small farms approximately equal to or fewer than four ha or 10 acres in size) enables the owner or manager to experiment with preserving and proliferating heirloom vegetables (Seed Savers Exchange 2019, Orgera 2019).

Precision agriculture developed in the late 1980s and early 1990s as technologies such as global navigation systems (for example the Global Positioning System or GPS), remote sensing and geographic information systems (GIS) were more widely implemented to optimize production on large farms. Integrated GPS-GIS precision agriculture practices accounted for variations within agricultural fields using site-specific applications with the goal of increased profit and increased yield, in part due to a decrease in input costs and targeted application of fertilizers, irrigation, drainage structures (Johnson et al. 1983, Lowenberg-DeBoer 1996, White 1997, Comis 1998, Zhang et al. 2002, Gebbers & Adamchuk 2010, Schimmelpfennig 2016). Increased profitability and a decrease in environmental impacts were achieved through the assessment of variables such as physical

soil properties, soil depth, drainage and moisture content; crop variability such as height and density; field variability such as elevation and slope and other factors such as weed, disease and pest infestation (Zhang et al. 2002). The typical use of precision agriculture, however, remains today at the broad scales of industrial farming and large fields covering multiple hectares of homogeneous crop monocultures.

Small farms and community gardens, on the other hand, enhance genetic variety and agrobiodiversity (O'Connor 2011, Pearsall et al. 2017, Orgera 2019) by the use of heirloom fruits and vegetables (O'Connor 2011, Barnett 2014). The Food and Agriculture Organization (FAO) of the United Nations concluded that the last 100 years witnessed the disappearance of 75% of crop genetic diversity as farmers world-wide have moved away from traditional and local seed sources to genetically homogenous varieties purchased through large seed companies (FAO 2019). Fortunately, organizations such as Seed Savers Exchange, a non-profit organization based in Decorah, Iowa, maintain over 20,000 varieties of heirloom plants and encourage small landowner farms and community gardens to plant local heirloom varieties. The Seed Savers Exchange focuses on collecting, preserving and sharing heirloom and rare plants in hopes of increasing and preserving genetic diversity as a safeguard against future disease, climate change and pest pressure (Seed Savers 2019). The Svalbard Global Seed Vault located in Norway is a world-renowned repository of seeds in a vault carved 100 meters into a mountain in permafrost substrate that ensures a stable temperature is maintained at minus 18 degrees C (Svalbard 2019). Svalbard receives seeds to preserve genetic material from all over the globe and the Seed Savers Exchange has deposited over 3,500 seed samples into the Svalbard Global Seed Vault in the last decade (Seed Savers 2018).

There are a multitude of reasons why individuals are increasingly turning to small landholder farming and/or becoming involved in community gardens. Motivations to participate in small farms or community gardens include personal enjoyment, a desire to interact and connect with members of the community, wanting to make their community a better place and fostering a feeling of connection with their cultural heritage (Bussell et al. 2017, Pearsall et al. 2017, Sonti & Svendsen 2018). Community gardens also help alleviate local food insecurity (Bussell et al. 2017). This is exemplified through the University of Georgia's UGArden food donations to the student pantry and Campus Kitchen (UGArden 2019). Some community or small farms also offer a volunteer trade - in exchange for volunteer hours on the farm, volunteers are paid in food items (author's personal experience). Experiential learning of young children working on-site in gardens and local farms showed a significant increase in knowledge of where food comes from (Kos & Jerman 2012). Bussell et al. (2017) discovered individuals and families who participated in community gardens reported that they had increased their fresh vegetable intake since becoming involved with their local community gardens. These farms and community gardens serve as connective hubs of community interactions, food sources and education tools; therefore, it is important to also provide small land holder/community gardeners with precision agricultural tools that have historically only been implemented on larger farms.

Potentially, the adoption of precision agriculture techniques may be lacking; farmers and managers may not be implementing the most efficient technologies or truly understand the long-term benefits of investing financially in new technologies (Tey & Brindal 2012, Schimmelpfennig 2016). They may be missing out on beneficial practices or new technologies to improve resource efficiency and crop yield. Given the numerous

positive social, cultural and nutritional benefits of small and community farms, it is important to ensure fine-scale local farms receive the same attention as large agricultural farms do in terms of access to information on geospatial technologies, precision agriculture and knowledge of other advancements for monitoring crop health.

The last several decades have witnessed a growth in popularity of farmers' markets in the United States. In less than 60 years, from 1960 to 2019, farmers' markets grew in number from around 100 to almost 9,000 (Greb 2019). As the number of local farmers' markets has grown, the U.S. Department of Agriculture (USDA) created an online National Farmers Market Directory (USDA 2020), searchable by identifiers such ZIP code, state-wide search or specific market name. The user interface also allows filters to be applied to see available products (e.g., fresh vegetables, plants in containers, baked goods, canned or preserved fruits, etc.) types of payment accepted or winter markets only. Organized websites like these allow for a faster and more efficient search, tailored to the user's needs. Additional information for individual markets includes location, number of vendors, day and time of market and a website link. As of February 1, 2020, there were 169 entries of local farmers' markets for the state of Georgia alone.

Application of Remote Sensing in Precision Agriculture

Geospatial technologies including remote sensing, Global Positioning System (GPS) and LIght Detection And Ranging (LiDAR), provide farmers with information that can be used to increase crop productivity and improve farming efficiency. Although crop and soil mapping has been conducted using aerial photographs since the 1950s (Goodman 1959 and 1964, Bowers & Hanks 1965, Evans 1972, Ryerson et al. 1997) and satellite images since the 1970s (Richardson et al. 1975, NASA 1978, Meyers 1983, Leon et al.

2003), until recently the data, equipment and computer analyses have not been readily accessible to fine-scale farm operations. The decrease in cost and increase in the availability of equipment, software and computers now allows integrated geospatial technologies to be used by all farmers to collect data on crop health, growth and effects of disturbances such as extreme weather events and damage due to pest species and herbivory. Low cost methods to monitor and manage crops at the small farm plot and community garden level are needed. For example, small unmanned aerial systems (sUASs) data acquisition with Structure from Motion (SfM) photogrammetric analysis and image processing, allows measurement of fine-scale plant structure, growth, insect damage, biomass, yield and recovery from extreme weather events. Quantified plant vigor and changes in yield can then be used to estimate the economic value of small farm production and assess damages resulting from droughts, floods, insect/fungus infestations and consumption and damage by wild animals. This research, conducted with support from the University of Georgia's Center for Research and Education at Wormsloe (CREW), Graduate School and Department of Geography Center for Geospatial Research (CGR), examines ways for small-farm agriculture and community gardens to be effectively and efficiently monitored using low cost and readily available solutions.

Precision agriculture is vital to maximize the productivity of fields and minimize the economic cost to the farmer. It is also a way to reduce farming-related environmental impacts by focusing resource application only on needed areas. The implementation of practices such as variable-rate fertilizer, pesticide, herbicide and irrigation application technologies, GPS tractor guiding systems and soil and yield mapping are most often seen on large farms (Schimmelpfennig 2016). It is inefficient and wasteful to over apply

fertilizers, pesticides, herbicides or over-irrigate in areas that do not require them. Ziliani et al. (2018) notes one of the most important aspects of intra-season monitoring; that site-specific issues will be noticed at “critical stages of the growth cycle” - allowing for solutions to be implemented before a loss in yield or harvest occurs. For example, if an area seems to be consistently underperforming, with plant heights consistently lower than other areas, perhaps the site has poor drainage or needs an application of a nutrient or fertilizer that the rest of the field does not. Underproductive portions of fields may also be identified and considered for the USDA Conservation Reserve Program that pays farmers to take unproductive and environmentally sensitive land out of production to restore native vegetation and promote biodiversity (Glaser 1985, Morefield et al. 2016, Meng 2019).

Farming is a long-term commitment and farmers utilize the same fields for years. It is beneficial to use 3D models of crops as a record to see how fields perform over time. They may show certain crops perform better in certain fields and be used to strategize efficient planting practices. 3D models also can be referred to for insurance purposes after destructive incidents, as measurable replicas and models of the fields prior to damage. Orthomosaics can assist in mapping areas of low productivity or damage.

Satellite Imagery and Aerial Image Acquisition and Processing

For precision agriculture, the spatial resolution of some satellite imagery is too coarse (Table 1). Medium resolution satellite imagery from the U.S. Landsat Program is freely available and includes images acquired by sensors such as Landsat 5 and 7 Enhanced Thematic Mapper Plus (ETM+) and Landsat 8 Operational Land Imager (OLI). These medium-resolution sensors acquire images with 30-m per pixel spatial resolution for visible, near infrared (NIR) and short wavelength infrared (SWIR). Landsat 7 and 8 are

currently functioning and Landsat 9 is slated to be operational in 2020 (NASA 2019a, 2019b, 2019c). Though datasets are free to download and use in programs such as Google Earth Engine and Earth Explorer, the spatial resolution is still too coarse for smaller fields on the order of 4 ha in size and results in pixels that depict multiple crop types. The Scan Line Corrector on Landsat 7 malfunctioned four years into its mission and resulted in data gaps in the imagery (NASA 2019a), making that dataset less effective. The temporal resolution or return time is 16 days for each satellite or 8 days if the data from two Landsat missions are combined (NASA 2019c). The European Space Agency (ESA) Sentinel 2A and 2B MultiSpectral Instrument (MSI) sensors acquire images at 10-m per pixel spatial resolution in the visible and NIR and 20-m spatial resolution for the SWIR portion of the electromagnetic spectrum with a return time of 10 days, or 5-day return time considering cloud-free imagery from both -2A and -2B MSI sensors (European Space Agency 2019). The Sentinel-2A and -2B imagery may be useful for larger farms and fields, although the 10-m Sentinel-2 imagery would not provide a fine enough spatial resolution for smaller or mixed-use fields. Unfortunately, return time does not guarantee useable imagery of the desired area. Cloud coverage is an issue, as it can obscure some or all of the target area on multiple returns. For smaller fields, especially during times of high cloud coverage or after a destructive event, this still may not be enough.

Table 1: Selected satellites comparing various attributes.

Cost	Name	Temporal	Spatial	Bands
Free	Landsat 4, 5, 7, 8	16 days per sensor	30 - m	Visible, NIR, SWIR
Free	Sentinel – 2A, 2B	10 days per sensor	10 - m 20 - m	Visible, NIR SWIR
Free	NAIP	1 to 3-year cycles	1 - m	Visible, infrared
Varies	sUAS	User defined	User defined	Visible
\$5,000	PlanetScope(DigitalGlobe)	Daily	3 - m	Visible, NIR
\$5,000	Rapideye (DigitalGlobe)	Daily	5 - m	Visible, red-edge, NIR
\$5,000	Skysat (DigitalGlobe)	Daily	.8 - m	Visible, NIR, pan

Although commercially available satellite imagery acquired by companies such as DigitalGlobe and Planet Labs, Inc. provides daily imagery at high spatial resolutions of <1 to 5-m and may capture the fine detail of community gardens and small farm crops, the data must be purchased and in the case of DigitalGlobe, may not be available for all study areas because it is acquired on a tasked-acquisition schedule vs. the global, synoptic and regular image acquisition of Landsat and Sentinel missions (DigitalGlobe 2019, Planet 2019). The purchase price of Planet Labs, Inc. imagery is expensive with the minimum order size costing \$5,000 (Planet 2019). Unfortunately, there is no guarantee that the satellite imagery will contain cloud-free coverage of the desired study area.

Airborne imagery acquired by the U.S. Department of Agriculture (USDA) National Agricultural Imaging Program (NAIP) is freely available for the U.S., since 2005. It has at 1-m spatial resolution with a contractual obligation to make every effort that imagery contains 10% or less of cloud coverage and imagery is orthorectified (USGS EROS Archive 2019). However, since NAIP imagery is acquired only once during the growing season for any particular area - currently on a three-year cycle - it would not be applicable to farmers monitoring their fields over a growing season (i.e., intra-seasonal monitoring) or in response to crop damage. Imagery collected also is exclusive to the United States and not applicable to international study areas (USGS EROS Archive 2019).

An alternative to satellite or aerial derived imagery is imagery acquired from small unmanned aerial systems (sUASs), also known as unmanned aerial vehicles (UAVs) or drones. sUAS acquired imagery has a significant advantage over satellite imagery – it can be acquired and checked for quality control almost immediately. While satellite data may take several days to be publicly available for use and the return time of the satellite can be

several days or weeks, depending on its orbit (See Table 1), sUASs can be reflown the same day or at a different height to capture sufficient and adequate data at optimal times to capture crops at particular stages of growth or immediately following a disturbance event. Users will not have to rely on the set revisit or spatial resolutions of satellite sensors that will not fit their needs.

sUASs are manufactured in a variety of sizes, wing types, weights, camera qualities and price points. Small UASs are defined by the Federal Aviation Administration as weighing less than 55lbs (25kg), including payloads (i.e. cameras or other sensors). The law states a sUAS may not exceed a speed of 100 mph and has a maximum flying height of 400 feet above ground level or 400 feet above a structure. These and other laws - daylight flights only and the remote pilot or assisting visual observer must maintain a visual line of sight at all time are important public safety precautions put in place to reduce the risk of injury and property destruction (FAA 2016).

Limitations for flying a sUAS would be unfavorable weather conditions such as precipitation, high winds, lack of daylight or extreme high or low temperatures. User derived limitations include spent batteries, recharge time for batteries or the number of extra batteries available for use.

The introduction of sUASs for agricultural image acquisition solves many of these issues (Jensen 2018). They provide the ultimate flexibility in terms of frequency and timing of flights, and they can be flown at various heights up to 400 ft. (approximately 122 m) to provide imagery, with pixel sizes on the order of cm or even mm spatial resolution, for community- and small farm-sized study areas ranging from approximately 0.5 to 4 ha (about 1 to 10 acres). Because of this flexibility, imagery captured by sensors on-board

sUAS are easily customized to the needs of the user. Discussing the use of sUAS for monitoring applications, Bendig et al. (2014) acknowledges “the method has potential for future applications by non-professionals (i.e., farmers).” Giving small landholder farmers the autonomy, authority and tools to monitor their crops in the most precise and accurate way possible will, hopefully, be a step towards increasing food security and productivity.

Because sUASs can be flown multiple times during a season, they are well-suited to conduct intra-season time series monitoring and studies. Intra-season time series studies consist of surveying fields or crops multiple times throughout the growing season. The areas are monitored for patterns of underperformance, damage, poor drainage or other impactful issues. The UASs may be flown at set intervals (e.g., every two weeks) or in addition, as an immediate response after a destructive weather or pest event. The ability to fly and acquire imagery from UAS sensors at user-defined frequencies allows farmers or researchers to record time-series imagery at any desired time interval. In recent years, there has been an increase in research of various agricultural crops, including intra-season time series studies and 3D modeling of crop height, using UAS collected imagery. Crops include eggplants, tomatoes, cabbage (Moeckel et al. 2018) Chinese cabbage and white radish (Kim et al. 2018), barley, (Bendig et al. 2014 and 2015) maize (Grenzdörffer 2014, Chu et al. 2018, Malambo et al. 2018), wheat (Grenzdörffer 2014, Holman et al. 2016), alfalfa and rape oilseed (Grenzdörffer 2014) and sorghum (Chang et al. 2017).

Photogrammetric Processing and Analysis of UAS Imagery

Photogrammetry and remote sensing applications have long been used in a variety of fields, ranging from historical and cultural preservation, ecology, forestry, natural resource and vegetation mapping (Remillard & Welch 1996, Holmgren & Thuresson 1998,

Yastikli 2007, Madden et al. 2009a, Madden et al. 2015, Madden et al. 2019). Uses such as monitoring coastal shorelines in Georgia, preserving historical and cultural buildings and monuments, and the assessment of vegetation damage after extreme weather events are examples of SfM projects conducted by the Center for Geospatial Research at UGA in the last five years (Madden et al. 2019). Photogrammetric concepts of SfM started in the 1950s and originated in the field of computer vision, but were not able to enter into mainstream use until the last two decades, as computing power increased and software became more readily available (Hartley & Zisserman 2003, Theriault et al. 2014, Jackson et al. 2016). The automated SfM process uses feature matching algorithms that are comprised of concurrent, highly redundant and iterative bundle adjustment procedures to match the overlapping images and extract features from them (Förstner 1986, Grün 1985 and 2000, Grün et al. 2004, Fraser & Cronk 2009). With these increases in computation technology, it became easier to work with 3D data as some datasets, such as DEMs, and LiDAR datasets became available for free or low cost through various online portals (Katsianis et al. 2008, Madden et al. 2009b, Agapiou et al. 2016, Richards-Rissetto 2017).

Structure from Motion (SfM), a photogrammetric process, estimates three-dimensional (3D) structures from multiple two-dimensional (2D) overlapping images (Westoby et al. 2012). Consecutive images for SfM analysis must overlap with each other to ensure distinctive features used in image matching, appear in multiple images and provide multiple perspectives of all features (Figure 1). Recent years have witnessed the advent of a variety of software programs such as MeshLab, Pix4D and Agisoft Metashape that use SfM processing to create 3D point clouds from overlapping images and allow the derivation of output products such as DEMs, CSMs, orthoimages and orthoimage mosaics

(or orthomosaics). Structure from Motion derives its name from the first step in its process. The object or area of interest stays static and the camera moves around the object, capturing images with significant overlap as pictured in Figure 1.

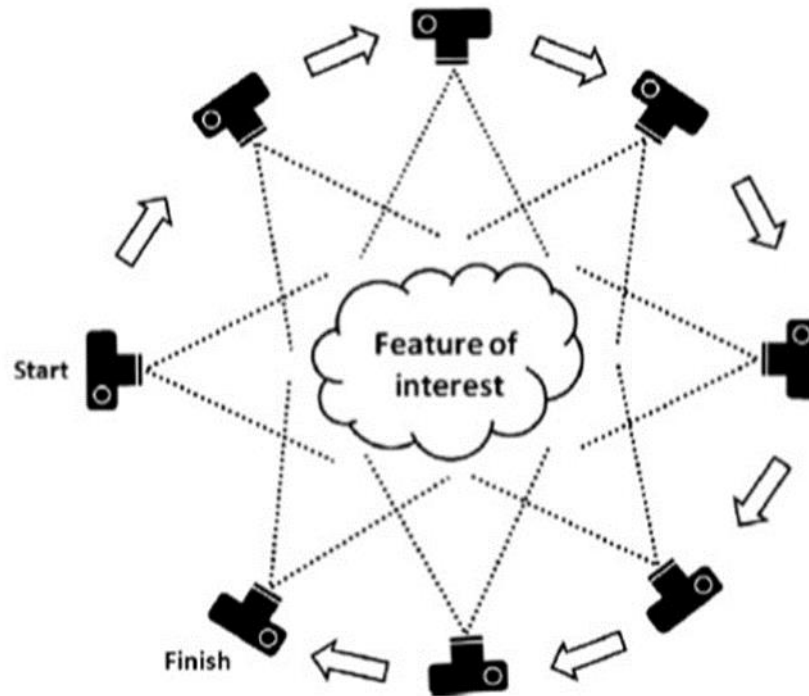


Figure 1: Depiction of overlapping imagery acquired for a feature of interest that will be processed by SfM to create a 3D model of the feature. Image credited to Westoby et al. (2012).

The basic workflow presented in software currently used to perform SfM, such as Agisoft Metashape, is often simplified to a few procedural steps, including: input overlapping imagery of the desired target, launch algorithms that detect matching points between images and construct a 3D point cloud and perform the creation of additional outputs such as a DEM, mesh and orthomosaic. However, the mathematical computations underlying these steps are complex. To gain a better understanding and appreciation of the complexity of the SfM process, examining some of the initial concepts upon which the SfM workflow is built is both helpful and necessary to ensure best decisions are made for

image acquisition and the selection of SfM parameters. The complex photogrammetric algorithms and processes in SfM performed within currently available software often operate in a “black box”, unseen and unexamined by most users. It is important that users understand the basic processes of SfM because the algorithms and methods differ slightly among software programs and user-input decisions for SfM parameters will affect the quality and accuracy of resulting products.

The software workflow requires an input of multiple images consisting of a large amount of image overlap (ideally 80 – 90%). The images do not need to be in specific order, nor does the software require *a priori* knowledge of the geometric position of the image collecting sensor. Although not necessary, embedded coordinates and information in the images from GPS-sensors will improve the efficiency of image matching and geometric reconstruction (Förstner 1986, Grün 1985 and 2000, Grün et al. 2004, Fraser & Cronk 2009, Cotten et al. 2019, Madden et al. 2019).

After the collection of imagery and input of images into the software, the first SfM process is feature matching. A feature is a distinct shape within the image that can be identified and extracted from multiple images, which is then stored in a database so the same feature can be matched in the additional images containing it (Förstner 1986, Grün 1985 and 2000, Grün et al. 2004, Fraser & Cronk 2009, Cotten et al. 2019). This is accomplished by identifying matching features, also referred to as tie points, on multiple images. An important “black box” concept to explore is *how* feature matching occurs. The Scale Invariant Feature Transform (SIFT) created by Lowe (1999), improves the quality of features being matched and extracted. The SIFT algorithm allows features to be matched regardless of image scale and rotation and has more robust matching in change of 3D

viewpoint, affine distortions, illumination changes and noise (Lowe 2004). This algorithm builds upon previous work developed for image matching on stereo matching using a corner detector designed by Moravec (1981), with a later improvement added by Harris & Stephens (1988) that allowed for better repeatability near edges and small variations within images, and later expanded to motion tracking and SfM recovery (Harris 1992). Building off this, Schmid & Mohr (1997) showed that invariant local feature matching could assist in image recognition issues by matching a particular feature within a large database of images and allowing features to be matched regardless of orientation changes between the two images. Lowe's (1999) improvements of added scale invariance allowed for better feature matching even while image distortions such as 3D viewpoint changed between images (Lowe 2004).

The second step, following the feature matching or tie point process step, is the image orientation that will occur based off the relationships determined in the feature matching or tie point process, using the Sparse Bundle Adjustment. The basis for image orientation and geometric reconstruction lies in photogrammetry and aerotriangulation of photographs (Lourakis & Argyros 2009, McGlone 2013). Aerotriangulation involved the alignment of analogue aerial images and prepared them for stereo measurement purposes. Using highly overlapping photos from a flight plan, the identification of tie points or pass points and known ground control points on the actual images, the camera positions and altitudes were then solved through mathematical equations (Wolf & Dewitt 2013). Although originally applied to a stereopair of two overlapping images, this photogrammetric process can be applied to an unlimited number of images. Wolf & Dewitt (2013) explain the term bundle adjustment performed in aerotriangulation refers to the

mathematical computation of equations representing “many rays of light passing through each lens position, constituting a bundle of rays. The bundles from all photos are adjusted simultaneously so that corresponding light rays intersect at positions of pass points and control points on the ground.” The bundle adjustment solves for the X, Y and Z positions of the targeted object points and the x, y and z positions of the camera locations and their omega, phi and kappa rotations (Wolf & Dewitt, 2013) and corrects for lens distortion. In this way, the geometry of the cameras’ positions and a sparse 3D point cloud of the target is created in its relative coordinate system (Wolf & Dewitt, 2013, Cotten et al. 2019). A sparse point cloud is then created.

The third step is the construction of a dense point cloud, where every individual point consists of XYZ coordinates, as well as the Red Green Blue (RGB) values from the imagery. The dense point cloud is an enhanced point matching from the already aligned images. This point cloud contains many more points than the sparse point cloud, and the density will vary due to quality, resolution and size of imagery. Processing time will also increase with larger datasets or higher resolution imagery (Cotten et al. 2019, Madden et al. 2019).

These are three required steps for SfM, but additional outputs derived from the 3D point cloud are possible through SfM or additional software. For example, a triangular irregular network (TIN) or mesh can be created by connecting adjacent exterior 3D points of the point cloud in a network of triangular facets to form a digital surface model (DSM) that mathematically models the uppermost surface of the 3D model (Little & Shi 2001, Westoby et al. 2012). Alternatively, if only the lowest ground points are selected, a bare earth digital elevation model (DEM) may also be computed. Once the DEM/DSM is

created, the pixel heights are used to orthorectify a mosaic of the images. Images are first orthorectified through the correction of inherent image distortion (e.g., relief displacement) and color balancing, then seamlessly stitched together as a mosaic (Wolf & DeWitt 2013). It allows for the orthomosaic to be used as a map with accurate location and distance measurements within it that can be used to also calculate area or volume. This is a useful and versatile product for users and can be input into a GIS program or serve as a base image map for other geospatial data such as locations collected with a GPS.

Software for Structure from Motion

The Agisoft Metashape Pro software is currently one of the most widely used to perform SfM and create 3D point clouds, DSMs and digital orthoimage mosaics using sUAS imagery. It should be acknowledged that imagery does not *need* to be from a sUAS to perform SfM and can, alternatively, be acquired from other devices such as mobile phone cameras or hand-held cameras. The Metashape software is designed to recognize points and features that appear in multiple photos (i.e., image matching), link common points together and create a smooth 3D model or dense point cloud from the multi-perspective image geometry (Fonstad et al. 2013, Koutsoudis et al. 2014, Madden et al. 2015, Cotten et al. 2017). Since SfM can be a computationally complex process and require hours of processing time when a large number (on the order of 100 or more) of sUAS images are being analyzed, the SfM images can be processed in separate batches using Agisoft Metashape Professional. Processing may take several hours; depending on the number of images used, the quality of the imagery and the settings selected for the created product/output. Products generated from the software include dense point clouds, that can, in turn, be used to produce DEMs or DSMs and interpolated 3D models. The 3D models

of small gardens can be created from low altitude sUAS images or ground photos that are acquired with approximately 80 – 90% overlap. These models can then be used to compute the height and volume of plant material in the garden. The 3D models, of the same area, created over time provide quantitative data on crop growth, yield and damage.

SfM and Vegetation

Moeckel et al. (2018) shows the accuracy of measurements derived from SfM products can vary between different species of plants - possibly due to the shape of their structure. For example, grain crops, such as wheat, barley and corn, grow tall and thin. Other crops, like leafy greens, have multiple overlapping broad edible leaves, while others have fruit at maturation and small inedible leaves. Due to their physiology, the growth form of crops effects the accuracy of plant measurements from 3D models created using SfM. The leaves and stalks of crops are pliable and may wave or bend in the wind. If the altitude above the intended target at which the sUAS is flown is relatively low (e.g., < 10 m), the sUAS can generate enough wind to make crops move – commonly known as “propwash”. Images taken in these conditions may be blurred, which can cause errors in the CSM height measurements (Chang et al. 2017). Image blurring causes the SfM algorithm to have issues finding matching points between images; points that are erroneously matched may affect 3D point extraction and the generation of the orthomosaic (Xu et al. 2016). Blurring and movement distort the actual object and it may appear different enough in the overlapping images to inhibit feature matching.

A study by Dandois et al. (2015) examined controllable parameters, flight altitude and percent image overlap, and naturally occurring weather variables, cloud cover and light, to see the effects on accuracy of 3D model reconstruction from sUAS imagery of

forests. They found the most accurate of their models came from flights conducted in cloud free conditions. Imagery collected during days with cloud coverage increased errors within the point cloud. While this is a valuable place to start, accuracy may differ according to various heights of vegetation. Tree canopies reach over several meters in height while some vegetation, including non-grain crops, grow less than a meter in height. A homogenous canopy will cast less shadow than one of varied height. As Dandois et al. (2015) measured heights of tree canopies reaching several meters as opposed to shorter vegetation, their recommendations may not hold true in all situations. Depending on the application, overcast days may be more beneficial to reduce shadows which may affect SfM processes, depending on factors such as height, canopy coverage and leaf overlap.

Dandois et al. (2015) notes “reduced image contrast can have a strong influence on the stability of image features”, resulting in an increase of dense point cloud position errors. Reduced image contrast can be the result of overcast days. Yet, the study also acknowledges that while direct or sunny lighting increases contrast, a negative trade-off is increased shadows in the imagery. Possibly, different species would do better under different conditions, as the shadow cast from a cabbage would perhaps interfere less with its volumetric and height measurements as compared to leafy greens, like collard greens or kale with many overlapping and flared-out leaves. An important consideration is noting while recommendations for optimal sUAS flight parameters and flying conditions can be made, real-world scenarios often differ from academic studies. Although a farmer with a limited amount of time may choose to collect imagery in less than ideal conditions, it would be vital for the farmer to understand the potential decrease in accuracy of their intended models.

Plant Height Monitoring for Estimating Crop Yield

Estimating plant growth via height measurements using sUAS imagery and 3D modeling has recently proven to be accurate for grain crops including maize (Chu et al. 2018, Malambo et al. 2018), sorghum (Malambo et al. 2018), barely (Bendig et al. 2014 and 2015) and wheat (Holman et al. 2016) and select vegetable crops (Kim et al. 2018, Moeckel et al. 2018). Measuring plant heights from 3D models is accomplished by subtracting the calculated height of the crop, known as the crop surface model (CSM), from the bare earth or digital elevation model (DEM) (Bendig et al. 2014, Grenzdörffer 2014, Kim et al. 2018, Moeckel et al. 2018). Plant height has shown to be an accurate way to predict crop biomass (Yin et al. 2011, Bendig et al. 2014) and predict yield (Yin et al. 2011, Bendig et al. 2015). The imagery to process and create the high spatial resolution DEM should be collected prior to the growing season, as it is a bare earth model. If a DEM is not created prior to the growing season, it can be established using measurements derived from models created when the plants are in very early growth stages and do not fully cover or obscure the ground. Once the DEM is established at T_0 , each set of subsequent images collected of the garden during the growing season or following a disturbance constitutes an individual 3D model or data set of $T_1, T_2 \dots T_x$ and produces a separate CSM data set for each time frame. The separate CSM data sets are then sequentially subtracted from the DEM to compute crop height, volume or yield for each time step. A series of CSMs can then be used to compute yield differences of crop loss in cases of disturbance and trends of crop growth over time. Monitoring yield is important as it can be a factor in the optimization of farming practices, potentially increasing the profitability of the farm and ultimately helping to alleviate food insecurity.

Unfortunately, oftentimes actual yield is less than potential yield (Anderson 2010; Mueller et al. 2012). As the global population is rapidly expanding, food security through increased food production will be an important goal. Anderson (2010) and Mueller et al. (2012) describe global and regional yield gaps, or the difference between observed yields compared to the potential or attainable yields in the same region. Increasing actual yield is in part due to management decisions and practices, including over or under nutrient application and irrigation (Anderson 2010, Mueller et al. 2012) and is part of precision agriculture. Active, intra-season and highly localized monitoring may help close this gap, increase food security and increase farm profitability.

SfM Compared to Other Crop Measuring Techniques

An examination of these sUAS and SfM studies with applications in agriculture reveals the authors often had different objectives in mind. Some like Grenzdörffer (2014), Chang et al. (2017), Moeckel et al. (2018) and Ziliani et al. (2018), attempted accurate measurements of crop height throughout the season, using multiple monitoring dates or an intra-season temporal study. Others, such as Bendig et al. (2014), attempted to estimate biomass from crop surface height and Holman et al. (2016) wished to determine phenotypes. While objectives may differ, they all show the benefits of geospatial technologies and sUASs to the farming community.

Studies used measurements taken by hand of the targeted crops in order to compare SfM measurements to the actual crop heights. Kim et al. (2018) found a high correlation of $R^2 = .95$ for Chinese cabbage, from height measurements taken by hand and SfM created crop surface models. Using a CSM created from SfM and UAS imagery and compared to validated measurements Moeckel et al.'s (2018) prediction model found a high correlation

of $R^2 = .89$ for tomatoes, $.97$ for cabbage and $.93$ for eggplant. Their results showed that the models underestimate true height. Though it does validate the SfM-UAS methodology of monitoring crops, measuring crops by hand is extremely labor intensive and time consuming. Regardless if it is simply measuring the plant from the ground to the highest point or destructive sampling involving the removal of the plant to record its true biomass and weight, validation data adds time, labor and cost - especially if comprehensively measuring multiple crops throughout an entire season.

The accuracy of crop surface heights derived from 3D models produced using UAS imagery and SfM has been assessed using comparisons of hand measurements of plant heights in the field, and comparisons with heights derived from terrestrial lidar data. Lidar (Light Detection and Ranging) or laser scanning is a highly accurate, yet expensive remote sensing technique used to measure distance. Lidar measures distance through a pulsed laser that reflects off the target and sends multiple returns back to the lidar sensor. This works by calculating distance through the speed of the return pulse. The first return would denote the tallest height (or closest distance) captured in that pulse, the second return, a slightly shorter height (or further distance) and so on (Renslow 2012). Depending on the density of the pulse, finer details may not be picked up. If there are obstructions such as vegetation canopies with no gaps, then the pulse will not be able to reach the ground or create a bare-earth model (Blair et al. 1999, Lefsky et al. 2002, Singh et al. 2016). It is used in a variety of applications and fields, including the creation of 3D models and digital elevation models of natural and cultural resources. A lidar sensor is an expensive tool to use and the collection of extremely large volumes of lidar data require special software for processing, making this geospatial technology more specialized and, perhaps, not appropriate for use

by the general public at this time. Lidar measurements are considered highly accurate in most applications and the use of lidar in precision agricultural has proved to be effective and important for crop management (Rosell et al. 2009, Llorens et al. 2011, Long & McCallum 2013, Eitel et al. 2014). Typically, lidar has been used in large or commercial scale agricultural applications to identify areas of underperforming crops.

Lidar is considered an accurate sensor for 3D reconstruction of plants (Underwood et al. 2017, Yuan et al. 2018) but an extreme drawback is expense and the large quantities of data it produces (Singh 2016). Yuan et al. (2018) compared the accuracy of terrestrial lidar to UAS-SfM for a temporal wheat crop height study. Lidar had the highest correlation ($R^2 = .97$) when comparing the lidar derived crop height measurements to manual measurements but UAS-SfM derived heights also had a high correlation ($R^2 = .91$). When Madec et al. (2017) compared the results of wheat plant height derived from terrestrial lidar to those of SfM, the study showed a strong correlation $R^2 (.98)$ between the two techniques. Ziliani et al. (2018) examined the accuracy of terrestrial lidar and UAS-SfM on maize, finding a correlation of $R^2 (.65)$ for crop heights and $R^2 (.99)$ for the DSM, and from those results, the authors determined UAS-SfM techniques can accurately reproduce the variability of maize crop heights throughout the season.

CHAPTER 3

STUDY AREA

This research will be conducted at two study areas in Georgia that are owned by the University of Georgia and represent small-farm growing conditions in the Piedmont and Coastal Plain physiographic regions of the Southeast – at the UGarden in Athens and the Center for Research and Education at Wormsloe on the Isle of Hope outside of Savannah, respectively (Figure 2).

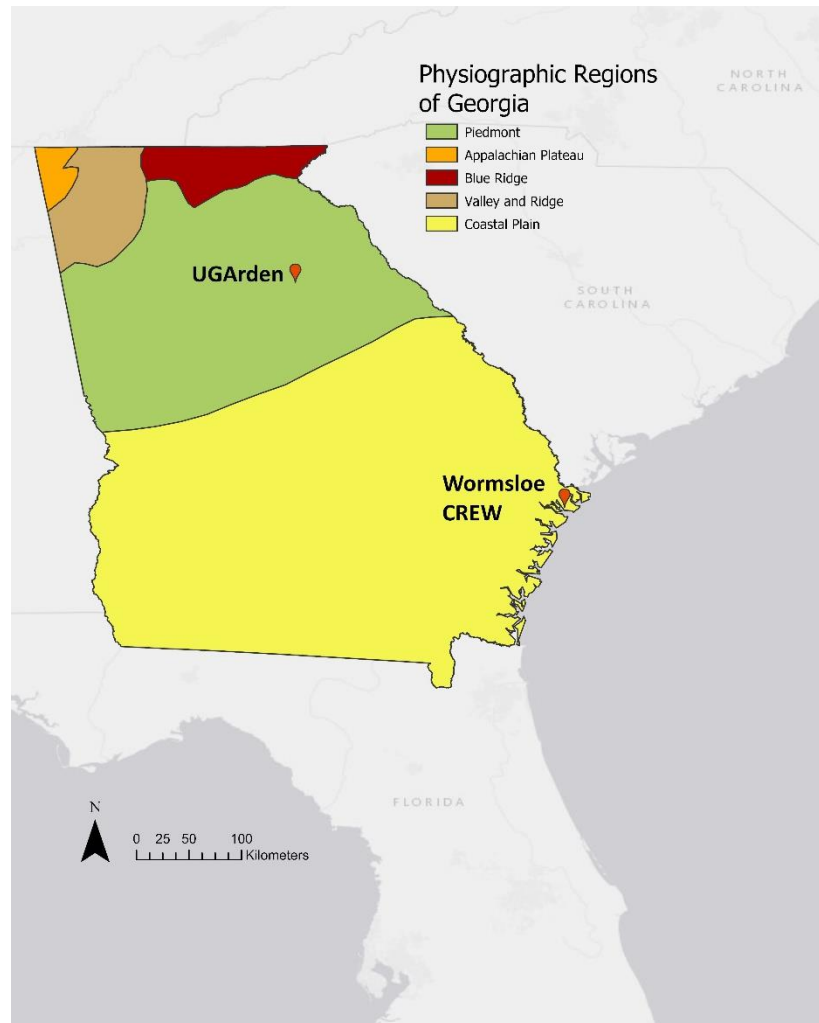


Figure 2: Study sites overlaid on the State of Georgia.

UGarden

UGarden is part of the University of Georgia's College of Agricultural and Environmental Sciences and is in the Piedmont physiographic region of Georgia. It is adjacent to the Georgia State Botanical Gardens, at 2500 Milledge Ave in Athens, GA (Figure 3). Operations are run by a combination of faculty, students, volunteers and interns affiliated with the University and the larger Athens community. Farm updates and blogs are available at their website: <https://ugarden.uga.edu/>. The first garden plot started in May

of 2010, initiated by the student organization, the Campus Community Gardening Initiative, and backed by funding from the UGA Horticulture Department. Financial assistance later expanded to include a Higher Education Grant from the United States Department of Agriculture (USDA) National Institute of Food and Agriculture. Currently, UGArden hosts several undergraduate, graduate and Freshman Odyssey courses and credited internships through the Horticulture Department, with an educational emphasis placed on sustainable farming practices. UGArden assists people suffering from food insecurity through donations of its harvest to the UGA Campus Kitchen Association and the UGA Student Food Pantry. Other outreach initiatives include promoting and encouraging healthy eating through cooking demonstrations and food sampling at the Athens Clarke County middle schools (UGArden 2019).

As the second largest physiographic region in Georgia, the Piedmont covers approximately 30% of the state. The elevation ranges from 152 m along the region's southern boundary to 366 m along the northern edge (See Figure 2) (NCDC 2020). The terrain is moderate and slope generally does not exceed 8° unless along the side of a valley (Markewich 1990). This region is distinguished visually by its red soils due to iron minerals from rocks such as granite and its numerous rocky outcrops formed from the hard bedrock located near the surface (GeorgiaInfo n.d.). Soils in the Piedmont are more susceptible to erosion as compared to the Coastal Plain because of the characteristically shallow soils (typically less than 1 m thick) (Markewich 1990) and the region's historically intense agricultural practices – particularly cotton (Forest Service 1994). Piedmont soils contain a higher clay content and less sand than those of the adjacent Coastal Plain (Markewich 1990).

The average summer temperatures range from 22 – 28 °C and the average annual precipitation is approximately 114 cm, but annual precipitation can vary greatly from year to year. The driest months occur in autumn. Annually, the region receives less rainfall and is slightly colder than the Coastal Plain (NCDC 2020). The growing season ranges from 205 – 235 days per year. The main forest types in this region are evergreen forests and oak-hickory-pine forests containing white, post and southern red oaks and pignut and mockernut hickories. In areas characterized by disturbance, loblolly and shortleaf pine tend to dominate (Forest Service 1994). Large agriculture farms commonly grow cotton, corn and peaches, among other crops (NCDC 2020). Smaller farms, such as UGArden, grow many varieties of crops including kale, collards, lettuces, tomatoes, squash and garlic.



Figure 3: Orthomosaic processed in Agisoft Metashape from sUAS flight imagery, georeferenced and overlaid on the study area of UGarden in ArcMap.

UGA Center for Research and Education at Wormsloe (CREW)

The second research site is the UGA Center for Research and Education at Wormsloe (CREW) campus located adjacent to the Wormsloe State Historic Site on the Isle of Hope. The Isle of Hope is an inner barrier island along the Georgia coast and is within the Coastal Plain physiographic region. Over the last ten years, the Wormsloe Institute of Environmental History and the UGA Graduate School have supported a variety of research projects at CREW utilizing concepts, theories and techniques from a variety of different disciplines, including geography, ecology, history and archeology (Wormsloe Institute for Environmental History, n.d.).

Located approximately 16 kilometers (10 miles) south of the city of Savannah, the northern end of the Isle of Hope is separated from the mainland by salt marshes adjacent to the Herb and Wilmington Rivers, the west side is surrounded by Shipyard Creek marsh and the south and east sides are surrounded by salt marsh tidal flats of the Skidaway River (Swanson 2012) (Figure 4). The flat terrain extends less than 20 km inland from the Atlantic Ocean and sandy soils support live oak hammocks, saw palmetto, slash pine and historically, longleaf pine forest (Swanson 2012). Animals such as deer, fox and raccoons live and thrive on the Isle, while oysters and other shellfish are abundant in the creeks and along the shore (Bragg 1999).

An emphasis of the Executive Director of Wormsloe CREW, Sarah Ross, is the awareness of traditional Coastal Plain farming practices that explores local food production, self-sufficiency and agriculture legacies of the southeastern U.S. Ms. Ross has created vegetable gardens on site to help preserve and proliferate heirloom varieties of various vegetables that were grown to sustain 18th century households along the Georgia

coast. As founder of a non-profit organization, Social Roots, she grows heirloom vegetables and saves the seeds for free donation to those who are also interested in preserving precious varieties for future generations. Her aim is to harvest seeds from between 450 - 500 heirloom varieties from collards, kale, greens and beans to the heirloom varieties of okra and peppers that are included in this study (Orgera 2019). She experiments with raised bed gardening nourished with compost created onsite. Two of her CREW gardens were selected as test sites (Figure 5 and Figure 6) for implementing best practices from sUAS image data collection and processing from UGArden for creating 3D models of small coastal farm plots.

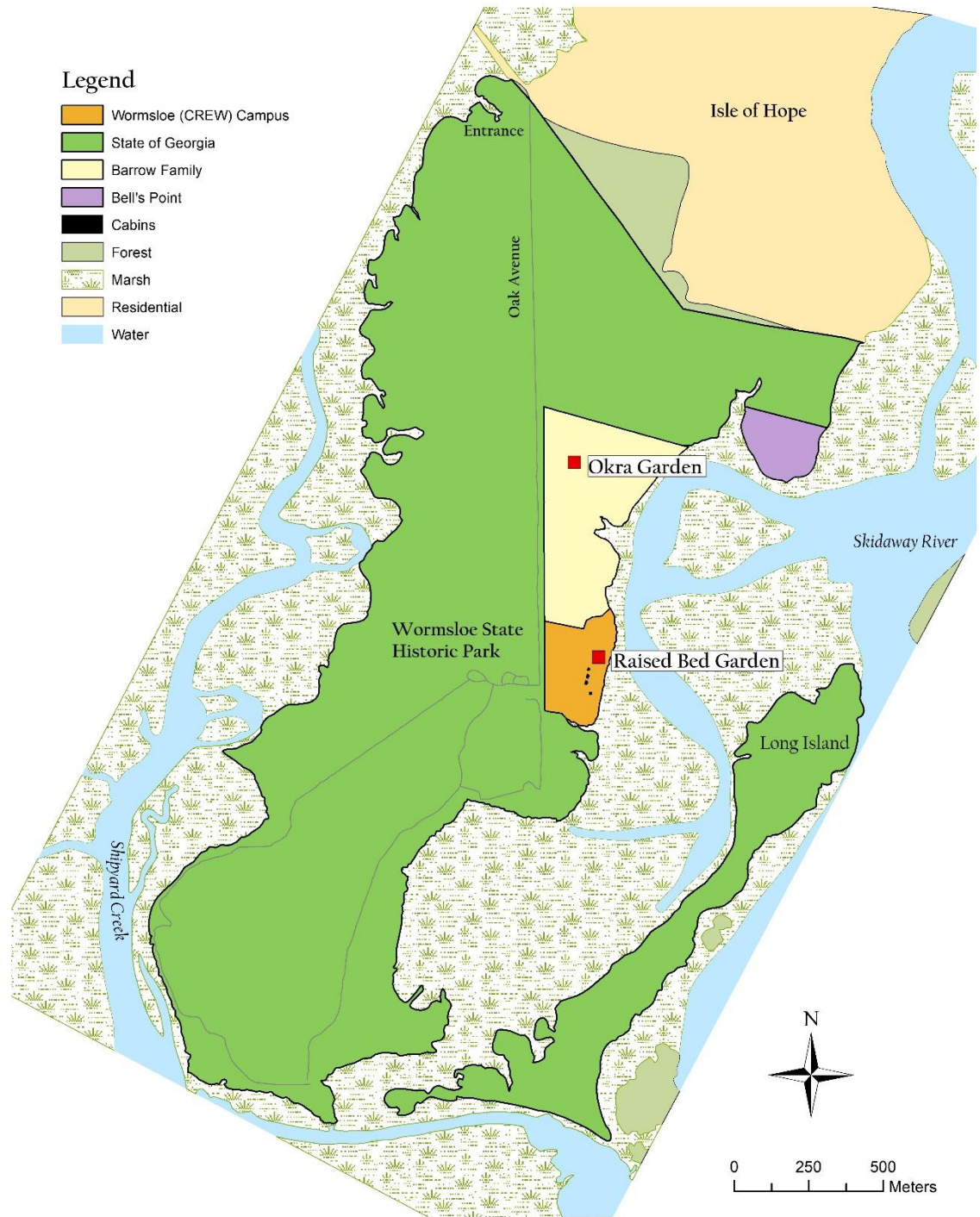


Figure 4: Map of Wormsloe and surrounding area. Garden sites are depicted by red squares. Data creation credited to Dr. Thomas Jordan, Center for Geospatial Research, University of Georgia, Athens, GA.



Figure 5: Aerial image of Wormsloe CREW garden outlined in red, adjacent to the Skidaway river marsh flats.



Figure 6: Aerial image of Wormsloe CREW raised bed gardens taken Sept. 10, 2019.

Unique in its ecological history, the Isle of Hope has been battered by hurricanes and shaped by centuries of human influence – starting from Indigenous Americans who were on the Isle centuries prior to European contact as found in archaeological evidence (Swanson 2012). From the arrival of Noble Jones and his family from Europe in the 1730s, who modified the Isle to create a working 18th century agricultural plantation, to today, the landscape has been shaped by forest clearing and the erection and eradication of various homes, structures, and trails over the last three centuries. It also bears the modifications of generations of agricultural and horticultural efforts - from a broad-scale cotton plantation to private gardens featured as a tourist destination in the 1930s, while in the continuous possession of one family (Bragg 1999). The original property has been divided with the bulk of the Island now owned by the State of Georgia under management by the Georgia Department of Natural Resources, a portion donated to the University of Georgia for the CREW campus and a portion still privately owned by descendants of Noble Jones (currently the Barrow family) (See Figure 4).

The Coastal Plain is the largest physiographic region of Georgia. It is predominately flat, with low lying marshes in many coastal areas. Elevations range from sea level to approximately 180 m (NCDC 2020). Soils on the Coastal Plain have a high sand content, with a low surface runoff, making it less susceptible to erosion than the Piedmont (Markewich 1990). The dominant forest type is loblolly and shortleaf pine, mixed with sweetgum, flowering dogwood, red cedar, southern red oak and hickories (Forest Service 1994).

Demonstrating the long farming history of the area, the first U.S. agriculture experiment station to be established on the Coastal Plain region in the United States is in

Tifton, Georgia. Today, 80% of Georgia's row crops are produced in the southern portion, making it integral to the area's economy. The area is also one of the United States' leading producers in pecans, blueberries, cotton, peanuts and vegetables (University of Georgia, 2019). A long growing season ranging from 200 - 280 days a year (Forest Service 1994), along with average annual precipitation of approximately 135 cm and average summer temperatures of 27 °C degrees create excellent growing conditions for agricultural crops (NCDC 2020). During the day, summer temperatures in this region will often exceed 32 °C and will drop to a range of 20 to 26 °C during the night (NCDC 2020). The Coastal Plain region has greater precipitation and higher temperatures than the Piedmont, contributing to a longer growing season.

Georgia's agriculture is vital not only to the state, but also to the national economy. In 2018, Georgia ranked 20th in the United States for crop commodities and crops consisted of 34% of Georgia's agricultural output. In 2018, Georgia ranked 5th or higher in the nation for peanuts, bell peppers, watermelon, cucumbers and blueberries and in the top ten for sweet corn, onions, snap beans and cabbage (USDA 2019). Georgia has over 42,000 farms that encompass over 3.6 million ha (9 million acres) in farmland (Wolf 2017). A comprehensive overview shows that in 2014, 88% of these farms were labeled as small by the USDA. According to the Bureau of Economic Analysis, 35,000 farms were owned either by sole proprietors or with non-corporate partners. In totality, agricultural industries contribute \$74.3 billion to Georgia's \$907.7 billion economy – just over 8% of the total economy. It also provides around 411,500 jobs (Wolf 2017).

METHODOLOGY

sUAS Flights to Acquire Imagery

To address my first two research questions related to the use of sUAS imagery to create 3D models of small farm plots at UGArden and at the Center for Research and Education at Wormsloe (CREW) campus, sUAS imagery was collected bi-weekly at the UGArden using a DJI Phantom 4 quadcopter. The Phantom was equipped with a 12.4 megapixel-camera with an image resolution of 4000x3000. Flight planning to ensure sUAS images are acquired using optimal flight parameters (e.g., camera tilt angle, flying height, forward and side overlap, speed and flight line locations) was performed using the mobile device application, Map Pilot, operating on an iPad mini tablet. This program requires the operator to input the desired image pixel size (e.g., 2 cm) and percent forward overlap (e.g., 80%), along with an outline of the study area that the user inputs by viewing an aerial image of the area of interest and touching four or more points, creating a bounding box and enclosing the area to be flown. The Map Pilot program then draws lines indicating adjacent flight lines and the operator can edit the length, orientation, number and starting/ending points. Flight lines extend past the bounding box of the targeted fields for quality control of imagery, specifically ensuring the entire field would be imaged and include the ground control points and features around the field needed for image-to-image registration. By inputting the desired pixel size and percent forward overlap, the app will determine the image acquisition interval and automatically capture sequential image frames along the flight lines. Figure 7 shows an example of overlap by depicting sequential images taken during a flight. The settings are saved within the application to be reused on subsequent data collection days. The program gives an estimated flight time, allowing the operator to

decide if the flight plan should accommodate a single battery charge or if automated settings will return the sUAS for a battery swap and then resume the mission. Saving the flight plan allows it to be recalled when needed in the field, ensure repeated flights acquire comparable sUAS images and to monitor the progress of the sUAS image collection during the flight. Figures 8 a-b illustrate the use of Map Pilot to develop a flight plan for the UGarden study plot. Figure 9 shows the settings in Map Pilot including the altitude, resolution, the maximum speed, predicted flight duration and storage space.

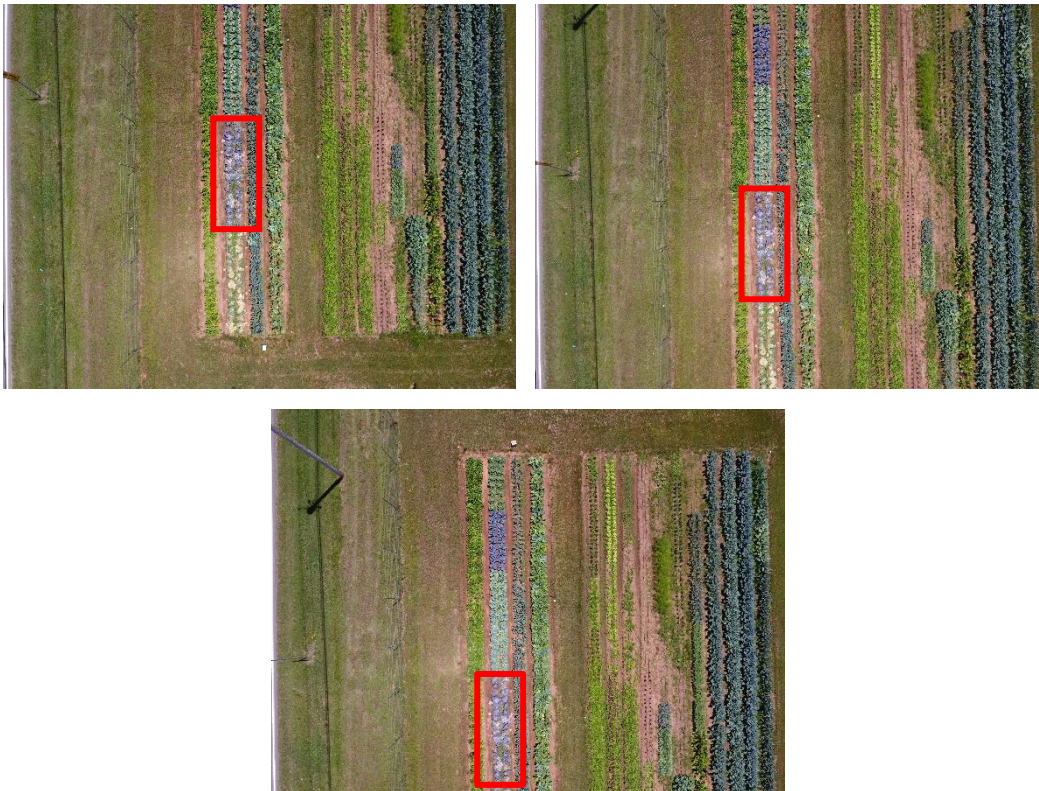


Figure 7: Sequential sUAS acquired imagery. The red box highlights the different placement in the images of the same cabbage patch during flight progression.



Figure 8 a-b: Map Pilot screenshots of UGarden flight plan (a) lengthwise flight lines and (b) widthwise flight lines of the field create a grid pattern when combined for multiple perspectives for optimal 3D models.

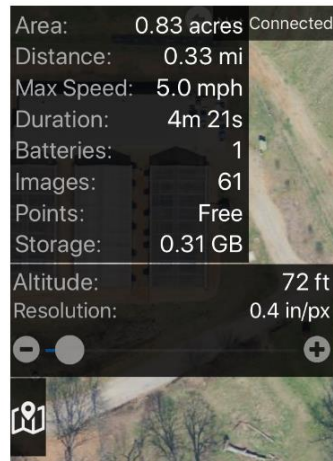


Figure 9: Map Pilot's flight plan information, including distance covered, estimated flight time and altitude.

The UGArden flight plan encompassed four plowed beds (Figure 10), with a focus on the 31 x 6 m bed highlighted in red in Figure 11. This bed consisted of 4 rows, each measuring about 1 meter in width with space on either side of each row for walking.



Figure 10: Aerial view of UGArden study site on March 19, 2019.



Figure 11: Aerial view of UGarden study site, with targeted bed outlined in red.

These garden rows included three different varieties of *brassica oleracea* of different shapes to compare the quality of derived 3D models and the accuracy of measurements made from the models. *Brassicas* (commonly known as cruciferous vegetables) are a genus of plants in the family Brassicaceae. While wild weed species exist, many cultivated varieties are important agricultural crops, including cabbages, broccoli, cauliflower, kale, kohlrabi and Brussels sprouts. Monitored varieties were 1) collard greens, which, at maturity have a cylindrical shape and large flat leaves; 2) kale, also of a cylindrical shape at maturity, but with thinner, more textured leaves that curl; and 3) cabbage, which has large, flat and broad leaves with the spheroid shaped cabbage head in the center of the plant at maturity (Figure 12a-c). The fourth row contained mustard greens, but they were not selected for this study due to time constraints required for field measurements and their finely dissected leaves.

Five sUAS flights of the UGarden study plot were conducted from March 19, 2019 to May 14, 2019 and spaced apart in time in approximately 2-week intervals (Table 2). The flights provided imagery needed to explore the temporal scale (i.e., frequency and timing of sUAS image acquisition) necessary for deriving accurate and efficient 3D model results from the photogrammetric analysis. The five flights occurred at an altitude of 22 m (72 feet), with the camera at nadir, in order to achieve a desired image pixel size of 1 cm (.4 inch) and to accommodate for the heights of powerlines and trees surrounding the field. Although flight plans were intended to be reused for all flights this did not happen. The 1st flight date had a flight plan (Flight Plan A) that was not able to be retrieved and a second flight plan was created for the 2nd and 3rd flight (Flight Plan B). Improvements on the flight plan were made by decreasing the size of the bounding box and leaving out extraneous

areas on the 4th flight were reused for the 5th flight (Flight Plan C) in an attempt to reduce data volume (see Table 2).



Figure 12 a-c: The three monitored varieties of crops as imaged from the ground on April 30, 2019 (a) collards (b) kale (c) cabbage.

The greater number of images acquired, the increase in total data storage needed. Though this creates large amounts of data, investment in external hard drives to save the collected images in a second location is imperative. These are the raw data sets and irreplaceable if lost. Data corruption or damage does occur, and it is necessary to have images saved in multiple locations. The five sUAS flights range of 160 – 205 images per date (See Table 2). The flight plan in Map Pilot used downloaded imagery of the area in advance of going to the gardens to fly the UAS in case cell phone coverage or internet connection was not available in the field. In addition to the straight flight lines following the length of the field, a second flight path was created to cover the field in straight flight lines going widthwise. Combined, the flight lines provide a grid pattern with adequate angles, coverage and photos to create 3D models (See Figure 8a-b).

Table 2: UGArden sUAS flight dates and data sizes.

Date	Number of Images	Flight Plan	Height	Total Image File Size	Individual Image File Size Range (MB)	File Type
03/19	172	A	22 -m	864 MB	4.81 – 5.56	.JPG
04/02	204	B	22 -m	1.03 GB	4.62 – 5.98	.JPG
04/16	205	B	22 -m	1.81 GB	4.66 – 5.62	.JPG
04/30	160	C	22 -m	842 MB	4.66 – 6.01	.JPG
05/14	164	C	22 -m	847.3 MB	4.64 – 5.56	.JPG

These large volumes of data are saved on the camera memory card within the sUAS. Imagery was then uploaded directly onto a computer used for processing (Dell OptiPlex 9020) from the memory card. Alternately, the images were uploaded onto a different computer and shared with the author via Google drop box in a zip file that was downloaded onto the computer. Separate folders were created for each flight date to store images in. These folders are backed-up on two external hard drives that reside in separate locations.

One flight date occurred at the Center for Research and Education at Wormsloe (CREW) on September 10, 2019. This flight used a DJI Mavic Air quadcopter with a 12-megapixel camera, acquiring a still image size of 4056 x 3040 and was flown at a height of 12 m (40 feet), with the camera at nadir. It was flown manually (due to the small area of coverage) using an iPhone 8 plus using the DJI GO 4.0 downloadable app. The targeted crops were: 1) heirloom pepper plants (Figure 13a-c) growing in a raised bed of mixed soils and organic fertilizers within beds approximately 6.16 m long, 1.45 m wide and .568 m high; and 2) heirloom okra planted directly in the plowed, coastal soil (Figure 14a-c). The pepper plant structure is bushy, with a growth range from about .66 m – 1.5 m in height with dense, thin leaves susceptible to movement in light breezes and the peppers visually standing out due to their bright, red color. The okra grew sparsely, with the plants being very tall (1 to 2 meters in height) and spindly, with small, sparse leaves. The pepper plants were in a raised bed garden located at the southern end of the property. The okra plants were in a garden plot at the northern end of the property.



Figure 13 a-c: Images of pepper plants at Wormsloe (a) aerial overview of raised bed garden, pepper plants outlined in red (b) ground image of pepper plants (c) pepper fruit.



Figure 14 a-c: Images of Wormsloe CREW okra garden (a) aerial overview of garden plot (b) ground image of okra (c) okra fruit.

Ground Control Points

Permanent markers serving as ground control points (GCPs) were anchored into the field site at UGArden for the duration of the project, (Figure 15) in order to overlay and ensure alignment and registration between the processed temporal data sets and maximize the accuracy of change analysis. Ground control points are needed to georegister the time series of dense 3D point clouds in order to correctly measure changes in the plant heights. The eight installed GCPs consisted of rebar pieces 61 cm in length hammered into the ground in March. 10 cm of the rebar remained above ground and were capped with orange rebar safety caps (Figure 16) to distinguish them from the vegetation. Multiple precautions were taken to ensure that GCPs were stable and securely located. At UGArden, they were placed at the edges of the fields and within the rows, where little to no interference would occur – (i.e., farm equipment would not be close to crops). At my request, the farm manager informed her crew of the placements of the targets and marked them with pink flags so they would not be disturbed or damaged by mowing or other equipment. During the different flights, it was apparent that the UGArden crew mowed around the targets. The grass growing within a radius of approximately 0.3 m around the individual targets was taller than the surrounding mowed areas. Before each flight, I checked each GCP and pulled out the grass/weeds adjacent to it to prevent tall grass from obscuring the GCPs in the sUAS images. I also ensured each orange rebar cap laid flat and was not askew.

GCPs were not used in the CREW gardens, as flying was a one-time occurrence and images would not need to be registered to each other. The structure of the raised bed provided corners and edges visible in the sUAS images that could be used to measure the

pepper plant heights. The okra garden was surrounded by a fence and fence posts visible in the images could be used as GCPs if desired.



Figure 15: The locations of the 8 ground control points are marked with yellow circles and blue flags in this orthomosaic of the UGarden study area.



Figure 16: One of the ground control points at UGArden.

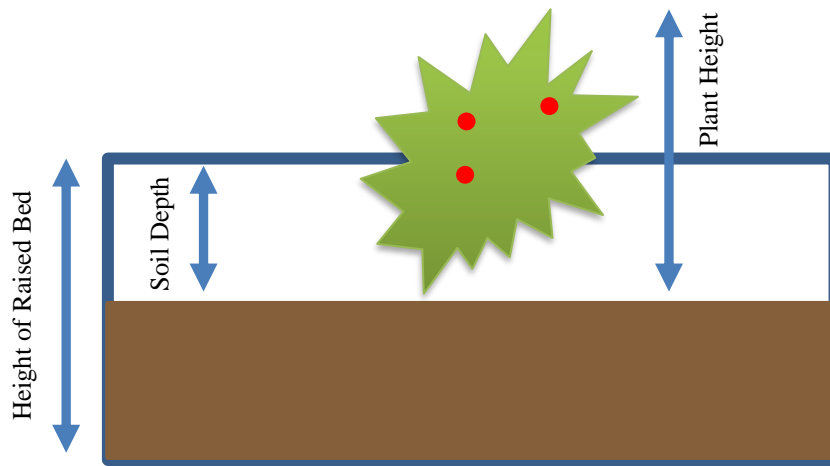
Field Measurement of Plant Heights

For accuracy assessment and validation of the plant measurements derived from the CSMs, field measurements of individual plant heights in the focus beds were taken within one day of the flights at UGArden. Height measurements were taken from the ground to the top of the plant using a measuring tape and recorded to the nearest cm (Figure 17a). The same plants were measured and recorded each time the sUAS was flown, in order to have comparable data. For example, if plant number 27 in the row was measured following the first flight, it would be measured for the duration of the study. Recorded measurements were then transferred to an Excel spreadsheet. At UGArden, the heights of collard, kale and cabbage plants were measured. These garden plants represent different growth forms and were selected to assess the relative accuracy of plant heights from the created 3D models.



Figure 17 a-b: Measuring plant heights for validation at (a) UGarden and (b) Wormsloe CREW.

At CREW, the heights of pepper plants were measured to the nearest cm. The monitored pepper plants were in a raised bed as depicted in Figure 17b. The height of the box, the average soil depth (from top of box to soil) and plant heights (from top of plant to soil) were measured with measuring tape and recorded. To compare these measurements in the dense cloud model, where the soil was not visible, the height of the box was added to the plant height and then the average soil depth was subtracted (Figure 18). These garden plants represent different growth forms and were selected to assess the relative accuracy of height in the created models.



$$\text{Measurable Model Height} = (\text{Height of Raised Bed}) + (\text{Plant Height}) - (\text{Soil Depth})$$

Figure 18: Visual diagram depicting how pepper plant model heights were calculated.

Aerial Image Processing and Structure from Motion to Create Orthoimages and 3D Models

The imagery was processed with Agisoft Metashape Professional software to perform Structure from Motion photogrammetry to perform multi-image matching and the creation of an image mosaic and 3D point cloud to derive a seamless orthoimage, a digital elevation model (DEM) and 3D models for each date of sUAS image acquisition (Figure 19a-c). From these products, the calculated crop surface model (CSM) enabled the plant heights to be measured and growth rates to be determined by subtracting the CSM from the DEM (CSM-DEM). The pixel size of orthoimages derived from images flown at 22 m (72 feet) is less than one cm spatial resolution (ranging from 7.6 to 8.8 mm) and the post spacing of the resulting DEMs and CSMs were approximately 3 cm (Table 3). The file sizes of the Metashape outputs are large and range from 2.5 – 3.42 GB of needed storage

space. This data should be saved in multiple locations, regardless of the file size. It can be reconstructed from the sUAS images if data is lost but would be an unnecessary use of time.

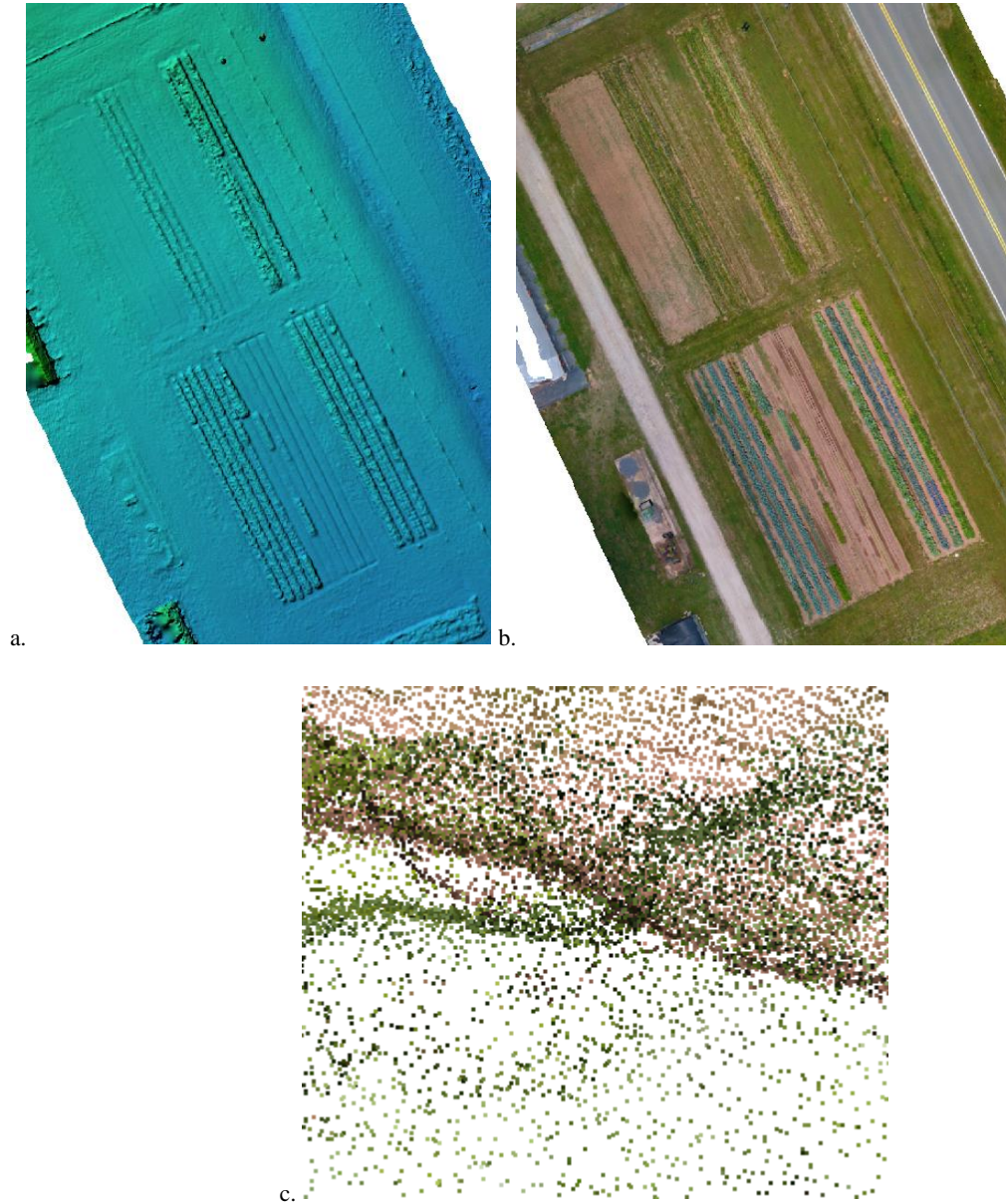


Figure 19 a-c: Examples of SfM product: (a) DEM (b) orthomosaic of images (c) dense point cloud.

Table 3: Agisoft Metashape information for flights at UGArden.

Date (2019)	Images Used	Tie Points	Dense cloud points	DSM Size	DSM Resolution (cm/pix)	Orthomosaic Resolution (mm/pix)	Orthomosaic Size	File Size (GB)
3/19	172/172	184,734	12,834,120	5,297 x 6,312	3.03	7.57	15,884 x 19,832	2.89
4/02	203/204	167,998	9,081,387	4,405 x 5,295	3.3	8.26	13,824 x 17,033	3.16
4/16	204/205	181,343	8,094,004	3,621 x 4,640	3.24	8.11	12,468 x 16,128	3.42
4/30	160/160	120,132	6,876,609	3,707 x 4,650	3.52	8.81	11,442 x 15,088	2.5
5/14	163/164	124,502	7,165,621	3,591 x 4,524	3.47	8.68	11,554 x 15,100	2.65

The same methodology was used at Wormsloe CREW to process imagery with the results depicted in Table 4. Okra is excluded from the rest of the study due to the software's inability to create an accurate model of it. Many of the okra plants captured in the sUAS images failed to appear in the model.

It is interesting to note that while the same settings in the program are used and it is imaging the same area each time, the data volume and resolutions differ. Even on datasets such as 4/30/19 and 5/14/19 which used the same flight plan, the resolutions of the orthomosaic and DSM still differ (possibly due to a slight increase in photos or differences in individual file sizes). Though 5/14/19 only uses 3 more images than 4/30/19 it was able to find over 4,000 more tie points in the first step of SfM and almost 290,000 more dense cloud points. Perhaps the imagery was of higher quality in 5/14/19 or contained image blurring in 4/30/19.

Table 4: Wormsloe CREW imagery processing information in Agisoft Metashape.

Date (2019)	Images Used	Tie Points	Dense cloud points	DSM Size	DSM Resolution (mm/pix)	Orthomosaic Resolution (mm/pix)	Orthomosaic Size	File Size (GB)
9/10	91/91	96,660	4,837,562	2772 x 2782	8.98	2.25	11,085 x 11,125	1.8

Digital images in .JPG file format were uploaded from the sUAS camera memory card to the computer and maintained in separate folders by date and flight height. Image file sizes have slight variation, generally ranging from just under 5 MB to 6 MB (See Table 2). Next, images from the flight were input into Agisoft Metashape Professional (Figure 20). The first step, photo alignment (Figure 21), is performed with a setting of “high quality” and a sparse 3D point cloud is created from the tie points. A dense point cloud using “medium quality” and “mild depth filtering” (Figures 22a-d) is then created. “Mild depth filtering” is the recommended setting for distinguishing finely detailed features in the images, such as plant leaves (Agisoft Metashape 2019). A 3D-tiled model (Figures 23 a-c, Figure 24) is then created from the dense point cloud, followed by a DEM if the field is bare of plants or a DSM once plants are growing. An additional final product is an orthomosaic image. The orthomosaic image is valuable because it is the photographs stitched together and geometrically corrected. Torres-Sánchez et al. (2014) used the orthomosaics to successfully map the vegetation indices of wheat and recommends their methods for even small field monitoring. Because distortions have been corrected, it can be used to make real world distance measurements. It is also the most visually stunning of the produced products and is useful as a promotional tool.

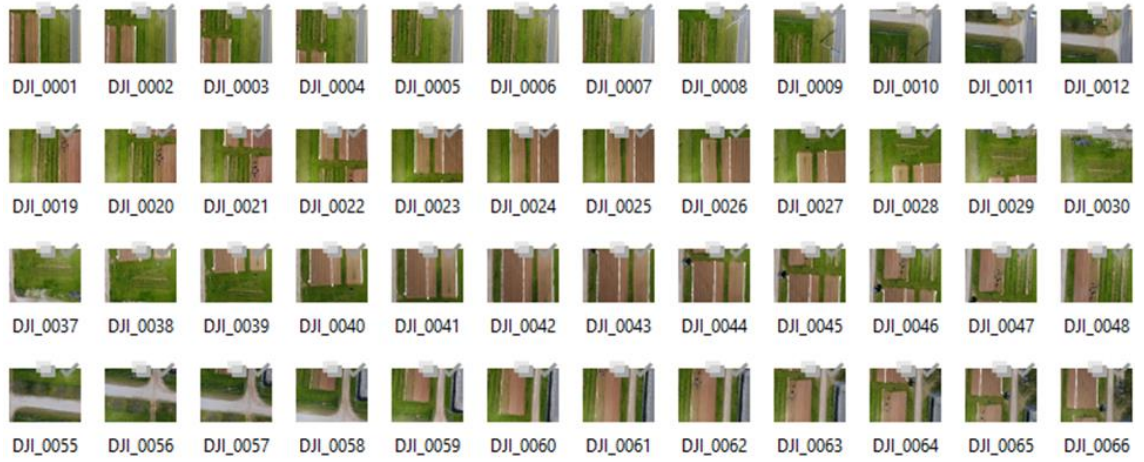


Figure 20: sUAS imagery to be input into Agisoft Metashape for processing.

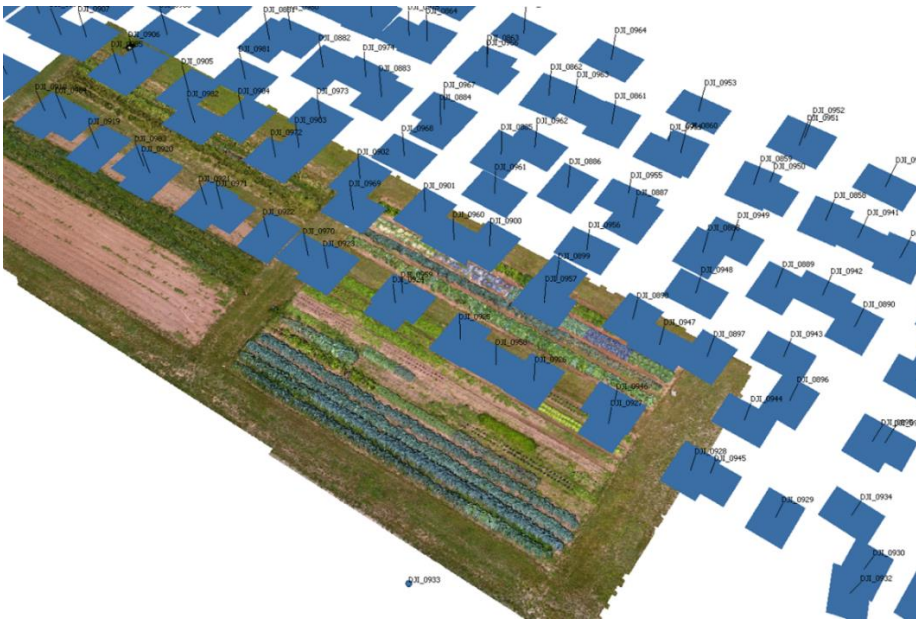


Figure 21: Location of sUAS photos and their alignment along flight lines to cover the study area plot at UGArden.

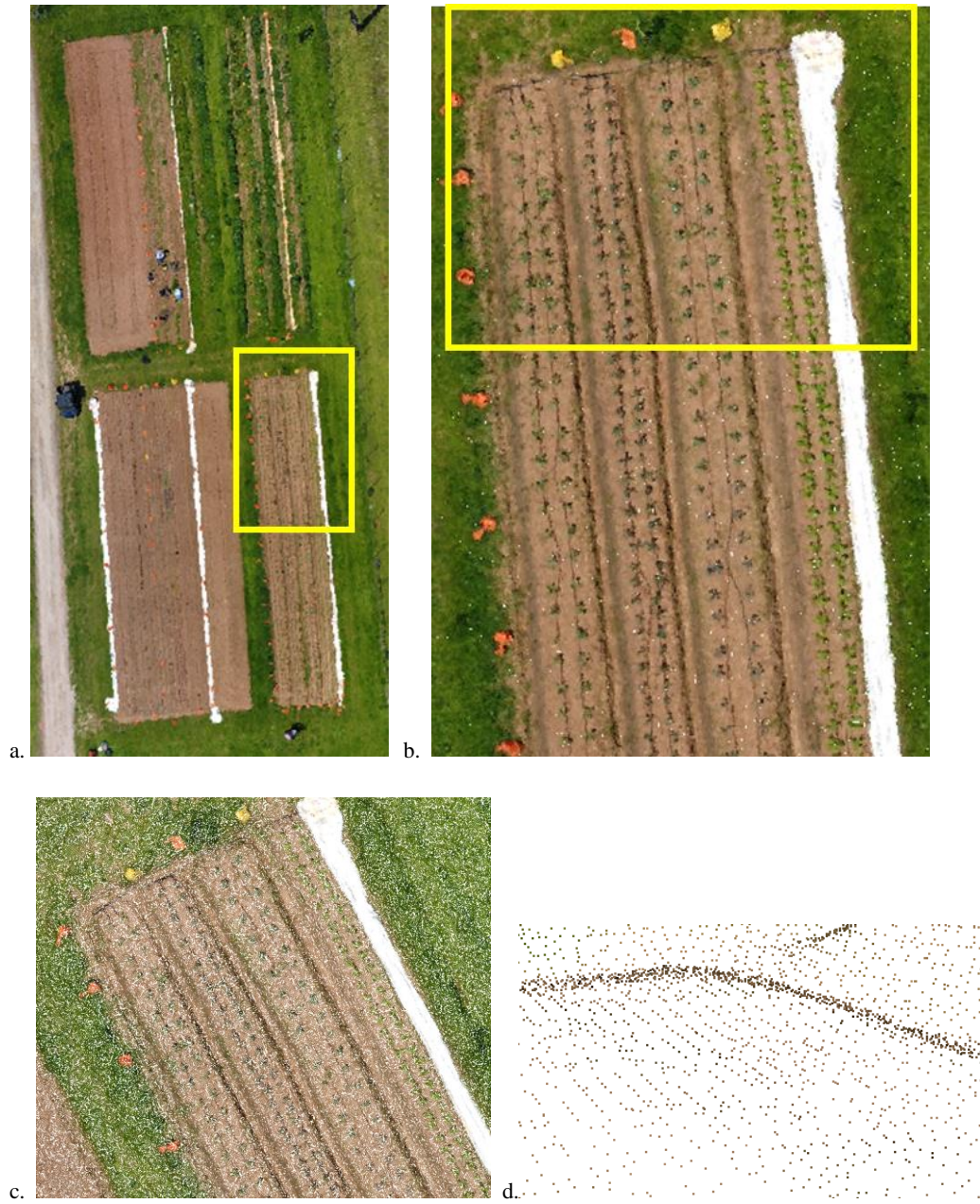


Figure 22 a-d: 3D dense point cloud from furthest distance (a) to closest (d).



a.



b.



c.



d.

Figure 23 a-d: Derived from the 4/16/2019 flight (a) Agisoft Metashape tiled model – images draped over the dense point cloud which creates CSM. Magnified view of (b) collards (c) kale (d) cabbage.



Figure 24: 3D model of raised bed gardens at Wormsloe CREW. Pepper plants are outlined in red.

CHAPTER 4

RESULTS

3D Model Processing

Once sUAS imagery was collected for both sites, I conducted the SfM processing to create 3D models of the vegetable crops grown at both research sites. Agisoft Metashape Professional software was utilized to process the overlapping imagery captured by the sUAS at UGarden and the gardens on the CREW campus. Because SfM processing is complex and often requires multiple hours to complete multiple image point matching and creation of 3D point clouds, different settings were explored in Agisoft Metashape to reduce the processing time. For example, processing for the first set of images was initially set to “high accuracy” at the dense cloud processing stage. The program was set to run overnight yet had crashed and did not produce a dense cloud. Using all the same parameters except setting the accuracy to “medium”, the results were processed in just a few hours and provided excellent clarity and detail. An example of the basic settings followed for output is featured in Figure 25. During different stages of processing (i.e., the creation of the tiled model and DEM), a region can be selected to ignore extraneous images or points to speed up the processing. For example, users can select the areas containing just the fields and target beds in the dense cloud and exclude features such as surrounding pathways and buildings. Unfortunately, this is not able to be done during batch processing. Batch processing allows the program to run continuously with the settings pre-selected and automatically saving the files after each step. It allows the user to run the program overnight

or for long periods of time without any additional input from the user. Imagery from April 2, 2019 was processed using batch processing and took 2 hours, 34 minutes and 11 seconds. When it was processed with only the fields of study selected after the creation of the dense cloud, it took 2 hours, 15 minutes and 25 seconds, a decrease of approximately 20 minutes.

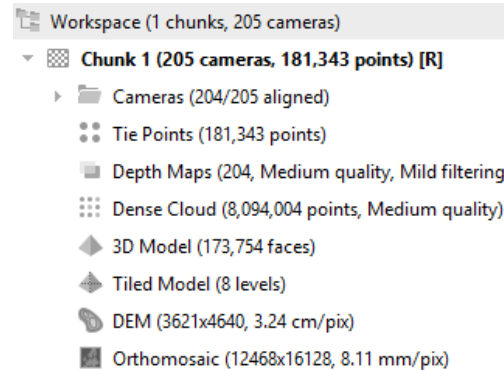


Figure 25: Example of processing steps and parameters in Agisoft Metashape from April 16, 2019 flight imagery.

Table 5 and Table 6 present the various processing times for the different data sets in Agisoft Metashape, showing the variation that can occur for the different amount of input images. Fewer input images did not always mean less total time. The image data set from 3/19/19 was the fastest processing data set but had more images than data sets for 4/30/19 and 5/14/19. The most time-consuming step is the creation of the depth maps and the dense cloud, which are produced at the same time. This is the step where the software is searching for and identifying more matches between the already aligned images to reconstruct scene geometry.

Table 5: UGArden flight dates with processing time in Agisoft Metashape (time abbreviated as hour:minutes:seconds).

Date	Tie Point Matching	Tie Point Alignment	Depth Maps	Dense cloud	3D Model	Tiled Model	DSM	Ortho-mosaic	Total
3/19/19	0:8:25	0:1:17	0:58:13	0:4:24	0:0:27	0:20:31	0:0:24	0:5:5	1:37:51
4/02/19	0:9:52	0:1:9	1:51:0	0:9:22	0:0:17	0:17:22	0:0:14	0:4:55	2:34:11
4/16/19	0:9:5	0:2:20	1:58:0	0:20:16	0:0:8	0:15:59	0:0:11	0:5:7	2:51:6
4/30/19	0:7:17	0:1:32	1:48:0	0:9:44	0:0:15	0:14:33	0:0:11	0:4:13	2:25:45
5/14/19	0:7:32	0:2:37	1:36:0	0:9:46	0:0:12	0:13:13	0:0:9	0:3:58	2:13:27

Table 6: Wormsloe garden imagery with processing time in Agisoft Metashape (time abbreviated as minutes:seconds).

Date	Tie Point Matching	Tie Point Alignment	Depth Maps	Dense cloud	3D Model	Tiled Model	DSM	Ortho-mosaic	Total
9/10/19	3:53	0:41	25:9	6:47	0:8	12:3	0:5	3:10	52:11

Plant Structure Estimation and Validation

To assess the growth of the crops over the growing season, each CSM was subtracted from the DEM to calculate height and monitor the plant growth. To do so, the CSM time series must be registered in the x, y and z directions. Due to the lower ability of the sUAS inertial measurement unit (IMU) to accurately record true above ground height of the sensor during image acquisition, inconsistencies arose in the 3D coordinates of the derived 3D cloud points. Although the x, y coordinates were more accurate in the models (i.e., in the range of a few cm) the z or approximate elevation values ranged from a perceived above ground level of 71 m at the lowest point for the March 19, 2019 flight to 175 m at the lowest point for the May 14, 2019 flight. This variation is depicted in Figure 26. Further actions, therefore, were required to align the datasets, in order to measure crop growth.

The solution to misregistration of the time-series of 3D models involved multiple steps. The orthomosaic from the first flight on March 19, 2019 was exported as a .tiff from Agisoft Metashape in NAD 83 (2007)/UTM Zone 17N and imported into ArcGIS Pro

where the x, y coordinates of the 8 GCPs were recorded in a .txt file. The file consisted of four columns containing the point number, the recorded x and y coordinates and the z coordinates. All 8 GCP z values were set to 0 in order to georegister the datasets to each other in the program QTModeler (Table 7).

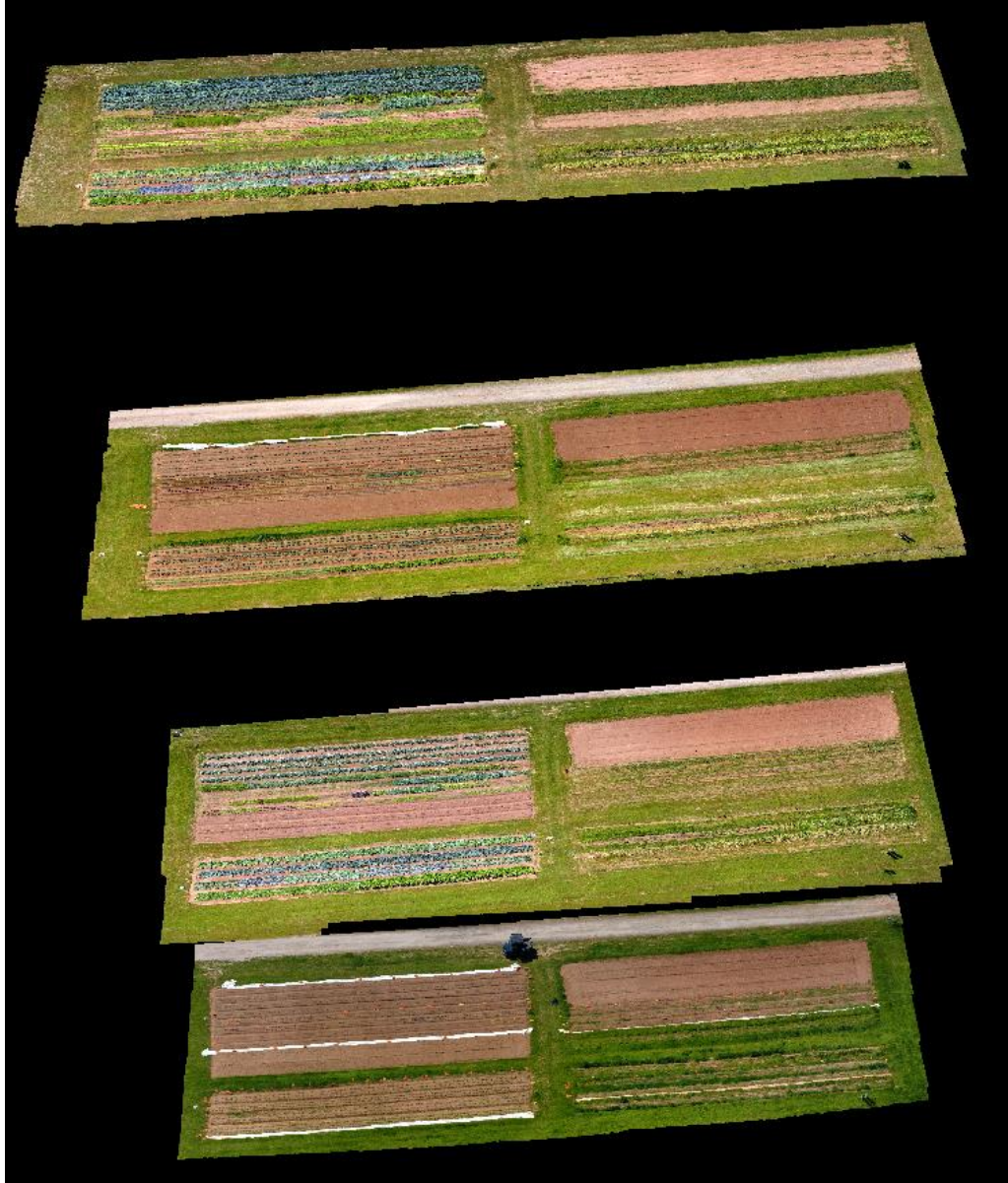


Figure 26: Models prior to georegistration (presented in QTModeler), illustrating the variation in z values.

Table 7: Ground Control Point coordinates and point number used to georegister models.

GCP	X	Y	Z
1	280596.8458	3753830.6678	0
2	280616.8252	3753840.0230	0
3	280610.0370	3753821.5330	0
4	280618.6308	3753821.7654	0
5	280612.1954	3753799.5401	0
6	280629.5310	3753793.6315	0
7	280625.2108	3753771.3139	0
8	280645.2278	3753780.1539	0

From Agisoft Metashape, the dense point cloud was exported as a .las file and imported into QTModeler. Using the georegister model function in QTModeler, each data set was georegistered by manually applying the recorded coordinates to the GCPs (see Table 7). The Root Mean Square Error (RMSE) after georegistration of the x, y, z coordinates of each data set are recorded in Table 8, showing the average offset of the different datasets. The z values have a noticeably higher mean, but that is due to the large difference in z elevations within the models.

Table 8: Calculated RMSE and mean x, y, z from the 8 GCPs after georegistration in QTModeler.

Flight Date	Mean X (m)	Mean Y (m)	Mean Z (m)	Roll (deg)	Pitch (deg)	Heading (deg)	RMSE (m)
3/19/2019	1.06	0.40	-74.50	-0.619	-0.581	-0.057	0.164
4/02/2019	-0.78	-1.71	-142.99	-2.684	1.240	-0.112	0.151
4/16/2019	-0.12	-1.64	-107.92	-2.114	0.147	-0.211	0.165
4/30/2019	0.35	-1.46	-106.10	-1.113	-0.436	-0.258	0.276
5/14/2019	-0.50	-0.57	-177.77	-1.778	1.270	-0.182	0.151
Mean of All Dates	0.002	-0.996	-121.856	-1.6616	0.328	-0.164	0.1814

A bare earth digital elevation model (DEM) can be made by flying imagery and creating a 3D model before crops emerge. If that imagery is unable to be captured due to

time constraints, an interpolated bare earth DEM may be created using the surrounding earth or dense cloud ground points between crops. In the case of this research, the first data collection flight on 3/19/2019 contained small seedlings. Since the leaves did not obscure the soil, ground points were easily measured and used to compute a bare earth model. As all the crops were transplanted, however, measuring the soil after transplanting would account for some soil disturbance. The crop surface model (CSM), depicts a continuous surface of the tops of the crops and can be used to measure the plant height of the crops using the profile analysis tool in QTModeler (Figure 27). In this study, each plant that had the field measurements recorded, was marked with a marker denoting the plant number in QTModeler (See Figure 27). Next, the profile analysis tool was drawn across each plant and the maximum height recorded in Excel. As the profile analysis tool measures the point cloud, a buffer was set at .03 m on either side of the drawn line, in order to capture and record the highest point of the plant (Figure 28).

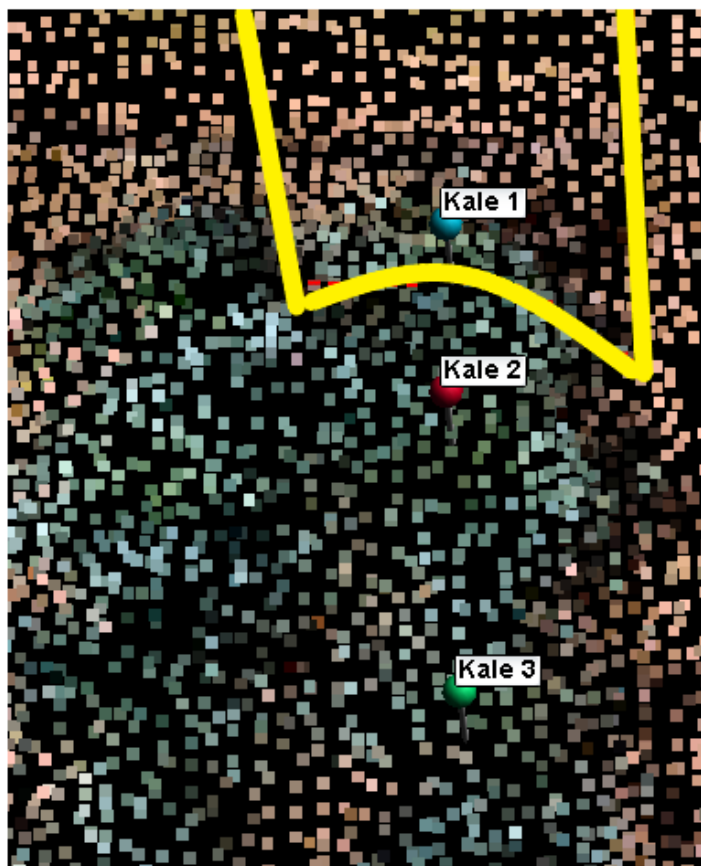


Figure 27: Example of profile analysis tool (in yellow) in QTModeler, over kale plant 1.

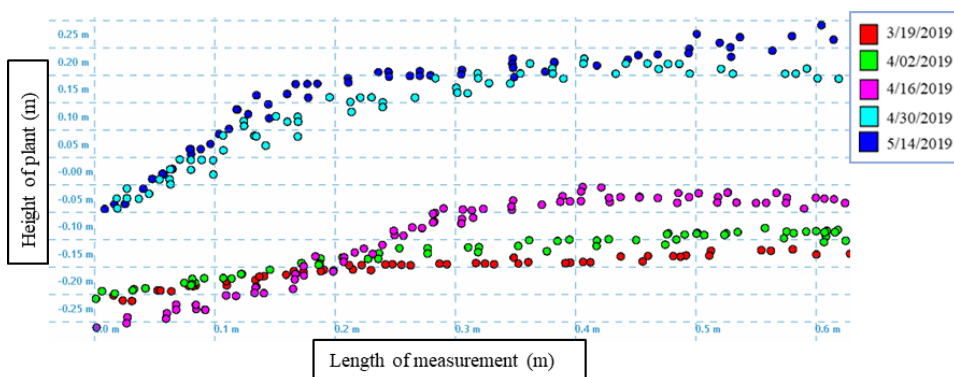


Figure 28: Example of profile analysis tool output, depicting sample heights in the UGarden datasets.

Calculating the measurements of the same plants from the different dates of CSM data sets allows for the quantification of change in plant growth. Subtracting the CSM by

the DEM will give the plant growth, height and a volume estimation ($\text{CSM} - \text{DEM} = \text{Plant Height}$). Subtracting an earlier CSM from a later CSM will also provide the plant growth between those two dates.

Results of Actual Field Measured Heights and Modeled CSM-DEM Plant Heights

Tables 9-12 depict the four crop types that were validated by hand measurements in the field and produced measurable 3D models. Results from the tables show an increase in plant height over time. The percent error illustrates how much the 3D model over- or under-estimated the height of the plant compared to the actual field measurements. The pepper plants in the raised beds obtained the greatest height and the largest range for both the actual heights and those measured within the model. At maturity, cabbage obtained the shortest height and smallest range. These two crop types, cabbage and peppers, though vastly different in height, growth form and leaf structure, had the two most accurate datasets. The pepper plants exhibited a strong linear correlation ($R^2=.99$) and a low average percent error (3.4%). The final temporal dataset for cabbage also had a strong linear correlation ($R^2=.61$) and a low average percent error (-.08%). During the first two flights, before the plants reached maturity, all three crop types at UGarden performed with extremely low accuracy (high percent error and low linear correlation).

Cabbage from 4/30/2019 performed the most accurately out of the temporal UGarden models, with strong linear correlation of an R^2 of .6129 and an average percent error of 0.08% underestimation. This range of error is small - underestimating by 3 cm or overestimating by 2.7 cm or -.12 – .15% percent error. In other words, the accuracy of estimated height measurements from the 3D models of cabbage were relatively consistent once the crop had reached maturity. Interestingly, the maximum height of cabbage never

exceeded 23.3 cm in this study, shorter than any of the measured collard and kale plants at maturation, yet the accuracy of the measurements from 3D models was lower for collard and kale plants. Cabbage has a more homogeneous canopy structure and this may be a possible influence on the higher accuracy of the 3D model at maturity. This indicates there are multiple factors that affect the accuracy of model measurement beyond plant height. The growth form, (i.e., plant structure, leaf types, stem heights....) may also be important. The growth form of cabbage is more compact and spherical in shape, with low growing broad leaves surrounding the cabbage head. This form appears to be more resistant to disturbance by slight breezes. This reduces the chance of image blurring during data collection, leading to greater accuracy in SfM point matching and creation of 3D models. This differs from collards and kale plants, which grow taller and have leaves that are more susceptible to breezes.

Pepper plants at Wormsloe were the tallest plants observed (all are over 88 cm) and had the largest range in actual plant heights (1 m). The model consistently overestimated the heights; with an average percent error of +3.41% and a small percent error range of +.19 – 7.9% (.17 to 9.9 cm). This plant is taller, denser and of a different growth type than the observed *brassicas* at UGArden. It should be noted that the peppers were observed on only one occasion because results from the UGArden study indicated the most accurate plant models were obtained later in the growing season when plants had reached their maximum heights and densities.

Table 9: Collards - actual field measured heights (cm) and model measured heights (cm) according to flight date.

Date	Field Min Ht	Field Max Ht	Field Range	Field Mean Ht	Model Min Ht	Model Max Ht	Model Range	Model Mean Ht	RMSE	R ²	Avg % Error
03/19	4.4	13.0	8.6	10.15	0.9	3.1	2.2	1.71	8.73	0.1253	-82.29
04/02	11.5	17.3	5.8	14.56	1.6	7	5.4	4.77	9.94	0.1933	-67.37
04/16	25.4	40.2	14.8	30.44	7.8	19.3	11.5	14.14	16.51	0.5899	-53.76
04/30	31.2	49.4	18.1	37.88	22	39	17	31.51	7.91	0.2739	-16.52
05/14	35.7	54.6	19.0	41.72	22.4	42.4	20	33.19	9.48	0.5632	-20.21

Table 10: Kale - actual field measured heights (cm) and model measured heights (cm) according to flight date.

Date	Field Min Ht	Field Max Ht	Field Range	Field Mean Ht	Model Min Ht	Model Max Ht	Model Range	Model Mean Ht	RMSE	R ²	Avg % Error
03/19	8.2	14	5.8	10.99	0.5	2.9	2.4	1.60	9.57	0.0121	-85.24
04/02	11.7	17.6	5.9	14.53	2.6	8.3	5.7	4.66	10.11	0.0022	-67.58
04/16	25.6	40.8	15.2	33.05	7.0	26.9	19.9	18.12	15.91	0.0861	-44.94
04/30	27.2	45.9	18.7	36.49	18.1	40.5	22.4	31.64	7.84	0.3097	-13.28
05/14	33.2	51.0	17.8	43.1	20	35.6	15.6	26.71	6.61	0.5355	-12.64

Table 11: Cabbage - actual field measured heights (cm) and model measured heights (cm) according to flight date.

Date	Field Min Ht	Field Max Ht	Field Range	Field Mean Ht	Model Min Ht	Model Max Ht	Model Range	Model Mean Ht	RMSE	R ²	Avg % Error
03/19	8.1	11	2.9	9.74	1.2	2.8	1.6	1.81	7.99	0.0003	-81.26
04/02	9.8	13.4	3.6	11.9	3.6	6.3	2.7	5.12	6.823	0.0829	-56.72
04/16	15.1	23.6	8.5	20.2	2.7	7.6	4.9	6.38	13.95	0.5128	-68.65
04/30	15.8	24.3	8.5	21.7	16	23.3	7.3	21.57	1.48	0.6129	-.08

Table 12: Peppers - actual field measured heights (cm) and model measured heights (cm) according to flight date.

Date	Field Min Ht	Field Max Ht	Field Range	Field Mean Ht	Model Min Ht	Model Max Ht	Model Range	Model Mean Ht	RMSE	R ²	Avg % Error
09/10	83.6	179.3	90.7	133.33	88.78	188.80	100.02	138.33	6.5	.9923	3.41

Of the four crop types observed, the final temporal dataset of cabbage at UGarden and the pepper plant model at Wormsloe CREW performed the most accurately, with the highest linear correlation, $R^2 = .56$ and $.99$ and lowest percent error $-.08\%$ and 3.4% ,

respectively (See Tables 11 – 12). Generally, the taller the plant within a specific crop type (corresponding to a later growth stage), the higher the accuracy of model heights compared to true plant height. The models for kale, cabbage and collards performed differently regarding percent error, range of percent error and correlation even if the individual crop type models are compared from the same flight date. This indicates multiple variables such as the plant structure, height, density, growth form and canopy may affect the software's ability to accurately construct models.

In Figures (29 - 46) the graphs visualize the linear correlation and R^2 of the different crop types for the different dates. These correlations illustrate how the heights derived from the 3D models compare to the measured heights of the actual plants. The 3D models came closer to the actual height when the crops were at maturation. The highest correlation for collards, kale and cabbage all occur during their final flights or the most mature stage of the crop (5/14/2019 for collards and kale and 4/30/2019 for cabbage). Pepper plants had the highest correlation of any plant type. Graphs are depicted for the individual crop type on the individual date, to be able to compare them over time (See Figures 29 – 42). They are also presented on a graph that combines all the flight dates and samples for the individual crop type (See Figures 43 – 45). When all flight dates are combined for individual crop type, they exhibit stronger correlations for collards and kale, but as it is known that the models exhibit low accuracy in early temporal series, the results are presented by both individual flight date and by all flight dates combined. Pepper plants only had one flight date and therefore do not need to be combined (Figure 46).

An observed trend is the underestimation of true plant height occurring in the temporal UGarden models. All models exhibit complete underestimation in the first three times series (3/19/2019 – 4/16/2019) (see Tables 9-11), with collards exhibiting complete underestimation in all flights (3/19/2019 – 5/14/2019) (See Figures 29 - 33 and Table 9). Overestimation does occur for kale and cabbage, but only in the final times series (4/30/2019 for cabbage (See Figure 42) and 5/14/2019 for kale (See Figure 37)). For kale, this is a total of five samples ranging from 0.93 to 6.90 cm overestimation or 2.5 – 22.8% percent error. Cabbage exhibits overestimation in five samples in 4/30/2019 (the final model for cabbage, due to harvesting) ranging from 0.13 to 3 cm or 0.6 – 15.2% percent error. It appears that within some crop types, plants at maturation exhibit a mix of over and underestimation of true plant height within the 3D models. It should be considered that adjacent plants, including those across the row and not measured for validation may be taller than the measured sample. At maturity, leaves overlap and may hide a shorter plant.

The respective residuals are calculated by subtracting the model height from the actual height (actual height – model height = residual) and are shown for each flight date (See Figures 29 - 42 and Figure 46) and for the combined flight dates (See Figures 43 – 45). For collards, residuals are high with a large range for the first three flight dates (2.5 cm – 20 cm). When the collards are at maturity and most of the plants exceed 31 cm in height, there is greater variation within the residuals and some fall close to 0. The fourth flight shows 6 residuals with values of < 2 cm (Figures 32b – 33b), but only one sample in the final flight has a residual of < 2 cm. Similar to collards, the residuals for kale plants for the first three flights have a large range (5 cm – 28 cm) (Figures 34b – 36b) . The fourth flight depicts the kale model performing with higher accuracy as 8 of the samples have

residuals of < 4 cm (Figure 37b). The overall range for residuals decreases on the fifth flight, when the plant is at peak maturity, with no residual > 10 cm (Figure 38b). While both collards and kale show a range containing lower residuals in the final flight, there is still a large range for plants over 30 cm. Plants over 30 cm may have residuals of < 2 cm but some of the tallest plants have residuals of > 15 cm.

For cabbage plants, the residuals never exceed 10 cm for the first, second and fourth flights (Figures 39b, 40b, 42b). The third flight has the highest residual values of any of the cabbage models (Figure 41b), however, this model had previously shown extreme underestimation that was not expected. The fourth and final flight for cabbage shows the model performing with higher accuracy as no residual value exceeds ± 3 cm. Pepper plants (Figure 46b) show that the residuals for all samples are < 10 cm. Since 4 out of the 5 actual height samples exceed 1 m in height, 10 cm is a relatively low residual.

When the residuals are combined for all flight dates (Figures 43b – 45b), the inconsistent pattern of residuals is shown. For collards and kale, residuals are consistently high prior to approximately 30 cm in actual plant height. After a plant is 30 cm or greater in height, residual values are a mix of low and high values. For cabbage, there is no consistent pattern when the flight dates are combined, due to the similar actual heights of the final two flight dates, but large variation of residuals between those two flight dates.

Results of Modeled vs. Actual Plant Heights by Individual Flight Date for Collards

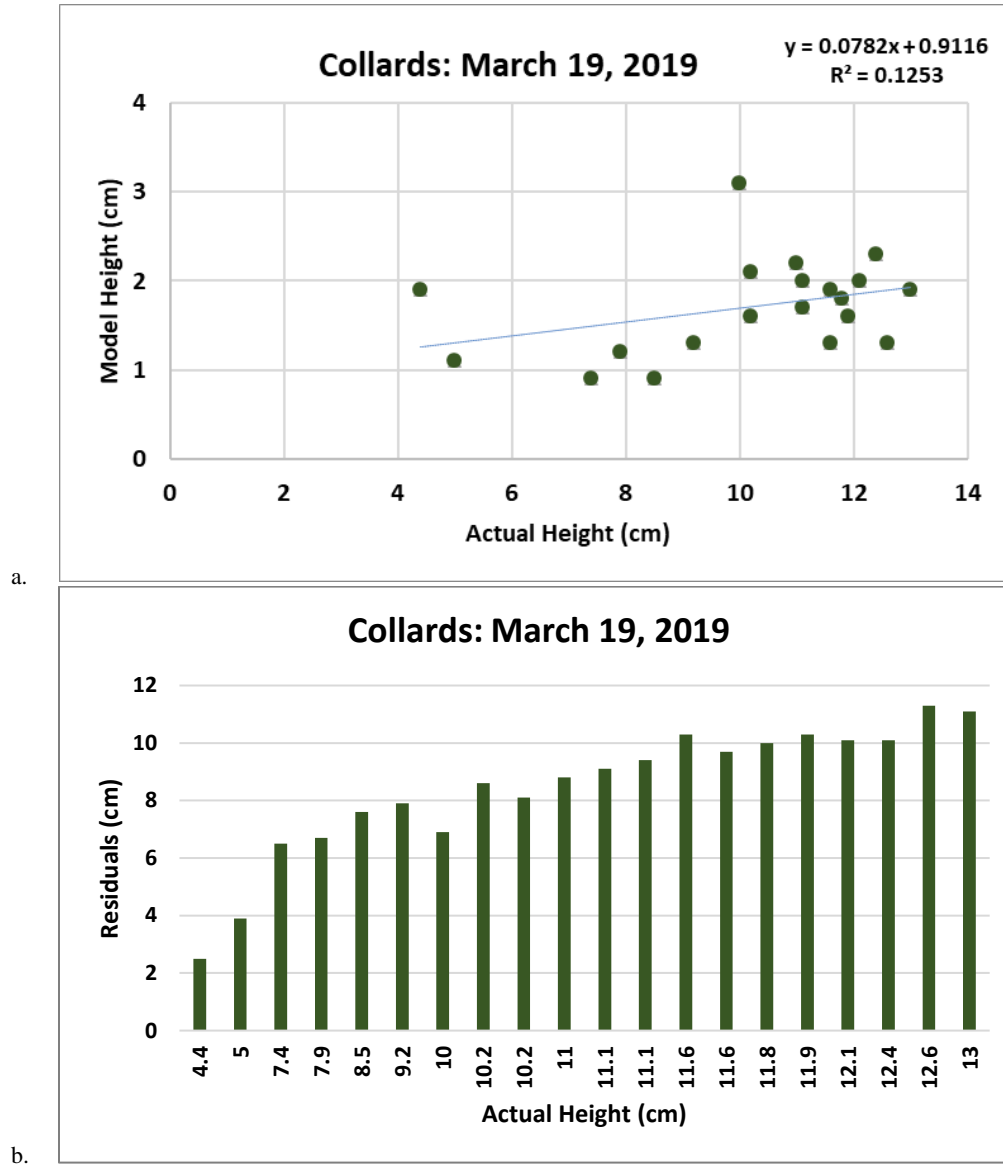
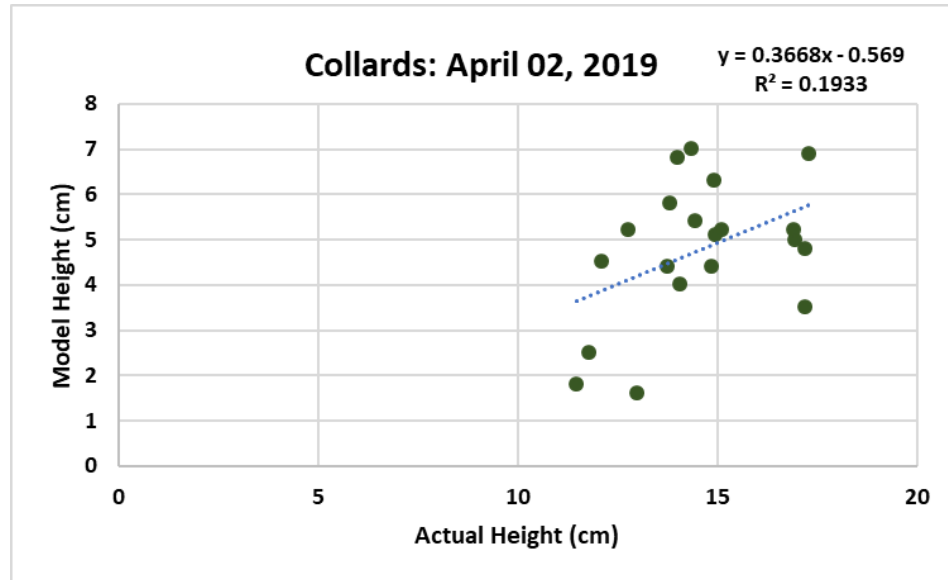
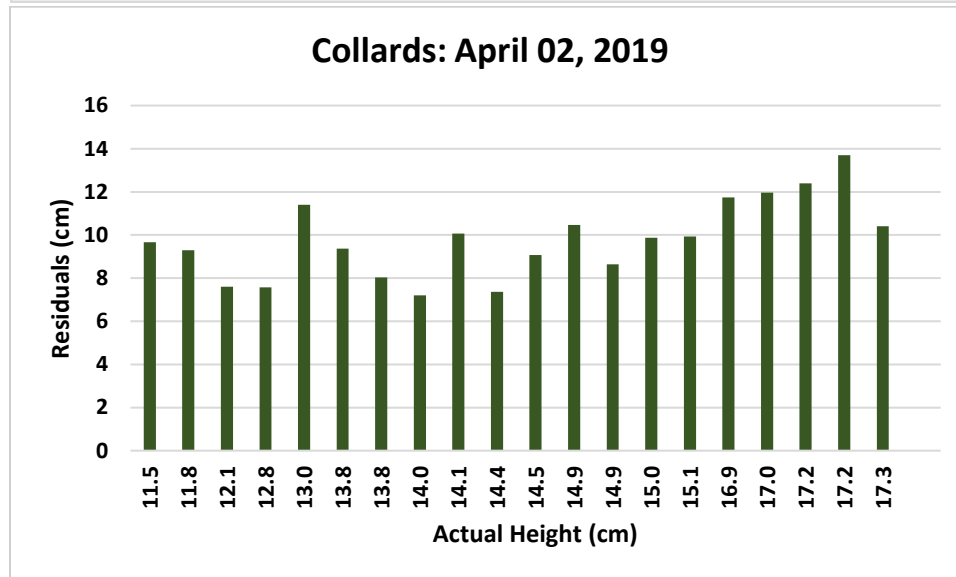


Figure 29 a-b: (a) Linear regression of modeled height to actual height of collards and (b) the respective residuals (3/19/2019).

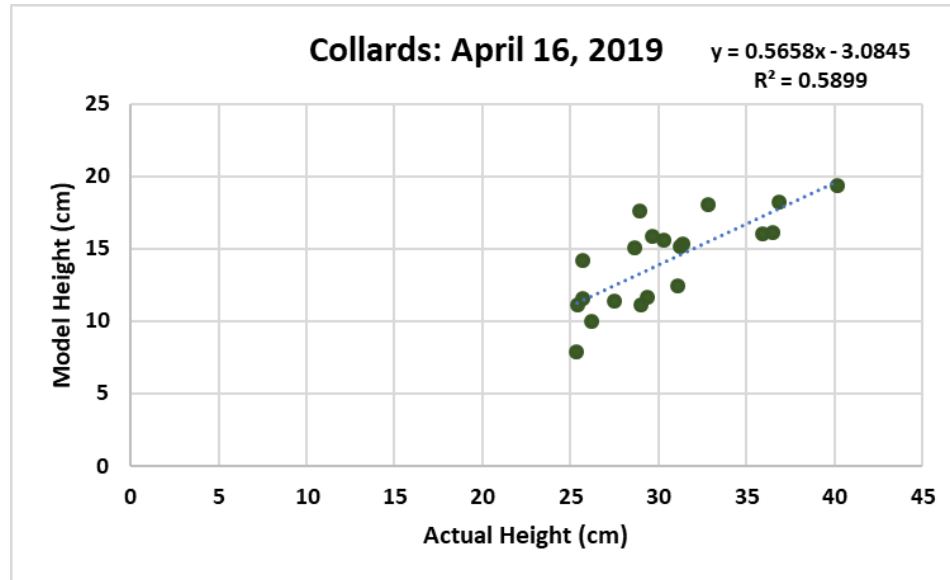


a.

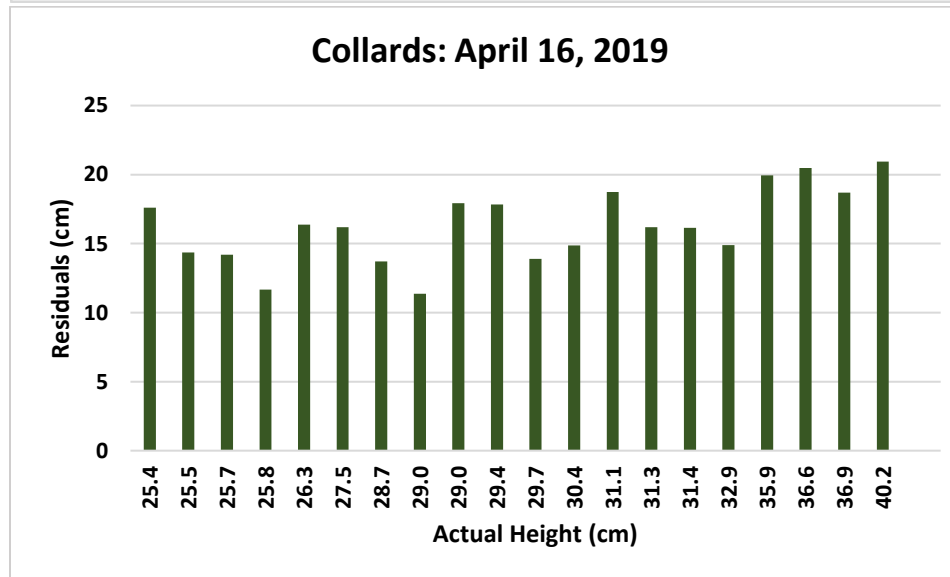


b.

Figure 30 a-b: (a) Linear regression of modeled height to actual height of collards and (b) the respective residuals (04/02/2019).

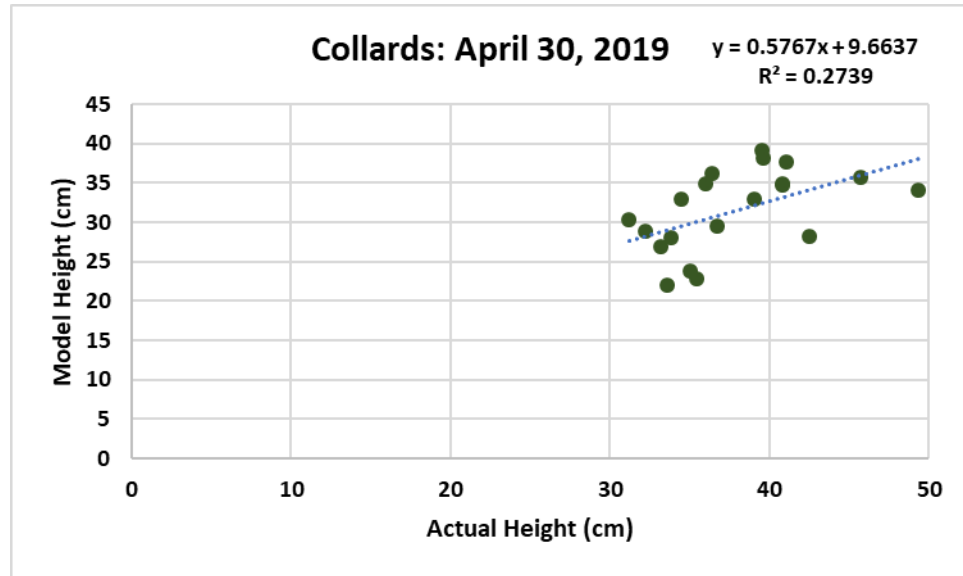


a.

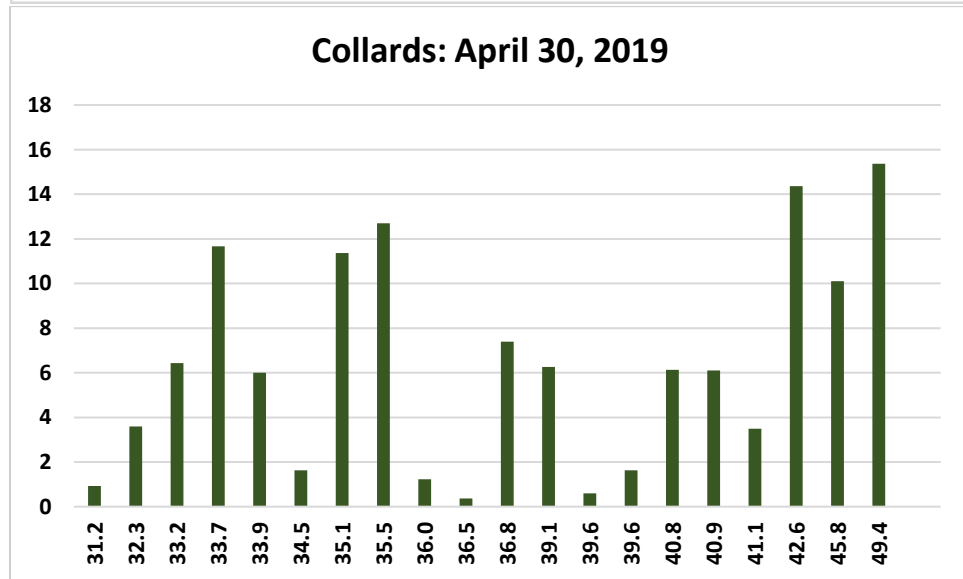


b.

Figure 31 a-b: (a) Linear regression of modeled height to actual height of collards and (b) the respective residuals (4/16/2019).

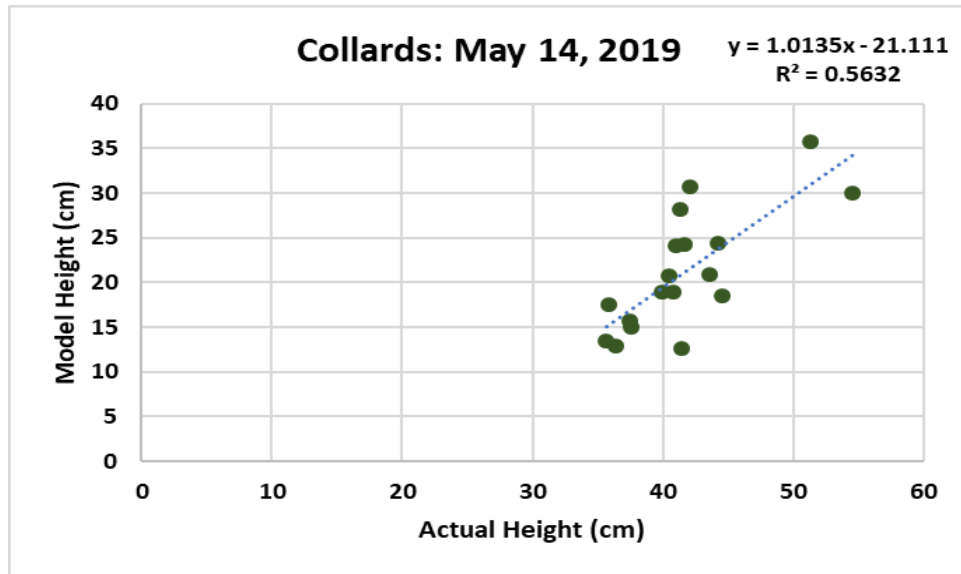


a.

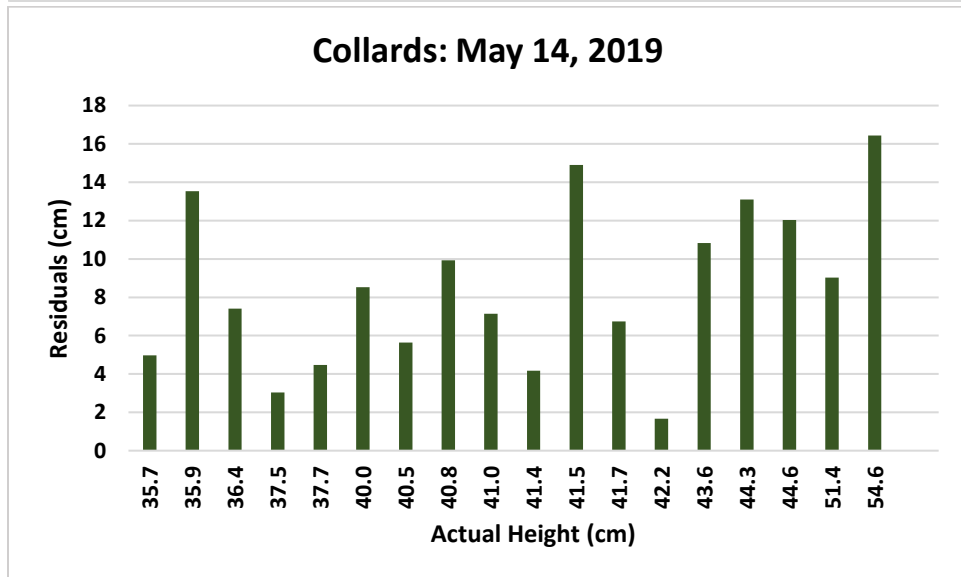


b.

Figure 32 a-b: (a) Linear regression of modeled height to actual height of collards and (b) the respective residuals (4/30/2019).



a.



b.

Figure 33 a-b: (a) Linear regression of modeled height to actual height of collards and (b) the respective residuals (5/14/2019).

Results of Modeled vs. Actual Plant Heights by Individual Flight Date for Kale

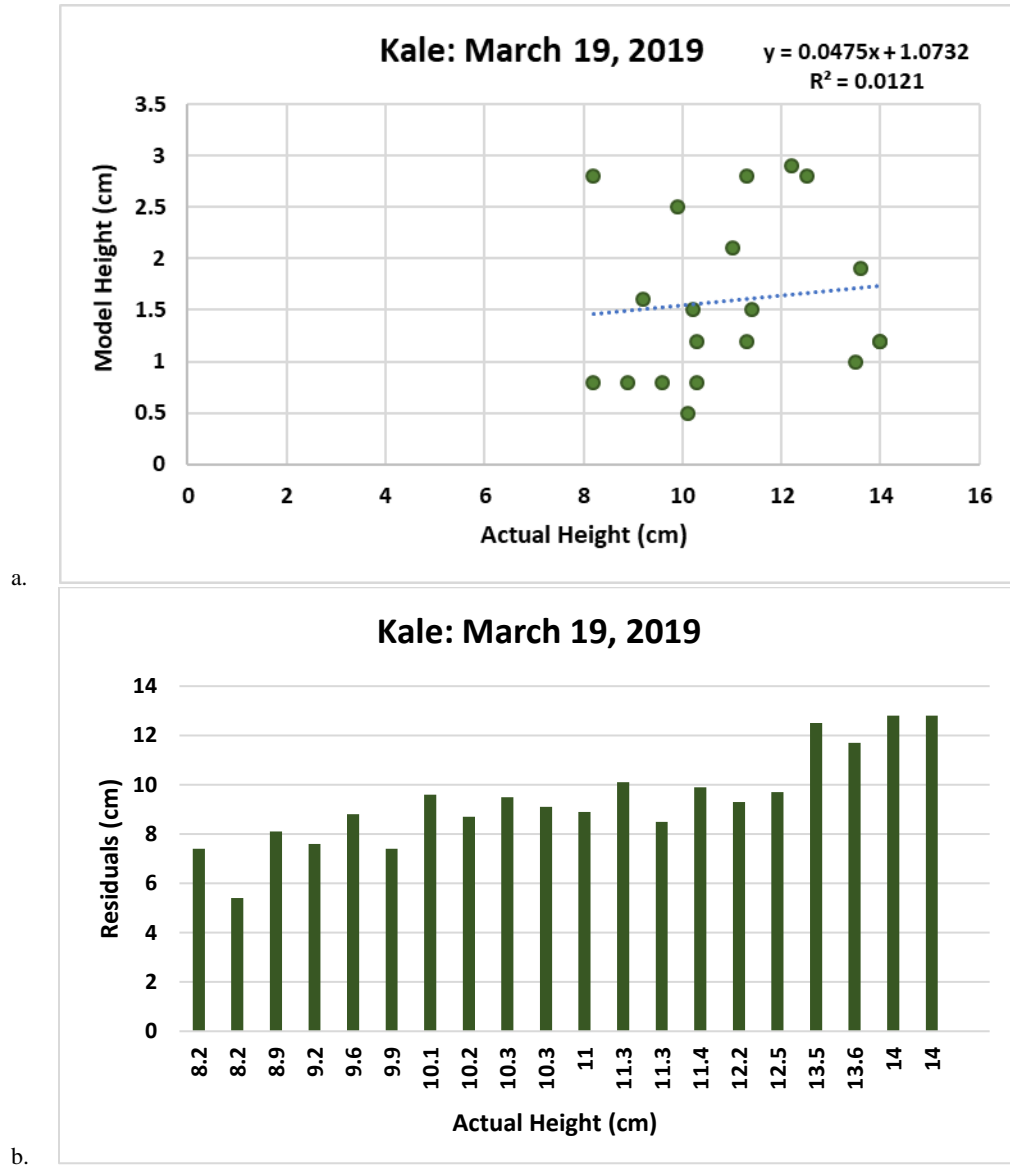
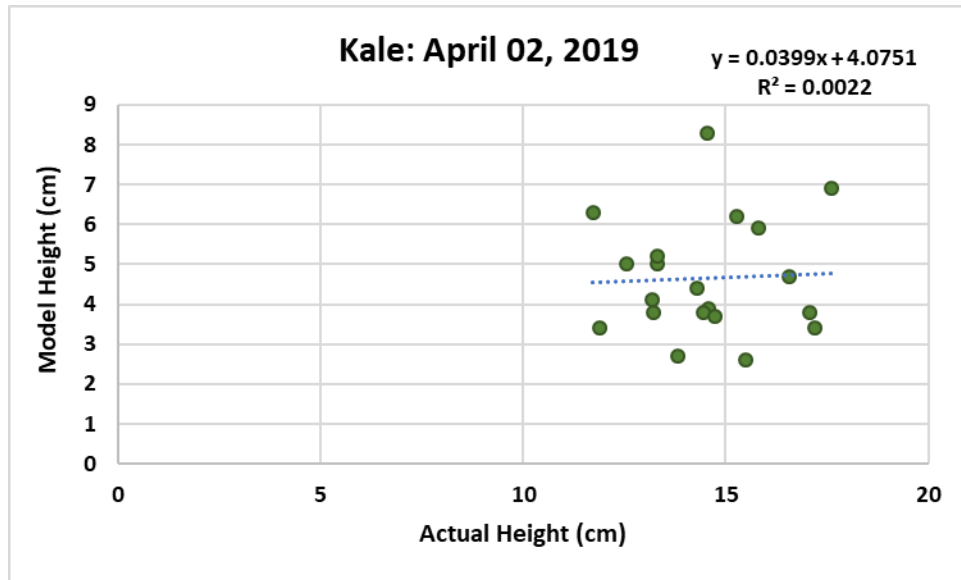
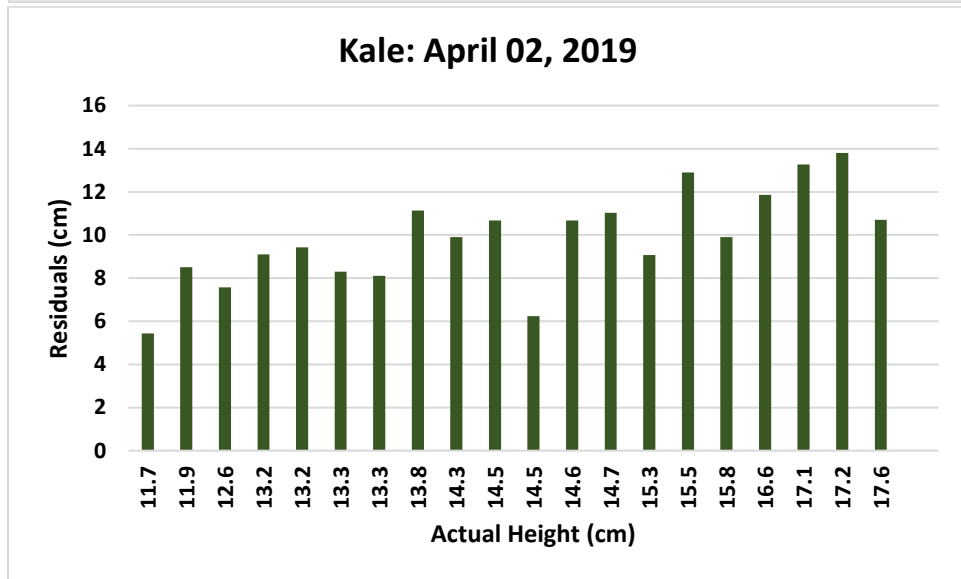


Figure 34 a-b: (a) Linear regression of modeled height to actual height of kale and (b) the respective residuals (3/19/2019).

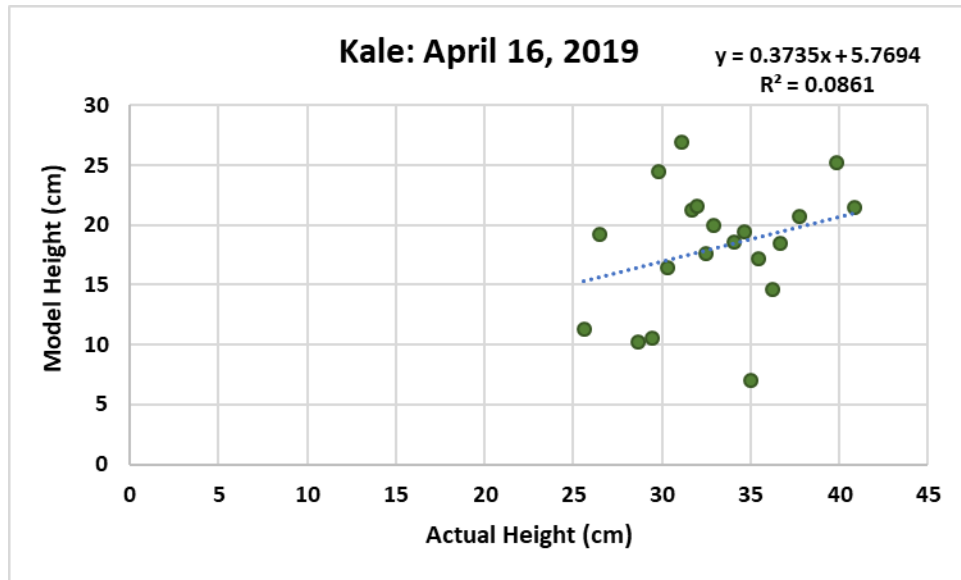


a.

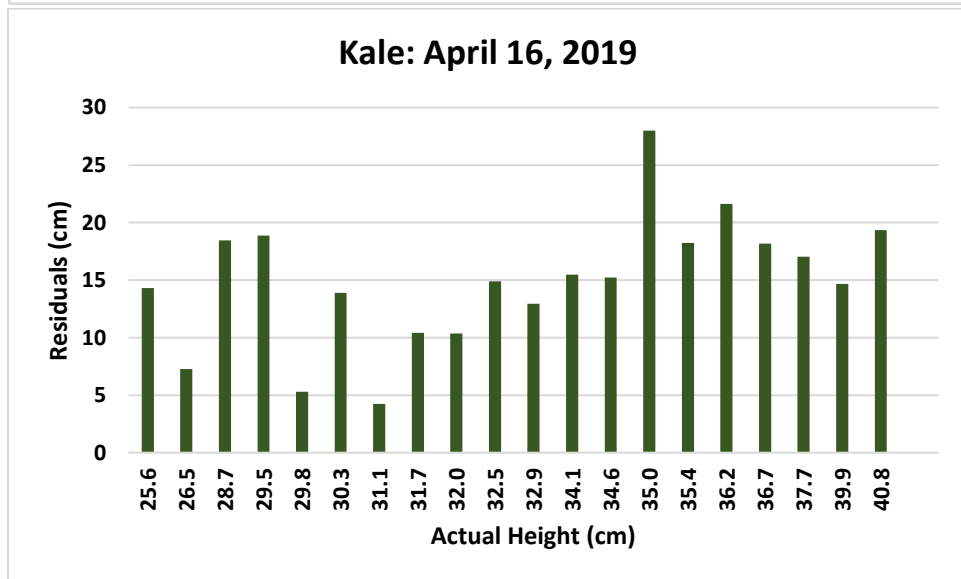


b.

Figure 35 a-b: (a) Linear regression of modeled height to actual height of kale and (b) the respective residuals (04/02/2019).

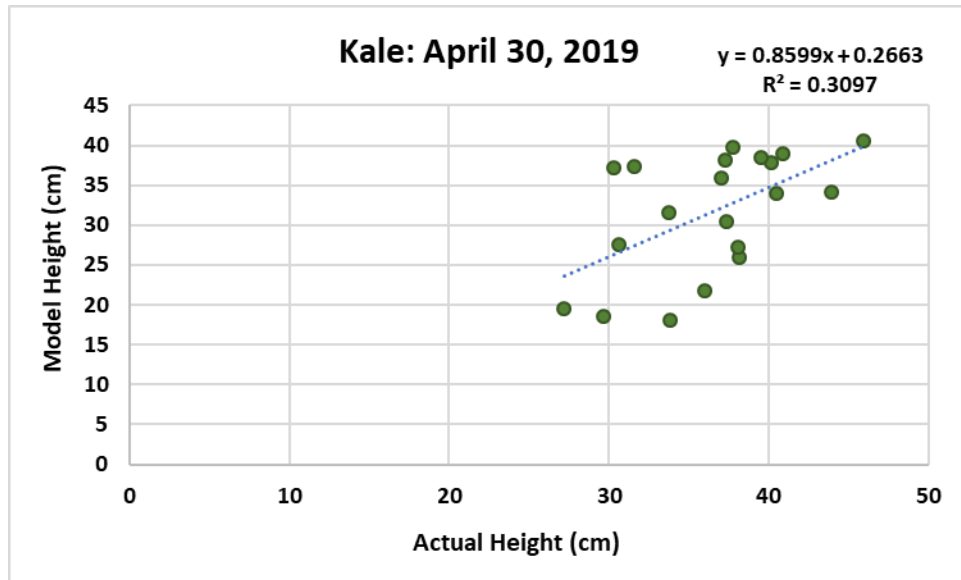


a.

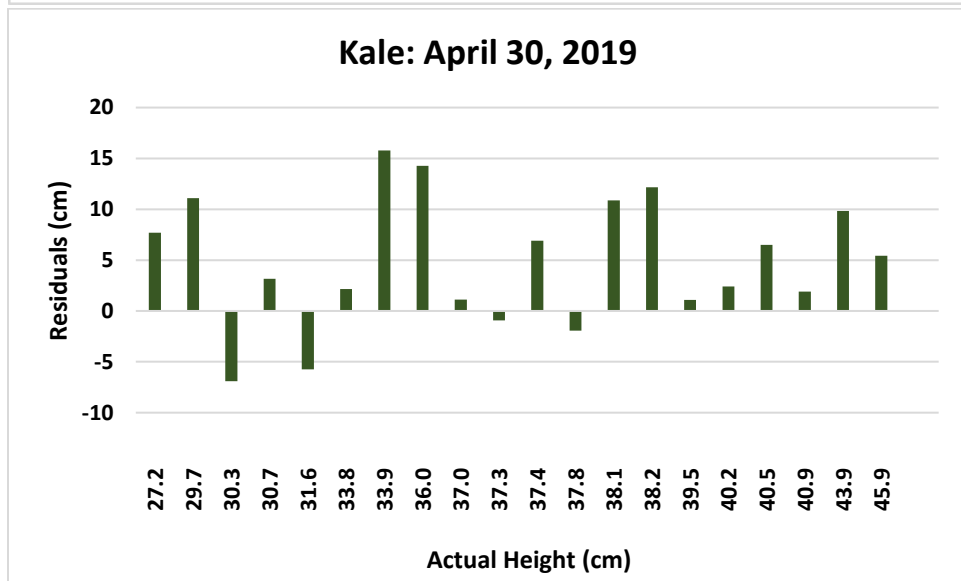


b.

Figure 36 a-b: (a) Linear regression of modeled height to actual height of kale and (b) the respective residuals (4/16/2019).

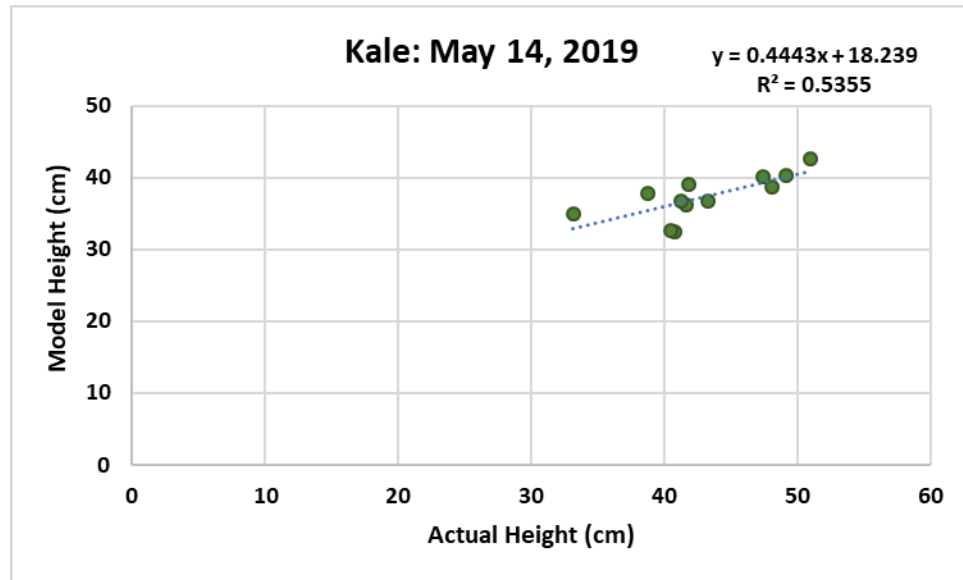


a.

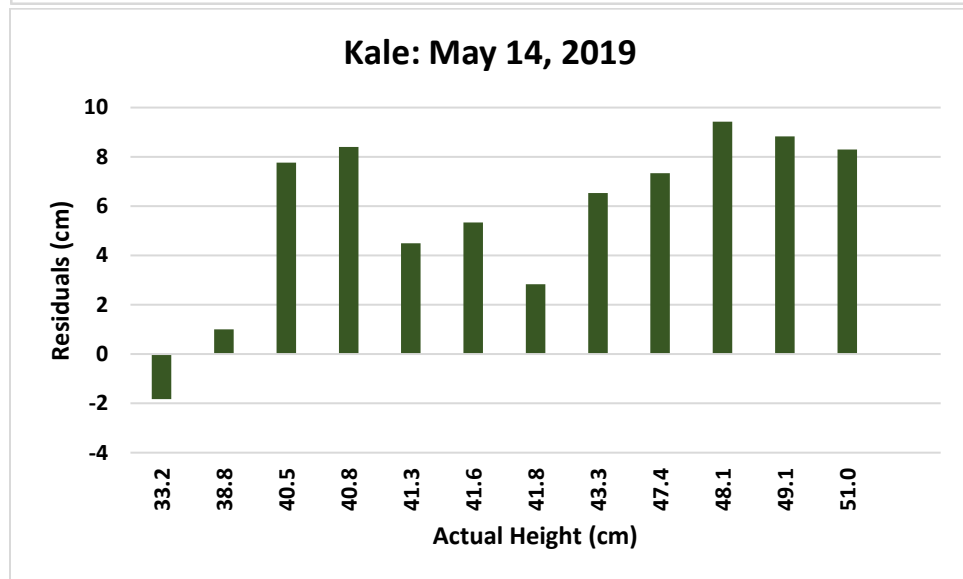


b.

Figure 37 a-b: (a) Linear regression of modeled height to actual height of kale and (b) the respective residuals (4/30/2019).



a.



b.

Figure 38 a-b: (a) Linear regression of modeled height to actual height of kale and (b) the respective residuals (5/14/2019).

Results of Modeled vs. Actual Plant Heights by Individual Flight Date for Cabbage

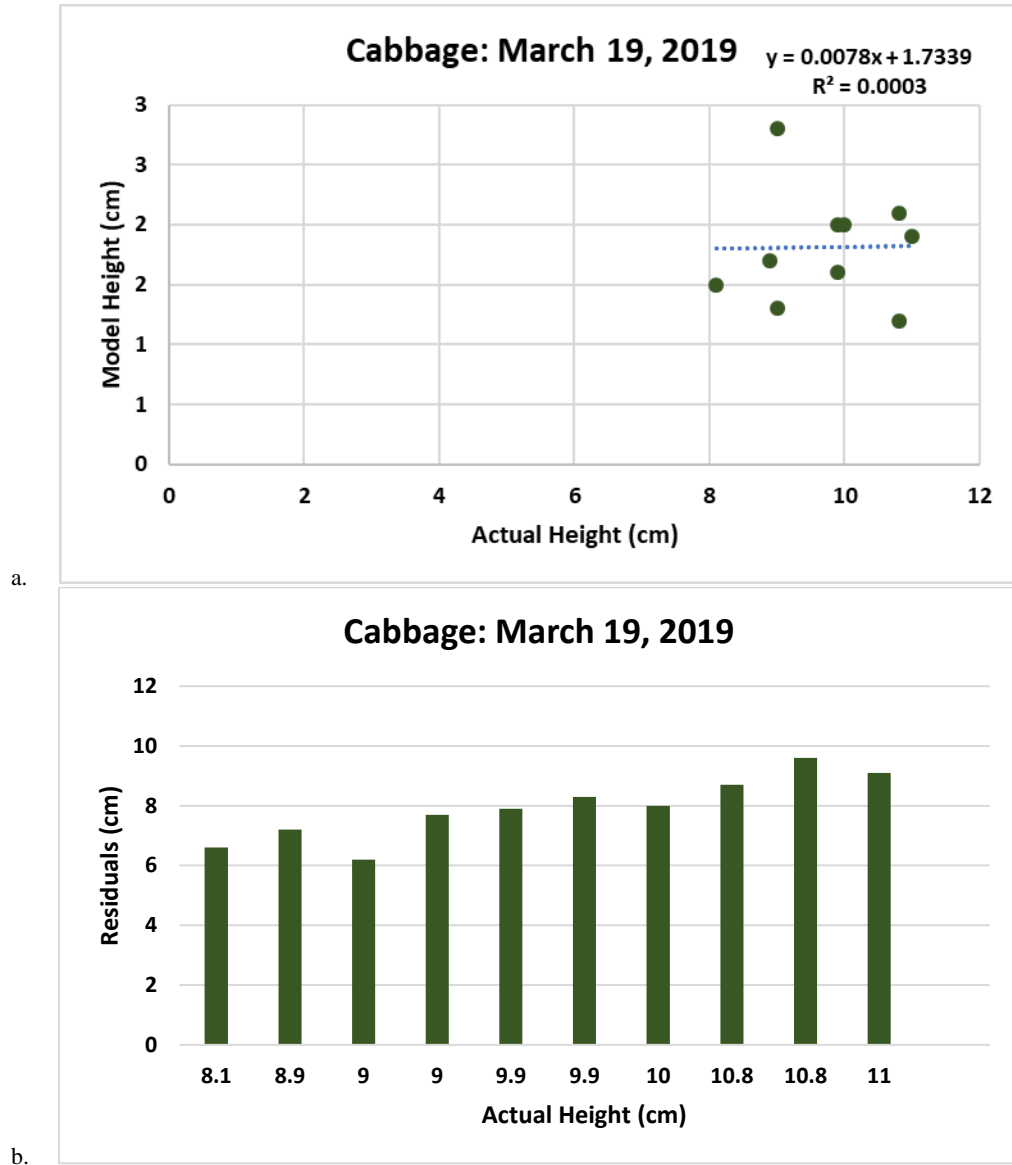
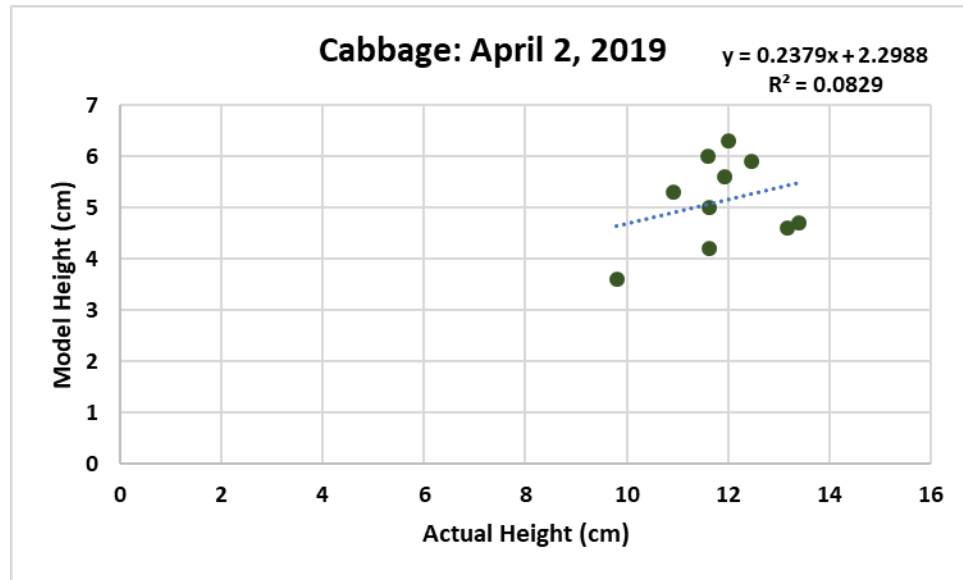
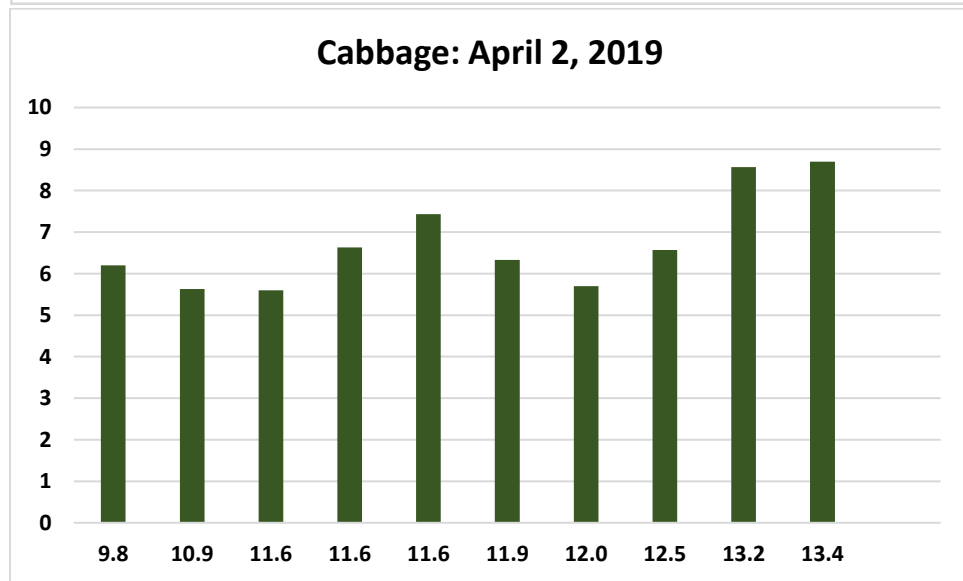


Figure 39 a-b: (a) Linear regression of modeled height to actual height of cabbage and (b) the respective residuals (3/19/2019).

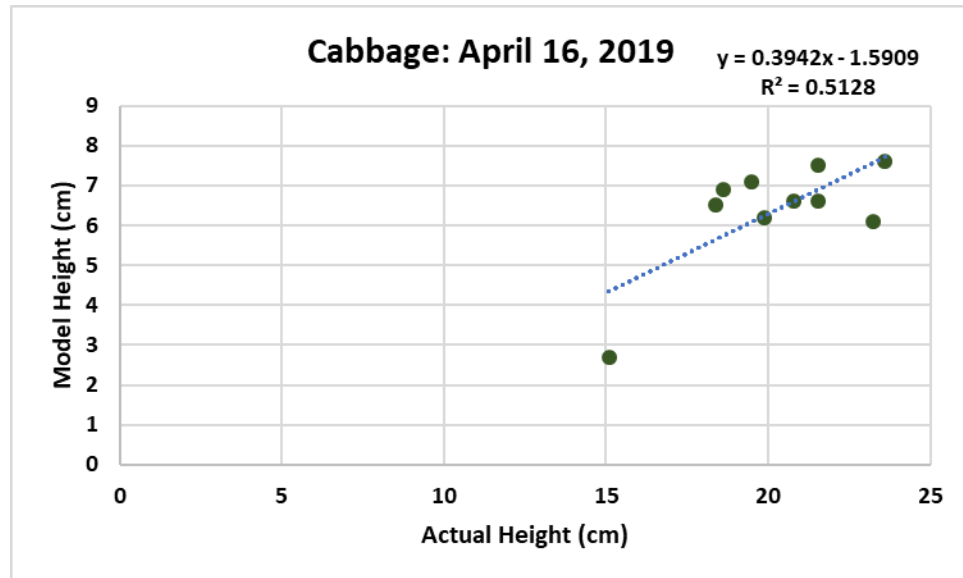


a.

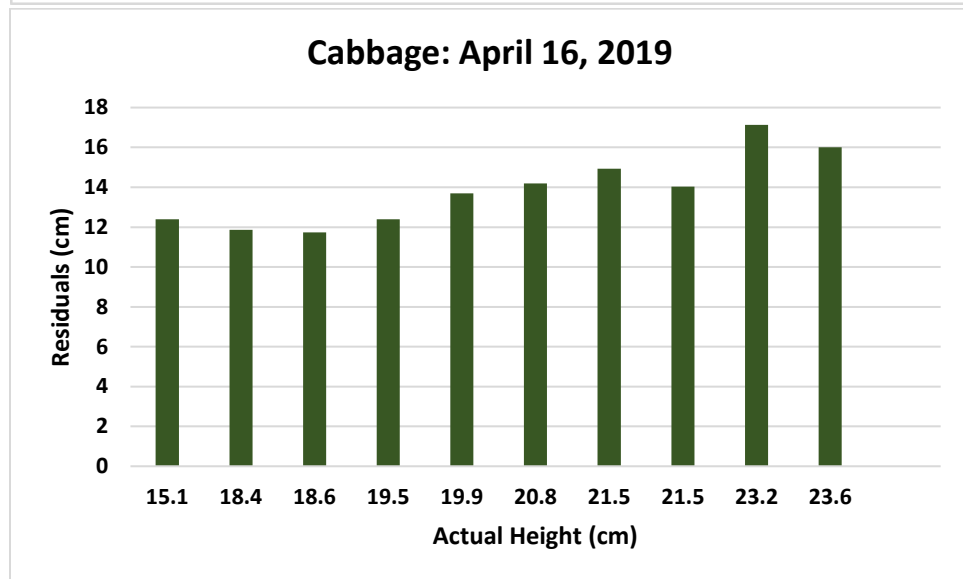


b.

Figure 40 a-b: (a) Linear regression of modeled height to actual height of cabbage and (b) the respective residuals (4/02/2019).

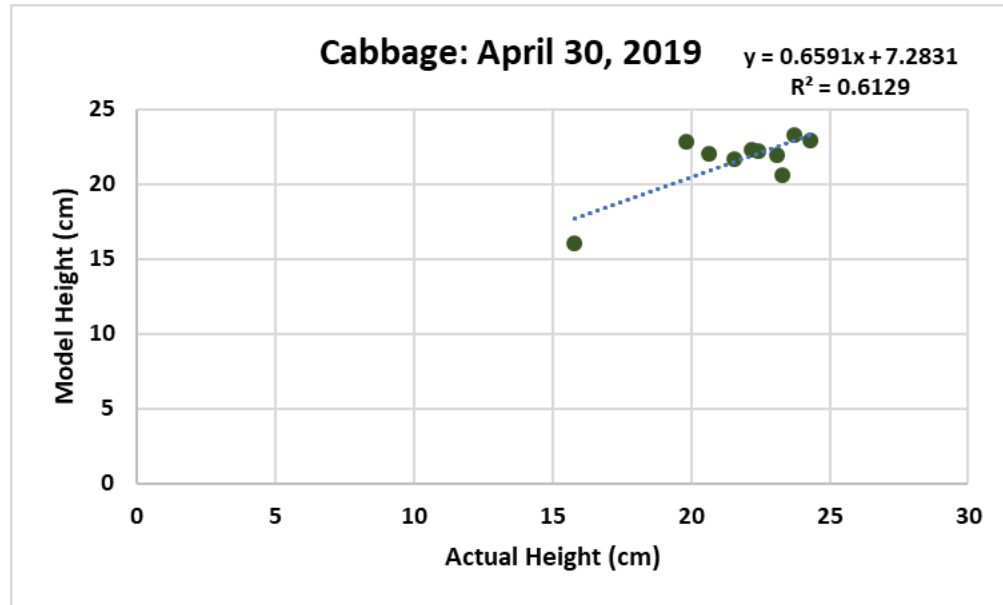


a.

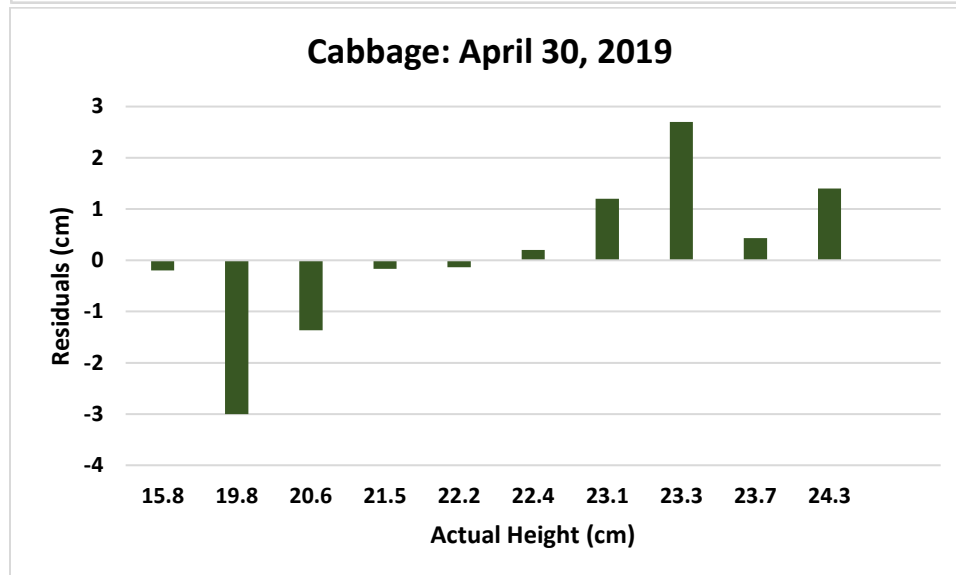


b.

Figure 41 a-b: (a) Linear regression of modeled height to actual height of cabbage and (b) the respective residuals (4/16/2019).



a.



b.

Figure 42 a-b: (a) Linear regression of modeled height to actual height of cabbage and (b) the respective residuals (4/30/2019).

Results of Modeled vs. Actual Plant Heights for All Flight Dates Combined

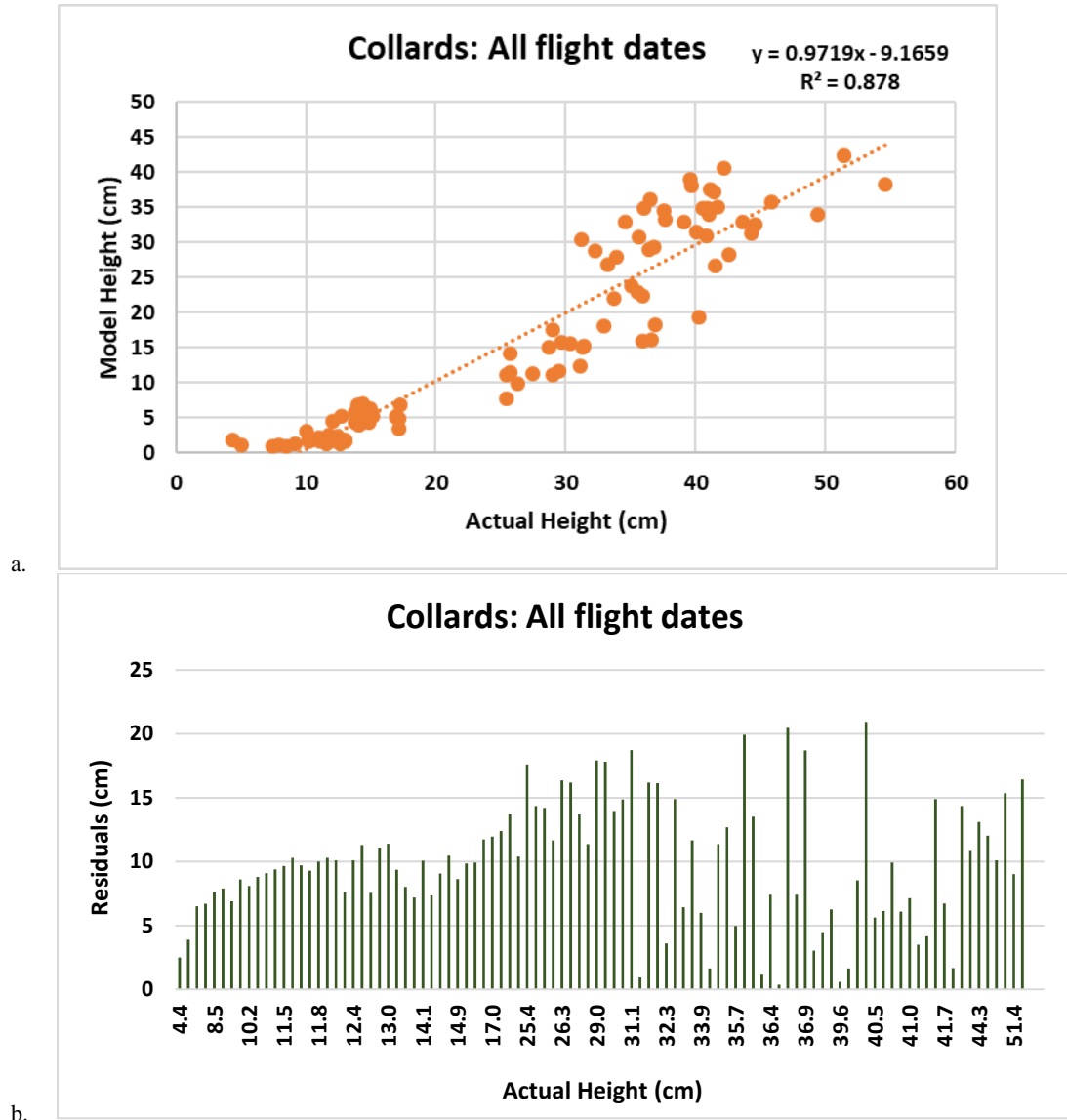
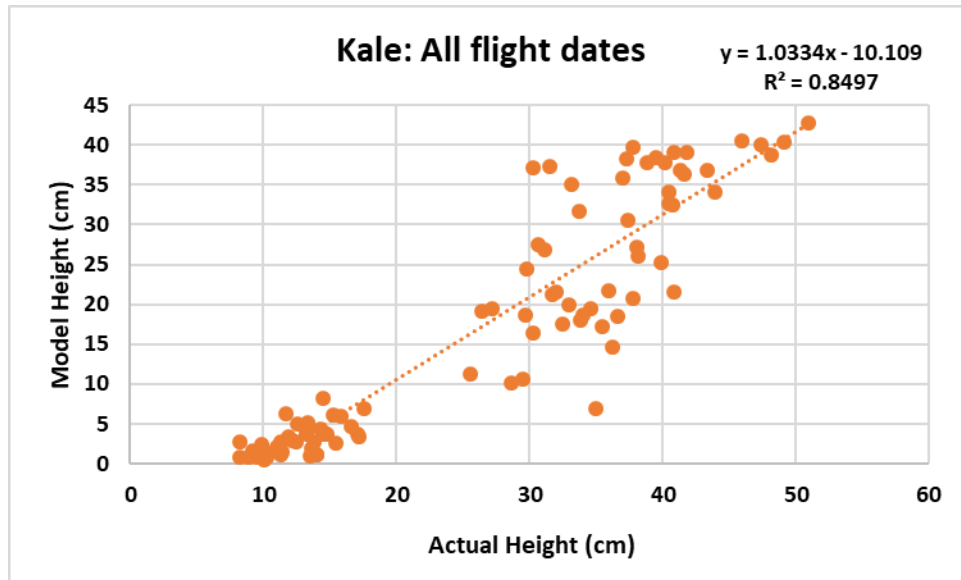
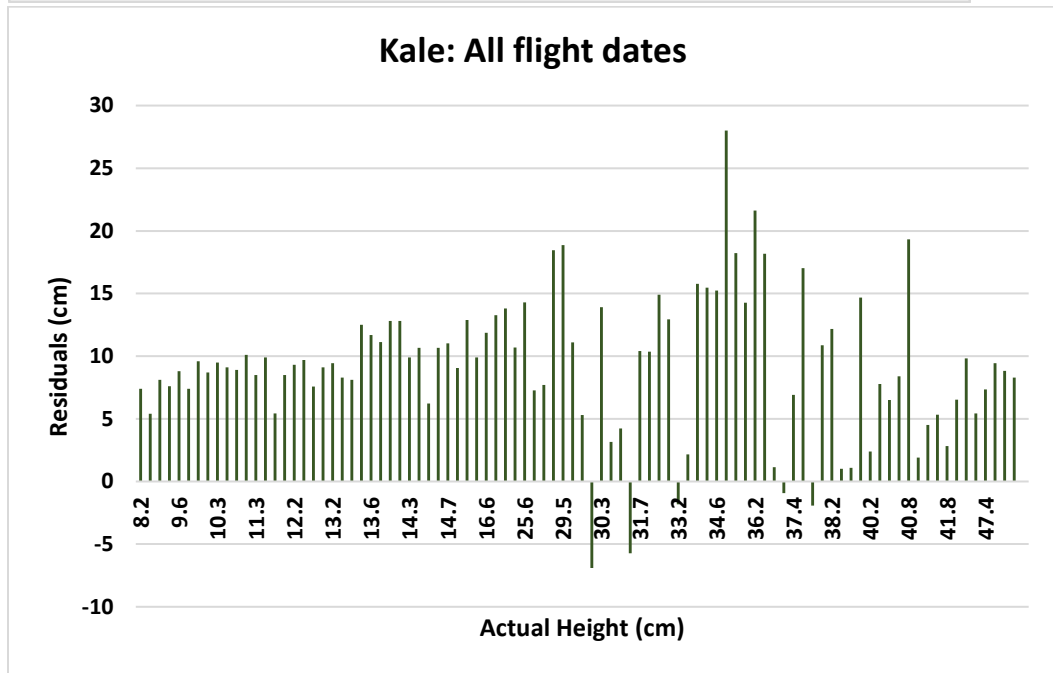


Figure 43 a-b: (a) Linear regression of modeled height to actual height of collards and (b) the respective residuals for all flight dates combined.

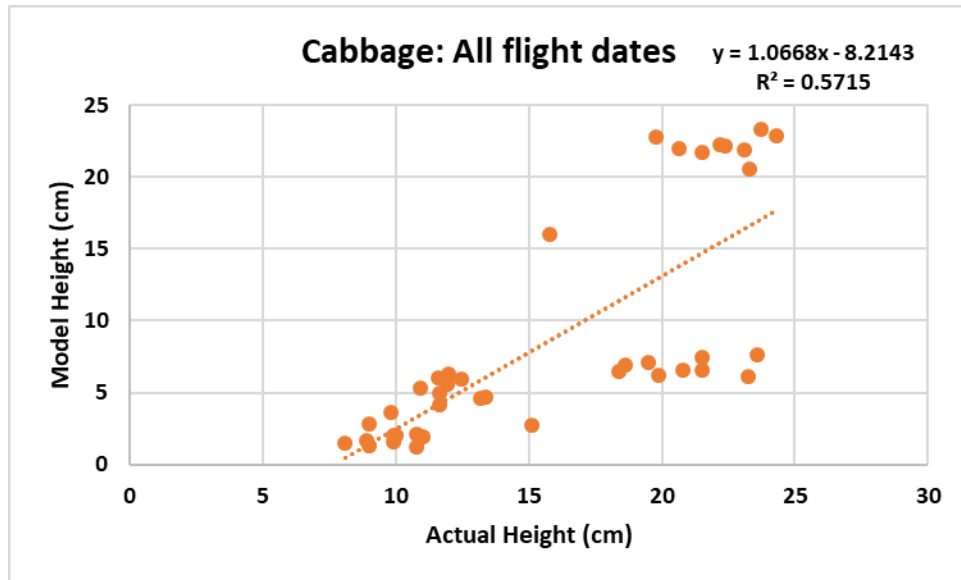


a.

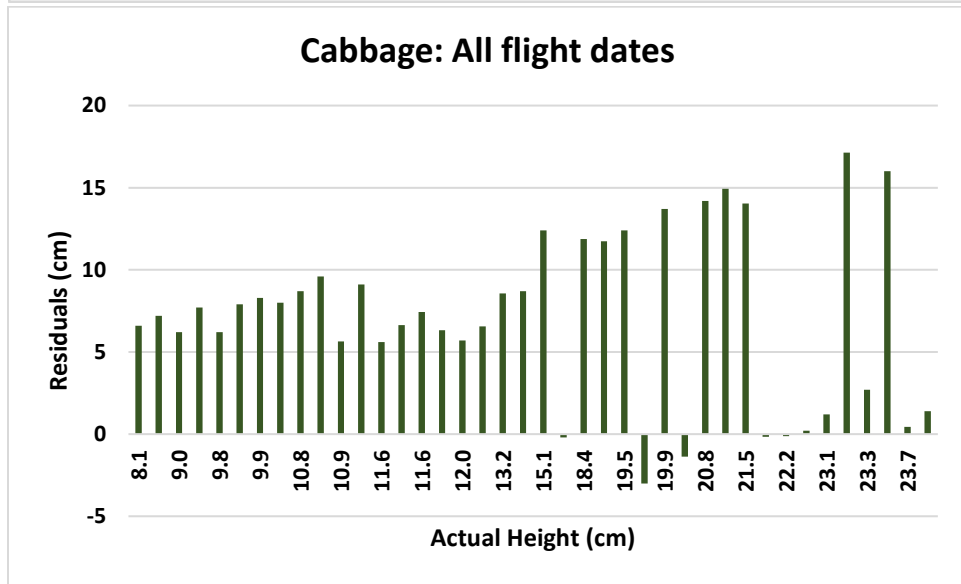


b.

Figure 44 a-b: (a) Linear regression of modeled height to actual height of kale and (b) the respective residuals for all flight dates combined.



a.



b.

Figure 45 a-b: (a) Linear regression of modeled height to actual height of cabbage and (b) the respective residuals for all flight dates combined.

Results of Modeled vs. Actual Plant Heights by Individual Flight Date for Peppers

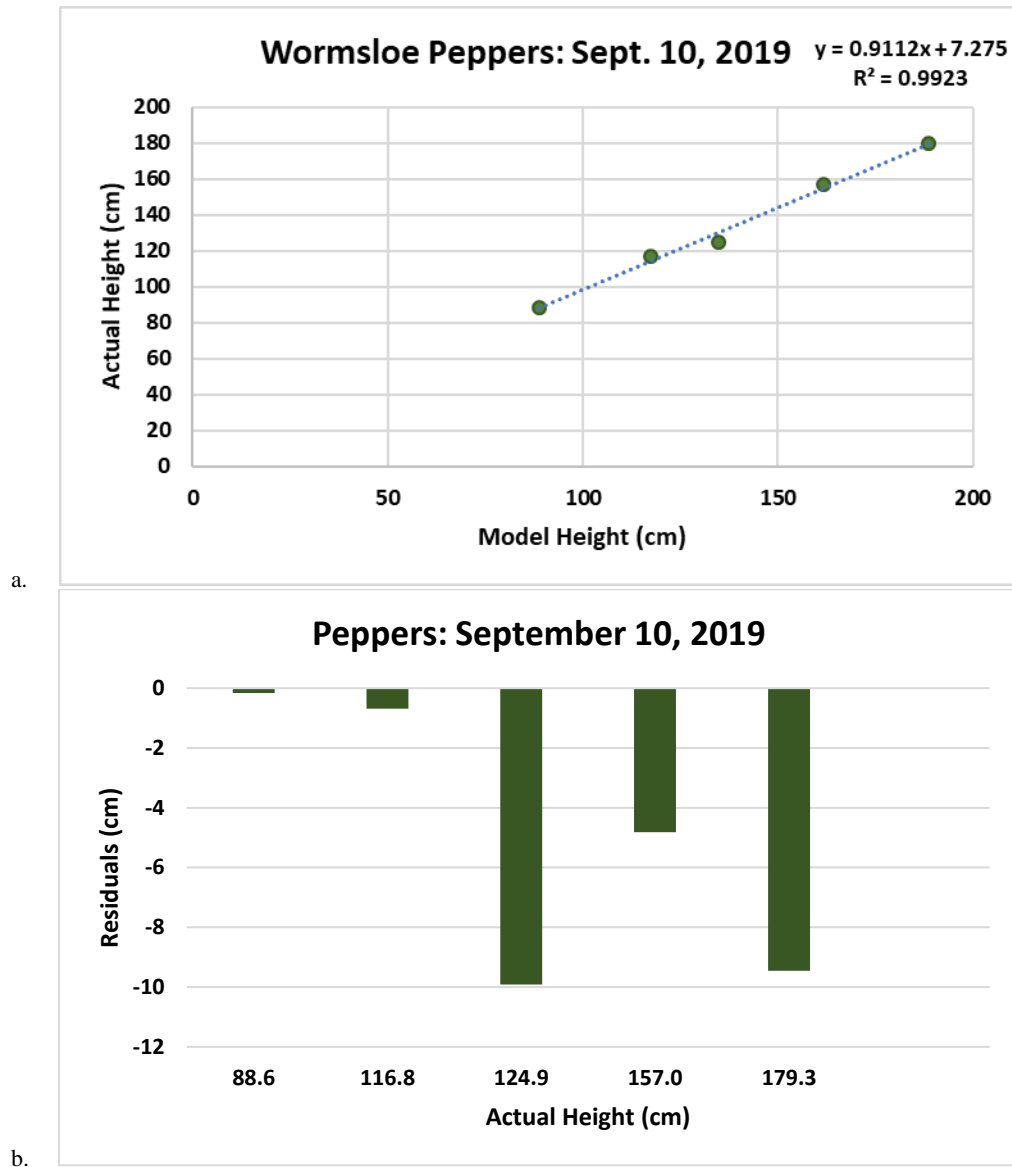


Figure 46 a-b: (a) Linear regression of modeled height to actual height of peppers and (b) the respective residuals (9/10/2019).

Percent Error of Plant Heights for All Flight Dates Combined

Generally, as the plant matured, grew taller and had a denser canopy, the percent error of plant heights derived from the CSM-DEM modeled surfaces decreased. This can be seen very clearly for both the collards and kale when plant heights are below 20 cm –

the percent error ranges from 50-95% (Figure 47 and Figure 48). The 3D models did not accurately reconstruct the height for these crop shapes below a certain height, yet there was still a percent error range of 33 and 26 when collards and kale were at full growth (i.e., all plants over 33 cm in height on 5/14/2019). Cabbage had similar high percent errors for the first two flights (ranging from 47-88%) (Figure 49). The third flight for cabbage saw an increased percent error (60% or higher) but had a smaller range of 19 cm. This appears as a distinctive cluster on the graph, sitting well below the linear regression line. The final flight for cabbage had the lowest percent error of any crop with an average percent error of .08% and this is also a distinct cluster on Figure 49 (clustered above the linear regression line). The pepper plants (Figure 50) have a range of <1% to 9% and an average percent error of 3%.

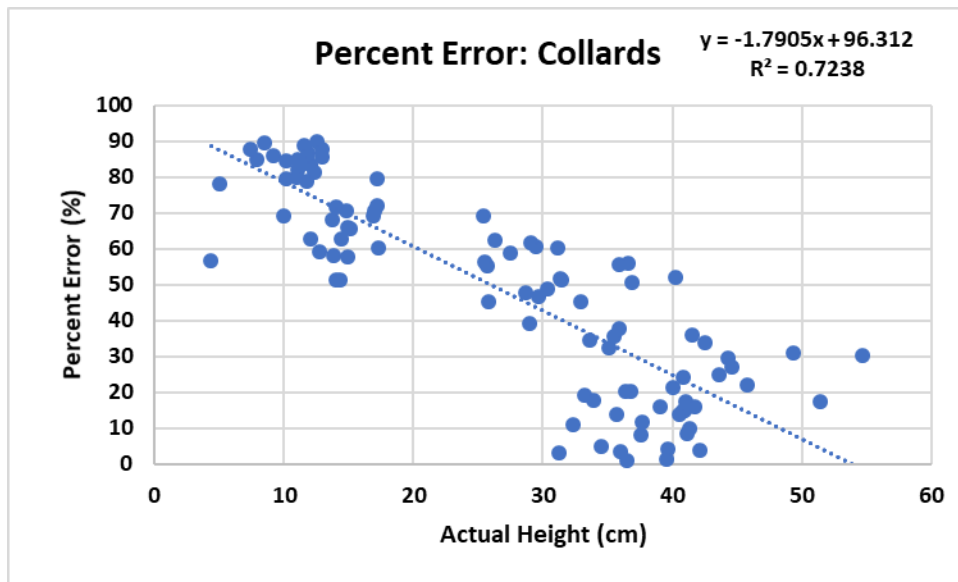


Figure 47: The percent error of the model as compared to actual plant height for all flight dates combined for collards.

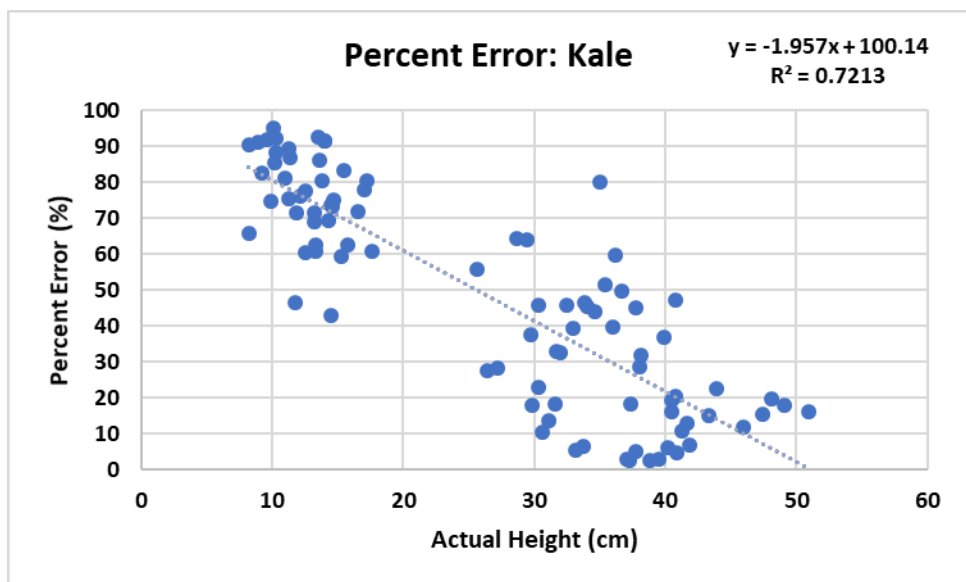


Figure 48: The percent error of the model as compared to actual plant height for all flight dates combined for kale.

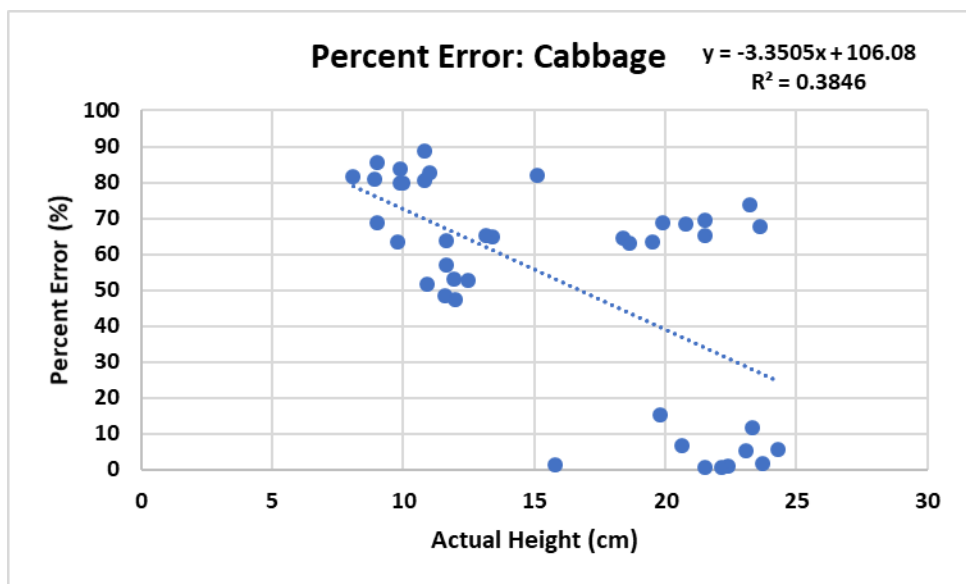


Figure 49: The percent error of the model as compared to actual plant height for all flight dates combined for cabbage.

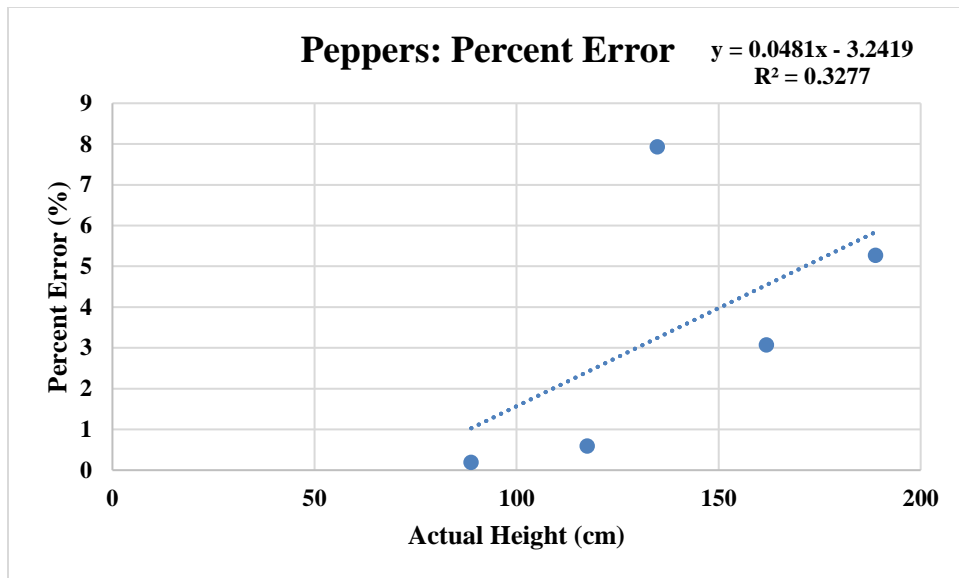


Figure 50: The percent error of the model as compared to actual plant height for pepper plants.



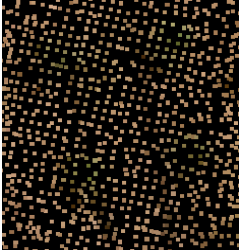


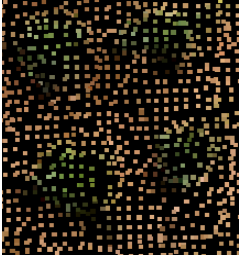


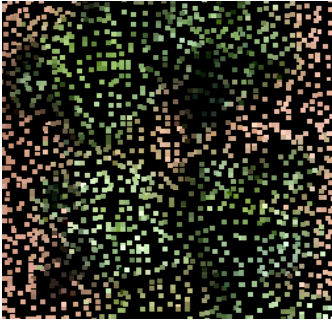


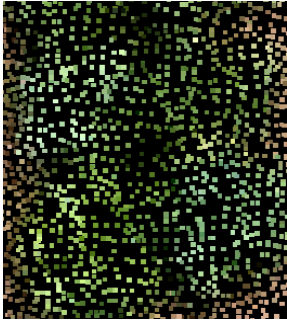

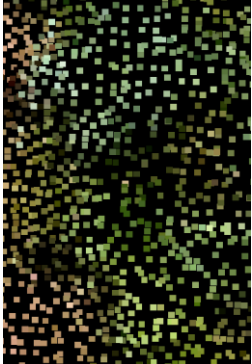
In the combined Figure depicted in Appendix A, the graphs of modeled vs. actual plant height are compiled by date and crop type. Slope increases over time for the temporal models. Collards appear to start exhibiting a pattern of clustering, showing less variation in actual vs. model derived heights starting on 4/16/2019. For 4/16/2019 and 4/30/2019, cabbage also exhibits less variation. Kale seems to show the least trend, at least for the first four flights.

Imagery Outputs

In Figure 51, all three crop types (collards, kale and cabbage) are depicted and ordered by date and crop type to visualize the stages of growth by an actual ground image, an example of the 3D tiled model and the dense point cloud. On the first flight (3/19/2019), the three crops were small seedlings, with no measured plant exceeding 14 cm in height. The largest expanses of soil are visible during this flight, and the DEM is created from these measurements. The second (4/02/2019) and third flight (4/16/2019) captured the

intermediate growth of the plants. During the second flight, the various leaf textures of the different crop types are more apparent, and some soil is still visible between plants. The third flight saw plants grow taller and become leafier. The fourth flight (4/30/2019) and the fifth and final flight (5/14/2019) captured the collard and kale plants at maturity. Some growth is seen between the fourth and fifth flight in collards and kale, but on average there was only a few cm of plant growth. The fourth flight captured cabbage at maturity while the fifth flight recorded the post-harvest of cabbage. Partial harvesting of a few leaves of collards and kale began just prior to the 4/30/2019 flight and continued until 5/27/2019, when the complete harvest of the kale and collards occurred. No data were collected for the post-harvest of collards and kale due to the high density of weeds in the garden beds upon their harvest. This was assessed during the final field visit which occurred on 5/27/2019. In Figure 51, when ground images were not able to be retrieved, a note was added to indicate “Image Unavailable.”

COLLARDS (a)

	Ground Image	Tiled Model	Dense Point Cloud
3/19/2019			
4/02/2019			
4/16/2019			
4/30/2019			
5/14/2019	Image Unavailable		

KALE (b)



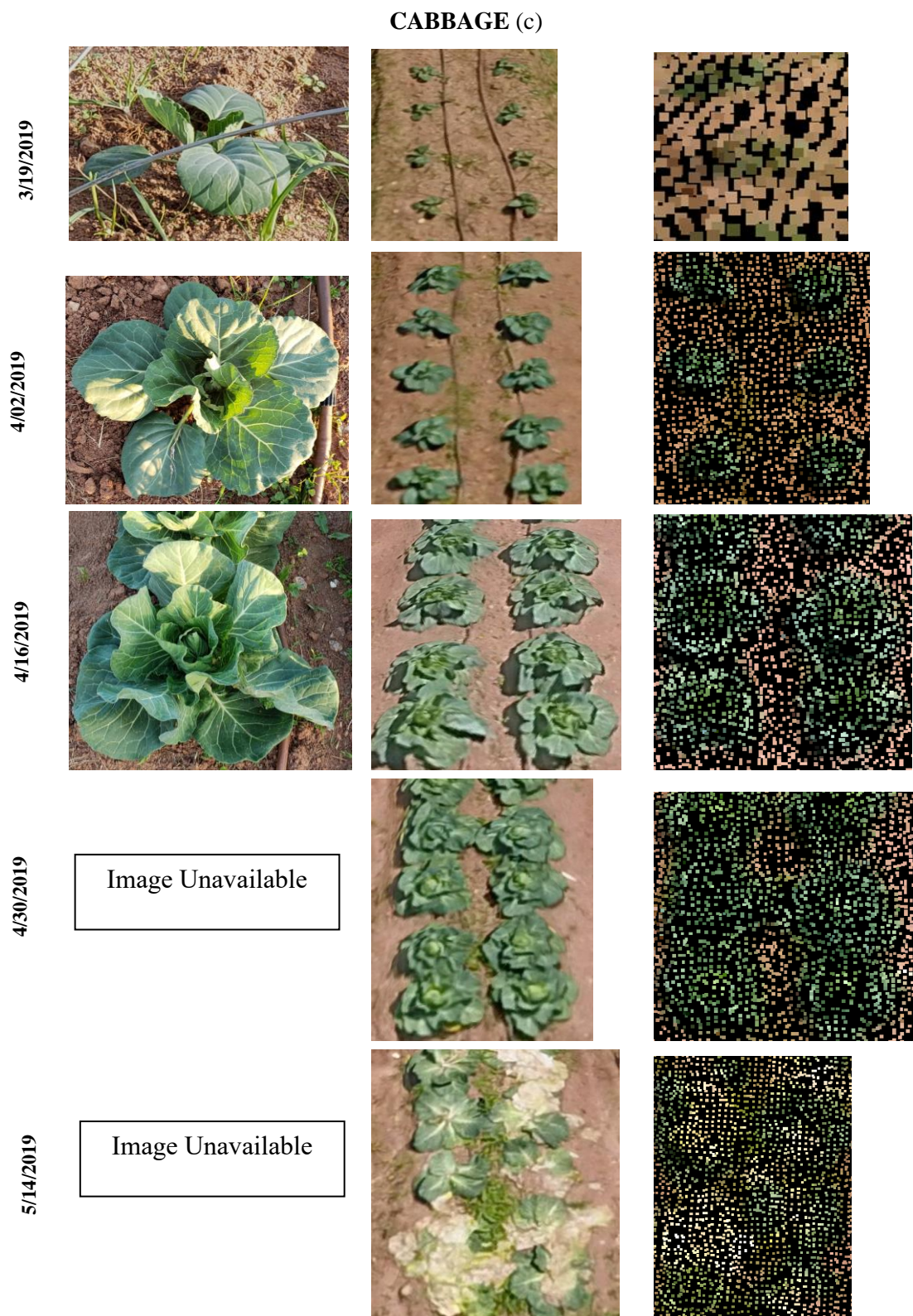


Figure 51: Actual image, tiled model and dense point cloud for all crop types, (a) collards, (b) kale and (c) cabbage at UGArden arranged by flight date.

Okra at the Wormsloe CREW garden did not produce results of adequate quality for analysis in this study due to its very thin growth form and sparse canopy. The SfM algorithm was not able to accurately detect okra as a separate feature or determine tie points during processing. As seen in Figure 52, okra plants were not reconstructed in the created 3D model.



Figure 52: Created 3D model of Wormsloe CREW okra garden. Red circles denote approximate location of where okra should have been.

Each set of field plot/garden sUAS imagery acquired at different dates created an individual data set that was processed as a separate CSM for each crop. The time series of 3D models and CSMs can be used to create a geovisualization of changes in the gardens over time. This deliverable product of an animation of growing plants created from the temporal models, can be used as a teaching tool showing the growth, senesce and decimation of the individual fields.

CHAPTER 5

DISCUSSION

Overall, the results from this study indicate a low-cost monitoring system was successfully developed for small landholder farms and community gardens approximately 4 ha in size using readily available sUAS equipment and photogrammetric software. The integrated system can be used to assess plant structure in terms of plant heights and rates of crop growth that can be used to estimate yield and plant biomass harvested, damaged or destroyed by extreme weather events, insects or grazing. Results also show there are optimal crop conditions needed to obtain plant height measurements from 3D models derived from remotely sensed sUAS images to accuracies in the range of 2 to 4 cm as compared to hand measurements of plant heights in the fields at different stages of crop growth.

For example, based on the results at UGarden, attempts to measure plants in the first stages of growth are not recommended. Though the earliest 3D models created from sUAS images acquired in the early spring were able to be used to detect subtle changes in the plant heights from the seedlings separated from the surrounding soil, the underestimation of the seedling heights was so extreme that the average percent error exceeded 80% for all plants on 3/19/2019. There was a slight decrease in average percent error in 4/02/2019, with average percent errors in the range of 55-68%. Even if modeled plant heights were not accurate, it was hoped the results would exhibit a pattern or trend that could be applied in order to better estimate plant heights from the CSM-DEM model

measurements. In other words, if modeled plant heights consistently underestimated actual heights by 10%, then actual plant heights could easily be calculated by increasing heights derived from the 3D models by 10%. Unfortunately, even models that seem to perform well such as kale from 5/14/2019, with a $R^2 = .53$ and average percent error of 12.6%, there was a range of 26 in percent error, from -20.6% to +5.5% of under- and over-estimation, respectively. This is a variation of up to 9.4 cm. With such a large range in error, the uncertainty of calculating crop heights of collards and kale, even in the later stages of growth, must be considered.

Issues with Processing, Intermediary Steps and Georegistering

Five dates of sUAS flights were selected to be included for the analysis of UGArden crop structure, based on the consistent use of the same flight altitudes, sUAS equipment, camera quality and the inclusion of established GCPs. Three previous experimental flights tested lower sUAS flying heights, however SfM processing of the sUAS imagery generated extremely high volumes of 3D point cloud data and required excessive processing times (e.g., a single flight date collected over 800 images). A different flight app (Pix4D) was initially used for some of the experimental flights, but later, Map Pilot was found to have a more user-friendly interface. These initial, experimental flights also did not contain the permanent ground control points, as those were installed after the first three sUAS flights due to recommendations by Dr. Thomas Jordan and by examples of other experiments. Visual inspection of models from the earlier flights at lower altitudes on the order of 10-15 m showed the increase in image detail did not add to the quality of the SfM products. It was, therefore, deemed a worth-while trade-off to fly the sUAS at a higher altitude, increase the image pixel size from less than one cm to about 2-3 cm and decrease the data volume

and processing time. The flight parameters were thus established and used to consistently fly the next five flights. The resulting imagery from these five flights was used for SfM analysis and the creation of 3D point clouds to derive DEM, CSM and plant heights from profiles.

After SfM processing of sUAS image data sets with the same settings in Agisoft Metashape Professional, the most time-consuming step was consistently the combined construction of the depth maps and dense point clouds (i.e., ranging from 1 hour and 2 minutes to 2 hours and 18 minutes), while the shortest step was the construction of the DSM (taking < 1 minute to create) (See Table 5).

One issue potentially effecting the accuracy of plant heights measured from 3D models was the georectification of the datasets. The average errors show that the data sets do not align exactly even in the X, Y direction, with the mean georegistration error for all datasets being .002 m in the X direction and -.996 m in the Y direction. The Z elevations had the highest mean error (-122.9 m) (See Table 8), which is to be expected since georegistration was necessary due to vast differences in z values (See Figure 26). But it would have been extremely hard to attempt any type of alignment without established GCPs. Turner et al. (2012) reported higher accuracy when using GCPs, by comparing 3D models of landscapes constructed with and without the use of GCPS. Many studies such as Bendig et al. (2014 and 2015) and Chang et al. (2017) did use high accuracy RTK GPS to georectify their resulting 3D models. However, due to the high-cost of RTK-grade GPS equipment on the order of \$15,000 to \$30,000, this was not considered in this study as feasible or accessible for a small landholder farmer to do so. In the georectification process, the Z values for many of the crops were on a negative scale (i.e., measuring a -.3 m) (Figure

53) due to setting the GCPs at 0 – some Z values then were measured as negative values if the micro-terrain dipped below the arbitrarily set elevation datum of zero. As this creates a local coordinate system, z values measure relative plant heights for these fields alone and can be compared to one another.

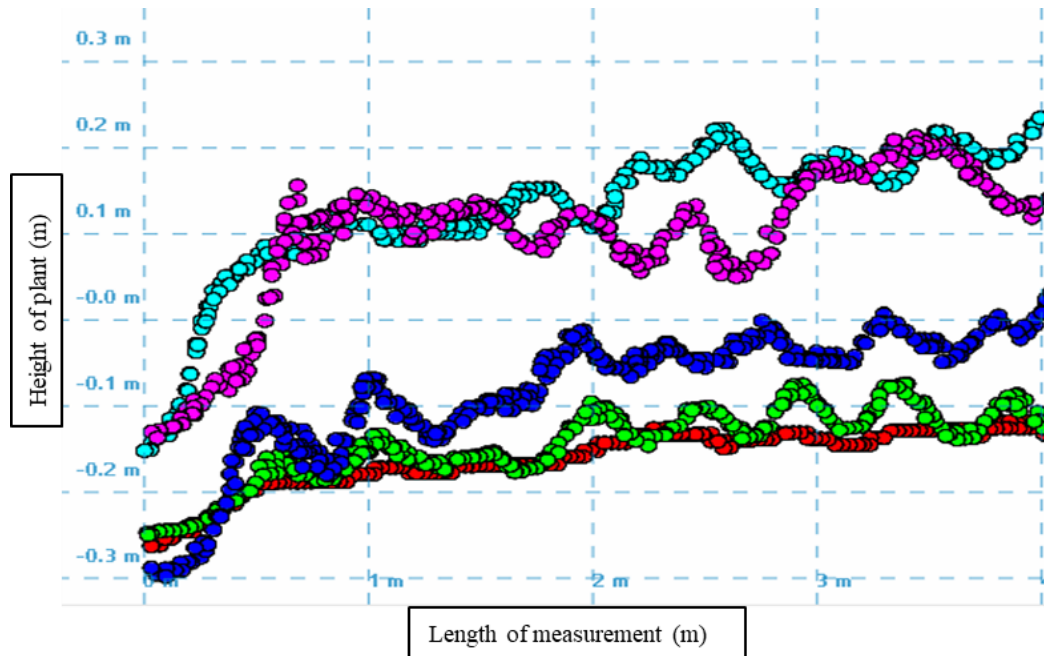


Figure 53: Crop height profile, depicting negative height values in QTModeler.

Comparison of Results to Similar Studies

My study appears to be unique in its accuracy assessment of the agricultural crops of collards, kale and peppers using the combined geospatial technologies of SfM model construction by sUAS-collected imagery to assess crop model heights. Although there are previous publications describing temporal agricultural crop monitoring studies using similar techniques, equipment and software, these are mostly limited to grain crops such as barley (Bendig et al. 2014, 2015), wheat (Holman et al. 2016) and maize (Chu et al. 2018, Malambo et al. 2018). Studies which focus on vegetable crops or examine how crop

growth forms influence accuracy are almost nonexistent. One study on vegetable crops does assess cabbage, tomato and eggplant (Moeckel et al. 2018); a second assesses Chinese cabbage and white radish (Kim et al. 2018). Since cabbage is one plant evaluated in this study, I will discuss my results as compared to those studies in more detail below.

Bendig et al. (2014) used UAS-acquired imagery and Agisoft Photoscan (a precursor to the Metashape software version used in this study) to construct temporal 3D models of barely; a tall, thin grain crop with a homogeneous canopy. Their findings showed a strong correlation ($R^2 = .92$) between model heights and true plant heights when all flight dates were combined. Interestingly, Bendig et al. (2014) did not present the correlation of modeled plant heights to hand-measured heights as data separated by individual flight dates. In this study, results were presented both ways, by individual flight date and combined for all flight dates. When flight dates for collards or kale are combined, the R^2 increased to .88 and .85, respectively. The individual temporal datasets, however, had lower correlations, ranging from a low of .125 for collards and .002 for kale. It may be beneficial for studies to separate out the individual flight dates for additional assessment of the importance of plant maturity on the success of UAS image-based SfM processing and derived products from 3D point clouds. Examining both data from individual dates and all combined dates, shows a broader picture of how crop phenology influences model accuracy, through changes in plant physiology, density and height over the crop's life span.

Results presented here present evidence that multiple variables influence the accuracy of plant structure measurements from 3D crop models, both between different crop types and within the same crop type during different points of its growth stage. Here

the different variables of plant height, crop canopy, plant/fruit color and flying conditions (wind, cloud cover) are addressed separately.

Plant Height

Grenzdörffer (2014) similarly found, crop heights in the early developmental stages are difficult to determine, because the plants are generally short and small. The minimum determinable height in that study was found to range between 5 - 15 cm. In the case of the UGarden in this study, the transplanted seedlings of measured crops (except for a few samples in collards) all exceeded 5 cm in height by the time of the first sUAS flight in March 2019. Although the SfM models were able to detect elevation changes, plant heights measured from the CSMs largely underestimated the actual heights. The model performed best with crops of a lower height with a compact growth form such as cabbage, over kale and collards, showing that height, as previously stated, is only one of the contributing variables. This is also exhibited through the results of the okra at Wormsloe CREW. The okra was very tall but did not reconstruct in the models due to its sparse canopy and growth form and thin, flexible leaves.

Wind and Clouds

Grenzdörffer (2014) also notes several concerns about the weather conditions when acquiring sUAS images for SfM, that are potentially applicable to this study. For example, it cannot be guaranteed that plant leaves and stems will not move during sUAS data collection due to any ambient or sUAS-induced wind from the rotor blades. Movement of plant leaves during the sUAS flight and image acquisition decreases the accuracy of 3D model reconstruction due to unmatchable features in overlapping imagery – a requirement during the first stages of SfM. Grenzdörffer (2014) notes, “even a little wind is enough to

cause problems.” Though precautions were taken for quality assurance by limiting flight days to low-wind conditions (including an instance of rescheduling, after arrival on site), light breezes can occur. Due to the physiology of kale and collards, especially at maturity, their long leaves are disturbed more by wind than the solid sphere of a cabbage head. Perhaps this is reflected in the high accuracy and low percent error of the final cabbage dataset, as compared to that of collards and kale. It should be noted that the UGarden fields are in a more open and exposed area, with forest wind break only on one side. The Wormsloe CREW site containing the raised-bed garden growing peppers, was a smaller area and closely surrounded by buildings (cabins and a garden shed), trees and other tall plants within the garden that better protected the garden from breezes. In addition to ambient wind, the sUAS operator must also monitor the down-draft wind created by the quadcopter rotor blades. If the flying altitude is too low relative to the crop plant height (e.g., approximately 5 to 10 m), wind generated by the sUAS will excessively move the plant leaves and stems. In this case, the sUAS must be flown higher at approximately 20 m.

Crop Canopy Structure

One previous study states crop model height is best determined if the canopy or crop surface is homogenous, dense and smooth (Grenzdörffer 2014). Results in my research similarly showed canopy structures that are sparse (such as early in the season) or with peaks marking the highest points of individual plants (such as the long leaves of kale and collards, specifically at maturity), will create 3D models that underestimate the true heights. High plant density is associated with later growth stages, as the plant grows and spreads out. My models generally performed with higher accuracy and stronger correlation

later in the season when the plants were taller, denser and the biomass or leaves obscured the ground. In later flights, collards and kale grew denser and obscured more of the ground, which hypothetically should increase the accuracy of 3D model measurements of plant structure. Correlation strength and plant height accuracy increased, but not as high as hoped compared to other vegetable studies (Moeckel et al. 2018, Kim et al 2018). This could be due to the wide variation in leaf heights. For example, the height range for collards and kale on the final flight were 19 cm and 17.8 cm, respectively. Possibly, the advantages of high plant density may be outweighed by disadvantages caused by the varying heights of the individual plants. The tallest leaves (and highest points measured) faced the greatest exposure to any breeze, as they extended above the majority of leaves of particular plants. The measured models underestimated every single sample height of the collards and all but five of the kale sample plants. The tips of individual kale leaves are only a few cm wide and may be hard for the software algorithm to identify and reconstruct, especially with a breeze. Comparatively, cabbage is solid and dense and obscured the ground on the final flight. It has a more homogenous height with a range of only 8.5 cm. This flight performed the best with the highest correlation and lowest percent error of any temporal model. Clearly, from my results, shorter plants that sparsely cover the ground do not produce accurate plant structure measurements from the 3D models of crops for all early growth stages.

Multiple variables, therefore, impact crop models including, the various growth forms, density or sparsity, height, homogeneity or heterogeneity of canopy. For example, cabbage, while still at a shorter height, performs better than the taller collards and kale. Cabbage, on its final dataset, has an R^2 correlation of .61 and average percent error of

-08%. Yet, the kale and collards that are over 20 cm taller than the cabbage do not achieve this level of accuracy, even within their highest correlated datasets. Pepper plants performed very well ($R^2 = .99$ and average percent error 4%) and were by far the tallest plant. Interestingly, they also had the largest variability in height (1 m), which supports the theory that different variables affect different plants to greater degrees. Pepper plant structure is different than the other four crop types. It is somewhat shrub like in structure and densely covered in small-sized leaves. It is one of two plant types observed in this study to have a color, texture and shape contrast of smooth, bright red fruits amidst the green leaves. This contrast may help with tie point recognition and 3D point cloud reconstruction. The canopy of the okra at Wormsloe CREW was extremely sparse, and even though it was tall and had a few okra fruits of contrasting shape and texture, the 3D models were not able to reconstruct the okra plants, even though they were able to reconstruct the garden bed itself. For okra, the extreme sparsity of its canopy may have outweighed the benefits of height and fruit contrast during reconstruction.

Underestimation of Plant Heights

A reoccurring theme is underestimation in the 3D model-measured plant heights, seen in my temporal studies and in other studies of grain crops such as barley (Bendig et al. 2014), maize, wheat (Grenzdörffer 2014) of white radish and Chinese cabbage (Kim et al. 2018) and predictive models of cabbage, tomatoes and eggplant (Moeckel et al. 2018). Of note, the 3D models of pepper plants consistently overestimated plant heights, which further research would need to be done to understand why. Hypothetically, it would be better to underestimate what exists than overestimate if it came to predicting yield or harvest. If yield overestimation occurs, issues may arise concerning planned monetary

budgets or insufficient food to feed people based on yield predictions. If models were used for insurance purposes, then the reverse would be true; underestimating a loss would result in undervalue in monetary payment.

The multi-temporal vegetable crop studies in the literature tended to report higher R^2 correlations than my temporal studies. For those that included cabbage in their experiments, cabbage was the vegetable that had the strongest correlation of actual and predicted plant heights. This is also seen in my study, specifically, the final assessment of cabbage when it has achieved its full height and density on 4/30/2019. Kim et al. (2018) reported Chinese cabbage had an R^2 of .95. It is worth mentioning that Chinese cabbage is a different species (*Brassica rapa*). It grows taller, with an elongated and oval growth form and has a color contrast of green and white as compared to the standard supermarket cabbage (*Brassica oleracea*), the cabbage examined in my study. Moeckel et al. (2018), while using a SfM- based prediction model, again had the highest correlation with cabbage with $R^2 = .97$ and the other vegetables eggplant (.93) and tomato (.89). My cabbage model did contain the lowest percent error and the highest correlation out of my temporal models but still had a lower correlation when compared to other studies. Although, the sUAS in a study conducted by Moeckel et al. (2018) was flown at approximately the same height (20m/65 ft), used the immediate predecessor (DJI Phantom 3 Pro) to my sUAS and an older version of the same modeling software used in my study used, it was a predictive study. These factors, plus human error in validation measurements, could account for some of the differences.

Vegetables in other studies that performed accurately (Kim et al. 2018, Moeckel et al. 2018) and the pepper plants I had in my study all have fruit with of contrasting color

and texture with the plant leaves and stems. The peppers were bright red and had a waxy, smooth texture and different shape compared to the rest of the plant. This would also be the same for fruited plants such as eggplant and tomato, with a different shape, texture and color standing out amongst the plant. It may be possible that these fruits help differentiate and create feature matches during SfM reconstruction.

Limitations

As previously noted, there were limitations to this work. Working with live vegetation can always pose problems and be a limitation for measurements, including possible human error in the actual measuring or recording of hand measurements of plant heights in the field. Possible breezes may have affected the accuracy of plant heights from 3D models, or the ability for the SfM algorithm to find sufficient or accurate tie points for the highest points or peaks of the plants. Unlike previous studies, my study did not incorporate the use of RTK GPS, which possibly could have helped with issues that occurred during georectification. For farmers who want to implement monitoring systems, there will be an initial financial investment and a learning curve and since some of these models have large ranges of percent error and underestimation, it may not be an appropriate monitoring system for everyone at this point in time – especially since it does not appear that enough crop types have been tried out.

Further limitations pertain to the sUAS itself – most low-cost sUAS systems cannot operate correctly if they are flown when the ambient temperatures are too high (40 C°). In the Coastal Plain of the southeastern U.S. and even into the upland Piedmont regions, most crops grow during the summer and temperatures may exceed 40 C° during the day. At this point malfunctions may happen during the flight - the controller screen may go gray or the

connection of the controller may be severed with the sUAS. This would be a potentially dangerous and costly situation if the sUAS crashes into something or plummets to the ground and breaks. Extreme heat occurs usually around mid-day but flying during early morning or evening has the issue of low sun angles which can cause shadows and decrease the accuracy of SfM modeling. Another possible perceived limitation of my study was the use of non-destructive sampling. Some studies use destructive sampling, which could allow for a better record of plant height to be taken (i.e. photographs for plant and height laid out on a ruler to be referenced or the ability to calculate biomass). Non-destructive sampling was chosen to follow the growth of the same individual plants throughout the course of the study. UGarden is also a working farm and I would not be allowed to do destructive sampling. The peppers at Wormsloe were grown to maturity for seed saving purposes; destructive harvesting would also have been impossible there.

CHAPTER 6

SUMMARY AND CONCLUSIONS

In summary, I explored and analyzed several combined geospatial techniques to attempt to make precision agriculture more accessible to fine-scale farms and community gardens, in hopes of assisting with local and sustainable crop monitoring. The first objective was to assess combined geospatial techniques appropriate for small landholder farmers. This was done through the use of Structure from Motion (SfM)-derived 3D models from sUAS-collected imagery and calculated model heights, as compared to the actual field heights of the crops. A large part of this was a temporal study conducted at UGArden in order to determine the most efficient methods to collect and store data. Since UGArden was in close proximity to the UGA campus, it made a bi-weekly temporal study feasible. These results also allowed me to fine tune my skills and methods in order to achieve my second objective, the application of these refined geospatial techniques to a farm (Wormsloe CREW) located on the Coastal Plain of Georgia. Several varieties of crops at both sites were examined in order to see how factors, such as growth form, height, canopy coverage, leaf structure and other aspects of plant physiology, may influence the accuracy of the measurements derived from 3D models, thus achieving my third objective.

Crops that performed with the highest accuracy in the 3D models vs. the actual plant height were those at maturity with dense canopies. This includes the pepper plants at Wormsloe CREW ($R^2 = .99$ and average percent error 4%) and cabbage at UGArden just prior to harvest ($R^2 = .61$ and average percent error -.08%). Multiple factors influence the

accuracy of the created 3D models. While height is a factor in low percent error and a higher correlation, other factors can outweigh it. For example, okra, the tallest plant observed, was 1 – 2 m in height and imaged at maturity yet had a very sparse canopy. The created 3D model was not able to reconstruct any of the okra plants, only reconstructing the garden bed.

Crops that had not reached maturity, such as the seedling of collards, kale and cabbage at UGArden had very low correlations ($R^2 = <.2$) and very high percent error (over 70%). This seems to be a combination of short height and sparse canopy, because as these crops grew taller and denser, generally the correlations became stronger and had a lower percent error. Cabbage, which has a homogenous canopy, had a stronger correlation and lower percent error. Collards and kale, even when the correlation was stronger and had a lower percent error, still had a large range within the percent error, likely due to the large range in actual plant height and the high peaks the leaves of the collards and kale exhibit. The leaf peaks may make it hard for the SfM algorithm to feature match especially as this type of growth form is susceptible to movement during light breezes which causes image blurring.

There are other factors that may have influenced the accuracy of the models. This includes errors incurred during the field measurements to validate the actual plant height. Errors may have occurred while measuring the plant itself or while recording or transferring the height values to the computer software. A significant concern is the errors that may have occurred during georegistration of the temporal datasets at UGArdens. As previously stated, the Z values for ground control points in each dataset were set to 0, but even a misalignment of a few cm would significantly affect accuracy, as the monitored

plants at UGArdens never exceed 55 cm in height. The bare earth model or DEM may also contribute to errors. The DEM is created from the height of the soil from the first flight and it is not unreasonable to speculate that the soil settled or has undergone micro erosion throughout the season. Again, even if the DEM changed by only a few cm, this error relative to the plant heights could contribute significantly to the accuracy of the created models.

Other factors such as data storage and organization must be considered when implementing these methods. The heights of the sUAS flights and resulting image resolution affects not only the volumes of data, but also the resolution and the accuracy of reconstructed 3D models. Flying too low may disturb plants in terms of leaf and stalk movement in the wind generated by the sUAS propellers and also generate large volumes of data. On the other hand, flying too high in order to reduce data volume, and therefore processing time, may not result in imagery of an adequately small pixel size (i.e., spatial resolution) that can accurately reconstruct 3D models for monitoring purposes.

Currently, monitoring crop growth requires an initial investment in equipment and software and there is a learning curve on how to use the equipment and software. Initially, the intent was to create an educational tool for small landholder farmers and community garden managers to autonomously monitor their crops and fields. After this study was completed, it was realized that a number of factors including the cost of multiple software licenses, specialized equipment and a relatively steep learning curve as more software programs were needed, may preclude the wide use of these techniques by small landowner farmers. Alternatively, the methodology described here may be most appealing and useful to small businesses that provide remote sensing services to the owners and managers of

small area farms and outreach services such as agricultural extension agencies. These techniques may still be appealing to individual farm owners who have an interest in learning new technologies and skill sets. Regardless of the type of users, these accessible techniques for acquiring, processing and analyzing imagery and 3D models of crops are still deemed to be valuable for monitoring crop growth and assessing damages in small area farms and community gardens.

Further Research

As these combined geospatial technologies have improved and decreased in cost, they have opened up the accessibility of specialized geospatial techniques to the broader public. Further research and repeated experiments, however, must be done before they can be truly accessible and widely usable. More vegetable crops will need to be examined to see how each of the variables influence the creation of accurate 3D models of crops at different times in their life cycle. Studies on other crops such as lettuces, squashes, asparagus, cauliflower, and a multitude of others, will need to be carefully conducted and examined in terms of their physiological differences. Only then, will these techniques become sufficiently accurate for the majority of farmers to feel confident in their use. Other options should be explored in order to accurately register, or align, Z-values in different temporal datasets. Other sUAS models should be explored. Indeed, new sUAS equipment has been released since the inception of this study. Additionally, there are other SfM software programs that may be explored, some open source and free and some requiring purchase or subscriptions. Time and repeated effort will ensure that the best geospatial techniques, practices and guidelines will be available for fine-scale farmers.

In conclusion, this study is important as it is a little explored aspect of precision agriculture, especially as it focuses on vegetable crops and fine-scale farming. Due to limitations in technology, precision farming for small landholder farmers and managers of community gardens has not received adequate attention until recently. Climate change, mass population increases, interruptions of food delivery systems and outdated or inefficient farming techniques will continue to contribute to local and global food insecurity and potential starvation. While these combined geospatial monitoring techniques may not have the accuracy or consistency for all crop types, it is a starting point. Results show that multiple factors contribute to the accuracy of model heights as compared to true plant heights. Further studies will need to be performed to better understand factors affecting the accuracy of derived 3D models of different crops and determine which crops may benefit most from these techniques.

REFERENCES

- Agapiou, A., Lysandrou, V., Themistocleous, K., & Hadjimitsis, D. G. (2016). Risk assessment of cultural heritage sites clusters using satellite imagery and GIS: the case study of Paphos District, Cyprus. *Natural Hazards*, 83(S1), 5–20. doi: 10.1007/s11069-016-2211-6
- Agisoft Metashape. (2019). Agisoft Metashape User Manual Professional Edition, Version 1.5. Retrieved From https://www.agisoft.com/pdf/metashape-pro_1_5_en.pdf
- Anderson, W. (2010). Closing the gap between actual and potential yield of rainfed wheat. The impacts of environment, management and cultivar. *Field Crops Research*, 116(1-2), 14–22. doi: 10.1016/j.fcr.2009.11.016
- Barnett, A., (2014, May 7). *Seed Saviour: I'm preserving our edible heirlooms*. NewScientist. <https://www.newscientist.com/article/mg22229680-100-seed-saviour-im-preserving-our-edible-heirlooms/>
- Bendig, J., Bolten, A., Bennertz, S., Broscheit, J., Eichfuss, S., & Bareth, G. (2014). Estimating Biomass of Barley Using Crop Surface Models (CSMs) Derived from UAV-Based RGB Imaging. *Remote Sensing*, 6(11), 10395–10412. doi: 10.3390/rs61110395
- Bendig, J., Yu, K., Aasen, H., Bolten, A., Bennertz, S., Broscheit, J., Gnyp M.L, and Bareth, G. (2015). Combining UAV-based plant height from crop surface models, visible, and near infrared vegetation indices for biomass monitoring in barley. *International Journal of Applied Earth Observation and Geoinformation*, 39, 79–87. doi: 10.1016/j.jag.2015.02.012
- Blair, J. B., Lefsky, M. A., Harding, D. J., & Parker, G. G. (1999). Lidar altimeter measurements of canopy structure: methods and validation for closed-canopy, broadleaf forests. *Earth Resour. Remote Sensing*, 76, 283-297.

- Bowers, S. A., & Hanks, R. J. (1965). Reflection Of Radiant Energy From Soils. *Soil Science*, 100(2), 130–138. doi: 10.1097/00010694-196508000-00009
- Boys, K., & Hughes, D. (2013). A Regional Economics–Based Research Agenda for Local Food Systems. *Journal of Agriculture, Food Systems, and Community Development*, 1–6. doi: 10.5304/jafscd.2013.034.012
- Bragg, W.H. (1999). *De Renne: Three Generations of a Georgia Family*. The University of Georgia Press, Athens, Georgia, 632 p.
- Bussell, M. R., Bliesner, J., & Pezzoli, K. (2017). UC pursues rooted research with a nonprofit, links the many benefits of community gardens. *California Agriculture*, 71(3), 139–147. doi: 10.3733/ca.2017a0029
- Chang, A., Jung, J., Maeda, M. M., & Landivar, J. (2017). Crop height monitoring with digital imagery from Unmanned Aerial System (UAS). *Computers and Electronics in Agriculture*, 141, 232–237. doi: 10.1016/j.compag.2017.07.008
- Chu, T., Starek, M. J., Brewer, M. J., Murray, S. C., & Pruter, L. S. (2018). Characterizing canopy height with UAS structure-from-motion photogrammetry—results analysis of a maize field trial with respect to multiple factors. *Remote Sensing Letters*, 9(8), 753–762. doi: 10.1080/2150704x.2018.1475771
- Comis, D. (1998) High-tech retrofitting of farm machinery. *Agricultural Research* 46 (11). 20
- Cotten, D., Jordan, T., Madden, M., and Bernardes S., (2017). Structure from motion and 3D reconstruction, pages 160-166, *In*, Chapter 7, Image Processing and Analysis Methods, Section 7, Bernardes, S. and M. Madden, (Chapter Eds.) *In*, Morain, S., A. Budge and M. Renslow (Eds.) *Manual of Remote Sensing*, 4th Edition, 12 Sections, American Society for Photogrammetry and Remote Sensing, Bethesda, Maryland, *In Press*.
- Dandois, J.P., Olano, M., & Ellis, E.C. (2015). Optimal altitude, overlap, and weather conditions for computer vision UAV estimates of forest structure. *Remote Sensing*. 7(10), 13895–13920 doi: [10.3390/rs71013895](https://doi.org/10.3390/rs71013895)

- DigitalGlobe, (2019). *Satellite Imagery*. Retrieved Dec 11, 2019 from <https://www.digitalglobe.com/products/satellite-imagery>
- DJI, (2019). *DJI Store*. Retrieved Nov 27, 2019 from https://store.dji.com/product/mavic-air?site=brandsite&from=buy_now_bar&vid=38961
- Eitel, J. U., Magney, T. S., Vierling, L. A., Brown, T. T., & Huggins, D. R. (2014). LiDAR based biomass and crop nitrogen estimates for rapid, non-destructive assessment of wheat nitrogen status. *Field Crops Research*, 159, 21–32. doi: 10.1016/j.fcr.2014.01.008
- European Space Agency (2019). *Spatial Resolution*. Retrieved Oct 24, 2019 from <https://sentinel.esa.int/web/sentinel/user-guides/sentinel-2-msi/resolutions/spatial>
- Evans, R., (1972). Air photographs for soil survey in lowland England: Soil patterns. *Photogrammetric Record*, 7:302-322.
- Federal Aviation Administration (FAA). (2016) *FAA News. Summary of Small Unmanned Aircraft Rule (Part 107)*. Federal Aviation Administration, Washington DC 20591. Retrieved from https://www.faa.gov/uas/media/Part_107_Summary.pdf
- Fonstad, M. A., Dietrich, J. T., Courville, B. C., Jensen, J. L., & Carbonneau, P. E. (2013). Topographic structure from motion: a new development in photogrammetric measurement. *Earth Surface Processes and Landforms*, 38(4), 421–430. doi: 10.1002/esp.3366
- Food and Agriculture Organization of the United Nations (FAO). (2019). *What is Happening to Agrobiodiversity?* Retrieved March 31, 2019 from <http://www.fao.org/3/y5609e/y5609e02.htm>
- Forest Service, (1994). *Chapter 20: Ecological Subregions of the United States*. (1994) Retrieved Oct 31, 2019 from <https://www.fs.fed.us/land/pubs/ecoregions/ch20.html>
- Förstner, W. (1986). A feature-based correspondence algorithm for image matching, *International Archives of Photogrammetry and Remote Sensing*, 26: 150–166.

- Förstner, W. & Wrobel, B.P. (2016). *Photogrammetric Computer Vision: Statistics, Geometry, Orientation and Reconstruction*, Springer International Publishing, Switzerland, 816 pp.
- Fraser, C. S., & Cronk, S. (2009). A hybrid measurement approach for close-range photogrammetry. *ISPRS Journal of Photogrammetry and Remote Sensing*, 64(3), 328–333. doi: 10.1016/j.isprsjprs.2008.09.009
- Gebbers, R., & Adamchuk, V. I. (2010). Precision Agriculture and Food Security. *Science*, 327(5967), 828–831. doi: 10.1126/science.1183899
- GeorgiaInfo. *Geographic Regions of Georgia*. (n.d.) Retrieved Oct 31, 2019 from <https://georgiainfo.galileo.usg.edu/topics/geography/article/geographic-regions-of-georgia>
- Glaser, L. K. (1985). Provisions of the Food Security Act of 1985. United States Department of Agriculture.
- Goodman, M.S., (1959). A technique for the identification of farm crops on aerial photographs. *Photogrammetric Engineering*, 25:131-138.
- Goodman, M.S., (1964). Criteria for the identification of types of farming on aerial photographs, *Photogrammetric Engineering*, 30:984-991.
- Greb, P., (2019) *Farm-Fresh Produce and You!* United States Department of Agriculture (USDA). Retrieved Sept 24, 2019 from https://tellus.ars.usda.gov/stories/articles/farm-fresh-produce-and-you/?utm_medium=email&utm_source=govdelivery
- Grenzdörffer, G. J. (2014). Crop height determination with UAS point clouds. *ISPRS - International Archives of the Photogrammetry, Remote Sensing and Spatial Information Sciences, XL-1*, 135–140. doi: 10.5194/isprsarchives-xl-1-135-2014
- Grün, A., 1985. Adaptive least square correlation: A powerful image matching technique. *South African Journal of Photogrammetry, Remote Sensing and Cartography*, 14(3): 175–187.
- Grün, A., 2000. Semi-automated approaches to site recording and modeling. *International Archives of Photogrammetry and Remote Sensing*, 33(5/1): 309–318.

- Grün, A., Remondino, F., & Zhang, L. (2004). Photogrammetric reconstruction of the Great Buddha of Bamiyan, Afghanistan. *The Photogrammetric Record*, 19(107): 177–199.
- Harris, C. & Stephens, M. (1988). A combined corner and edge detector. In *Fourth Alvey Vision Conference*, Manchester, UK, pp. 147–151.
- Harris, C. (1992). Geometry from visual motion. In *Active Vision*, A. Blake and A. Yuille (Eds.), MIT Press, pp. 263–284.
- Hartley, R. & Zisserman, A., (2003). *Multiple View Geometry in Computer Vision*, Cambridge University Press, Cambridge, UK.
- Henneberry, S. R., Whitacre, B.E., & Agustini H.N. (2009). An Evaluation of the Economic Impacts of Oklahoma Farmers Markets. *Journal of Food Distribution Research* 40(3): 64–78. doi: [10.22004/ag.econ.99760](https://doi.org/10.22004/ag.econ.99760)
- Holman, F., Riche, A., Michalski, A., Castle, M., Wooster, M., & Hawkesford, M. (2016). High Throughput Field Phenotyping of Wheat Plant Height and Growth Rate in Field Plot Trials Using UAV Based Remote Sensing. *Remote Sensing*, 8(12), 1031. doi: 10.3390/rs8121031
- Holmgren & Thuresson. 1998. Satellite remote sensing for forestry planning - A review. *Scandinavian Journal of Forest Research*. V 13 issue 1-4 pp. 90 – 110
- Jackson, B. E., Evangelista, D. J., Ray, D. D., & Hedrick, T. L. (2016). 3D for the people: multi-camera motion capture in the field with consumer-grade cameras and open source software. *Biology Open*, 5(9), 1334–1342. doi: 10.1242/bio.018713
- Jensen, J.R., 2018. *Drone Aerial Photography and Videography: Data Collection and Image Interpretation*, (Kindle Book 1), 304 p.
- Johnson, C.E, Schafer, R.L., & Young, S.C. (1983).Controlling agricultural machinery intelligently *Agricultural Electronics -1983 and Beyond*. Proceedings of the National Conference on Agricultural Electronics Applications, American Society of Agricultural Engineers, St Joseph (1983)
p. 114–119

- Katsianis, M., Tspidis, S., Kotsakis, K., & Kousoulakou, A. (2008). A 3D digital workflow for archaeological intra-site research using GIS. *Journal of Archaeological Science*, 35(3), 655–667. doi: 10.1016/j.jas.2007.06.002
- Kim, D.-W., Yun, H., Jeong, S.-J., Kwon, Y.-S., Kim, S.-G., Lee, W., & Kim, H.-J. (2018). Modeling and Testing of Growth Status for Chinese Cabbage and White Radish with UAV-Based RGB Imagery. *Remote Sensing*, 10(4), 563. doi: 10.3390/rs10040563
- King, R. P., Hand, M.S., Digiacomio, G., Clancy, K., Gomez, M.I., Hardesty, S.D, Lev, L. & McLaughlin, E.W., (2010). *Comparing the Structure, Size, and Performance of Local and Mainstream Food Supply Chains*, Economic Research Report No. 99., Economic Research Service, U.S. Department of Agriculture (USDA), Washington DC.
- Kos, M., & Jerman, J. (2012). Preschool children learning about the origin of food, on local farms and in the preschool garden. *Nutrition & Food Science*, 42(5), 324–331. doi: 10.1108/00346651211266836
- Koutsoudis, A., Vidmar, B., Ioannakis, G., Arnaoutoglou, F., Pavlidis, G., & Chamzas, C. (2014). Multi-image 3D reconstruction data evaluation. *Journal of Cultural Heritage*, 15(1), 73–79. doi: 10.1016/j.culher.2012.12.003
- Lefsky, M.A., Cohen, W.B., Parker, G.G., Harding, D.J., (2002). Lidar Remote Sensing for Ecosystem Studies: Lidar, an emerging remote sensing technology that directly measures the three-dimensional distribution of plant canopies, can accurately estimate vegetation structural attributes and should be of particular interest to forest, landscape, and global ecologists, *BioScience*, 52(1) 19–30, doi: [/10.1641/0006-3568\(2002\)052\[0019:LRSFES\]2.0.CO;2](https://doi.org/10.1641/0006-3568(2002)052[0019:LRSFES]2.0.CO;2)
- Leon, C.T., Shaw, D.R, Cox, M.S., Abshire, M.J., Ward, B., Wardlaw III, M.C. & Watson, C. (2003). Utility of remote sensing in predicting crop and soil characteristics. *Precision Agriculture*, 4(4), 359-384. doi: 10.1023/A:1026387830942

- Little, J., Shi, P. (2001) Structural Lines, TINs, and DEMs. *Algorithmica* 30, 243–263.
<https://doi.org/10.1007/s00453-001-0015-9>
- Llorens, J., Gil, E., Llop, J., & Escolà, A. (2011). Ultrasonic and LIDAR Sensors for Electronic Canopy Characterization in Vineyards: Advances to Improve Pesticide Application Methods. *Sensors*, 11(2), 2177–2194. doi: 10.3390/s110202177
- Long, D. S., & McCallum, J. D. (2013). Mapping straw yield using on-combine light detection and ranging (lidar). *International Journal of Remote Sensing*, 34(17), 6121–6134. doi: 10.1080/01431161.2013.793869
- Lourakis, M.I.A. & Argyros, A.A., (2009). SBA: A software package for generic sparse bundle adjustment. *ACM Transactions on Mathematical Software*, 36(1): 1–30, doi:10.1145/1486525.1486527.
- Lowe, D.G. (2004). Distinctive Image Features from Scale-Invariant Keypoints. *International Journal of Computer Vision*, 60(2), 91–110. doi: 10.1023/b:visi.0000029664.99615.94
- Lowe, D.G. (1999). Object recognition from local scale-invariant features. In Proceedings of the seventh IEEE International Conference on Computer Vision, Corfu, Greece, 1999. Vol 2. pp. 1150-1157.
- Lowenberg-DeBoer, J. (1996). Precision Farming and the New Information Technology: Implications for Farm Management, Policy, and Research: Discussion. *American Journal of Agricultural Economics*, 78(5), 1281-1284. doi:10.2307/1243507
- Madec, S., Baret, F., Solan, B. D., Thomas, S., Dutartre, D., Jezequel, S., Hemmerlé, M. Colombeau, G. & Comar, A. (2017). High-Throughput Phenotyping of Plant Height: Comparing Unmanned Aerial Vehicles and Ground LiDAR Estimates. *Frontiers in Plant Science*, 8. doi: 10.3389/fpls.2017.02002
- Madden, M., Jordan, T. & Masour, J. (2009a). Orthoimages and Forest-Agriculture-Urban Conversion 1938-1980 for the Chattahoochee River National Recreation Area, Final Report to the U.S. Department of Interior, National Park Service, Public Service

- Cooperative Agreement Number P534007A185, Center for Remote Sensing and Mapping Science, The University of Georgia, Athens, GA, 46 p
- Madden, M., Jordan, T., Kim, M., Allen, H. & Xu, B. (2009b). Integrating remote sensing and GIS: From over-lays to GEOBIA and geo-visualization, In M. Madden (Ed.) *The Manual of Geographic Information Systems, American Society for Photogrammetry and Remote Sensing*, Bethesda, MD, pp. 701–720.
- Madden, M., Jordan T., Bernardes, S., Cotten, D., O’Hare N., & Pasqua, A. (2015). Unmanned Aerial Systems (UAS) and Structure from Motion (SfM) Revolutionize Wetlands Mapping, In, R. Tiner, M. Lang and V. Klemas (Eds), *Remote Sensing of Wetlands: Applications and Advances*, CRC Press Taylor & Francis Group, Boca Raton, Florida, 10: 195-222.
- Madden, M., T. Jordan, S. Bernardes, C. Goetcheus, K. Olson and D. Cotten. (2019). Small Unmanned Aerial Systems (sUAS) and Structure from Motion (SfM) for Identifying, Documenting and Monitoring Cultural and Natural Resources, In, J.B. Sharma (Ed), *Applications of Small Unmanned Aircraft Systems: Best Practices and Case Studies*, CRC Press Taylor & Francis Group, Boca Raton, Florida, 179-209.
- Malambo, L., Popescu, S., Murray, S., Putman, E., Pugh, N., Horne, D., et al., Bishop, M. (2018). Multitemporal field-based plant height estimation using 3D point clouds generated from small unmanned aerial systems high-resolution imagery. *International Journal of Applied Earth Observation and Geoinformation*, 64, 31–42. doi: 10.1016/j.jag.2017.08.014
- Markewich, H., Pavich, M., & Buell, G. (1990). Contrasting soils and landscapes of the Piedmont and Coastal Plain, eastern United States. *Geomorphology*, 3(3-4), 417–447. doi: 10.1016/0169-555x(90)90015-i
- McGlone, J.C. (Ed. in Chief), (2013). *ASPRS Manual of Photogrammetry*, 6th edition, American Society for Photogrammetry and Remote Sensing, Bethesda, MD.
- Meng, Nick, 2019. A Geospatial Decision Support Tool to Evaluate the Economic Outcomes of

- Targeted Conservation Delivery, M.S. Thesis Publication, Warnell School of Forestry and Natural Resources, The University of Georgia, 96 p.
- Meyers, V.I., (1983). Remote sensing applications in agriculture, Author-Editor In, R.N. Colwell (Ed.-in-Chief), *Manual of Remote Sensing, Vol. II Interpretation and Applications*, American Society of Photogrammetry, Falls Church, Virginia, pp. 2111-2228.
- Moeckel, T., Dayananda, S., Nidamanuri, R., Nautiyal, S., Hanumaiah, N., Buerkert, A., & Wachendorf, M. (2018). Estimation of Vegetable Crop Parameter by Multi-temporal UAV-Borne Images. *Remote Sensing*, 10(5), 805. doi: 10.3390/rs10050805
- Morefield, P. E., LeDuc, S. D., Clark, C.M. & Iovanna, R. (2016). Grasslands, wetlands, and agriculture: the fate of land expiring from the Conservation Reserve Program in the Midwestern United States. *Environmental Research Letters* 11(9):94005.
- Moravec, H. (1981). Rover visual obstacle avoidance. In *International Joint Conference on Artificial Intelligence*, Vancouver, Canada, pp. 785-790.
- Mueller, N. D., Gerber, J. S., Johnston, M., Ray, D. K., Ramankutty, N., & Foley, J. A. (2012). Closing yield gaps through nutrient and water management. *Nature*, 490(7419), 254–257. doi: 10.1038/nature11420
- National Aeronautics and Space Administration (NASA). (1978). *Independent Peer Evaluation of the Large Area Crop Inventory Experiment (LACIE)*, National Aeronautic and Space Administration, Johnson Space Center, NASA JSC-14550, NTIS, Springfield, Virginia.
- National Aeronautics and Space Administration (NASA). (2001). *Precision Farming*. Retrieved Dec 11, 2019 from <https://earthobservatory.nasa.gov/features/PrecisionFarming>
- National Aeronautics and Space Administration (NASA). (2019a). *Landsat 7*. Retrieved Nov 27, 2019 from <https://landsat.gsfc.nasa.gov/landsat-data-continuity-mission/>
- National Aeronautics and Space Administration (NASA). (2019b). *Landsat 8*. Retrieved Oct 24, 2019 from <https://landsat.gsfc.nasa.gov/landsat-data-continuity-mission/>

- National Aeronautics and Space Administration (NASA). (2019c). *A Landsat Timeline*. Retrieved Nov 27, 2019 from <https://landsat.gsfc.nasa.gov/a-landsat-timeline/>
- National Climatic Data Center (NCDC) (2020). Climate of Georgia. Retrieved April 13, 2020 from https://www.ncdc.noaa.gov/climatenormals/clim60/states/Clim_GA_01.pdf
- O'Connor, T., (2011). Inherit the Earth: Why Treasure Heirloom Foods. *Horticulture Magazine*, 108(4), 30-35. Accessed <http://www.seasonalwisdom.com/wp-content/uploads/2011/01/HortMag-Inherit-the-Earth.pdf>
- Olson, K. A. (2018). The town that food saved? Investigating the promise of a local food economy in Vermont. *Local Environment*, 24(1), 18–36. doi: 10.1080/13549839.2018.1545753
- Orgera, A., (2019, April 29). Seed Life. *Savannah Magazine*. Retrieved Feb 2, 2020 from <https://www.savannahmagazine.com/seed-life/>
- Pearsall, H., Gachuz, S., Sosa, M. R., Schmook, B., Wal, H., & Gracia, M. A. (2017). Urban Community Garden Agrodiversity and Cultural Identity in Philadelphia, Pennsylvania, U.S. *Geographical Review*, 107(3), 476–495. doi: 10.1111/j.1931-0846.2016.12202.x
- Planet, (2019). Pricing. Retrieved Nov 27 from <https://support.planet.com/hc/en-us/articles/360021049373-What-is-the-minimum-order-value-and-how-much-does-it-cost->
- Remillard, M. & Welch, R., (1996). Remote Sensing and GIS for Landscape Assessment of Fuel Hazard in Yellowstone National Park, Final Report to the US Forest Service, Southeastern Forest Experiment Station, Contract # 12-11-008-876 Supplement 159, Center for Remote Sensing and Mapping Science, University of Georgia, Athens, GA: 37 p.
- Renslow, M. S. (2012). Airborne topographic lidar manual. *American Society of Photogrammetry and Remote Sensing*, Bethesda, MD (2012)
- Richardson, A.J., Wiegand, C.L., Gausman, H.W., Cuellar, J.A. & Gerbermann, A.H. (1975). Plant, soil and shadow reflectance components of row crops, *Photogrammetric Engineering and Remote Sensing*, 41(11):1401-1407.

- Richards-Rissetto, H. (2017). What can GIS +3D mean for landscape archaeology? *Journal of Archaeological Science*, 84, 10–21. doi: 10.1016/j.jas.2017.05.005
- Rosell, J. R., Sanz, R., Llorens, J., Arnó, J., Escolà, A., Ribes-Dasi, M., et al., Palacín, J. (2009). A tractor-mounted scanning LIDAR for the non-destructive measurement of vegetative volume and surface area of tree-row plantations: A comparison with conventional destructive measurements *Biosystems Engineering*, 102(2), 128–134. doi: 10.1016/j.biosystemseng.2008.10.009
- Ryerson, R.A., Curran, P.J & Stevens, P.R. (1997). Applications in agriculture. In, W. R. Philipson (Ed.-in-Chief), *Manual of Photographic Interpretation*, 2nd Ed., American Society for Photogrammetry and Remote Sensing, Bethesda, Maryland, pp. 365-397.
- Schimmelpfennig, D. (2016). *Farm Profits and Adoption of Precision Agriculture*, Economic Research Report No. 217. Economic Research Service, U.S. Department of Agriculture (USDA), Washington DC. 10.22004/ag.econ.249773
- Schmid C., & Mohr R., (1997) Local Grayvalue Invariants for Image Retrieval. *IEEE Transactions on Pattern Analysis and Machine Intelligence*, Institute of Electrical and Electronics Engineers, 1997, 19 (5), 530–534. doi:10.1109/34.589215
- Seed Savers Exchange. (2018). *Svalbard, SSE Mark a Decade of Safeguarding Seeds Together*. Retrieved March 31, 2019 from <http://blog.seedsavers.org/blog/celebrating-svalbard>.
- Seed Savers Exchange. (2019). *Our Story*. Retrieved March 31, 2019 from <https://www.seedsavers.org/story>.
- Singh, K. K., Chen, G., Vogler, J. B., & Meentemeyer, R. K. (2016). When Big Data are Too Much: Effects of LiDAR Returns and Point Density on Estimation of Forest Biomass. *IEEE Journal of Selected Topics in Applied Earth Observations and Remote Sensing*, 9(7), 3210–3218. doi: 10.1109/jstars.2016.2522960
- Smithsonian Gardens. (2019). *Grown from the Past: A Short History of Community Gardening in*

- the United States*. Retrieved April 14, 2019 from <https://communityofgardens.si.edu/exhibits/show/historycommunitygardens/intro>
- Sonti, N. F., & Svendsen, E. S. (2018). Why Garden? Personal and Abiding Motivations for Community Gardening in New York City. *Society & Natural Resources*, 31(10), 1189–1205. doi: 10.1080/08941920.2018.1484971
- Svalbard Global Seed Vault, (2019). *10 Years (2008-2018) safeguarding seeds for the future*, Norwegian Ministry of Agriculture and Food, <https://www.seedvault.no/>. Last accessed April 23, 2019.
- Swanson, Drew A., 2012. *Remaking Wormsloe Plantation: The Environmental History of a Lowcountry Landscape*. University of Georgia Press, Athens, Georgia. 251 p.
- Tey, Y.S., & Brindal, M. (2012). Factors influencing the adoption of precision agricultural technologies: a review for policy implications. *Precision Agriculture* 13: 713–730. doi: 10.1007/s11119-012-9273-6
- Theriault, D. H., Fuller, N. W., Jackson, B. E., Bluhm, E., Evangelista, D., Wu, Z., et al. Hedrick, T. L. (2014). A protocol and calibration method for accurate multi-camera field videography. *Journal of Experimental Biology*, 217(11), 1843–1848. doi: 10.1242/jeb.100529
- Torres-Sánchez, J., Peña, J., Castro, A. D., & López-Granados, F. (2014). Multi-temporal mapping of the vegetation fraction in early-season wheat fields using images from UAV. *Computers and Electronics in Agriculture*, 103, 104–113. doi: 10.1016/j.compag.2014.02.009
- Turner, D., Lucieer, A., & Watson, C. (2012). An Automated Technique for Generating Georectified Mosaics from Ultra-High Resolution Unmanned Aerial Vehicle (UAV) Imagery, Based on Structure from Motion (SfM) Point Clouds. *Remote Sensing*, 4(5), 1392–1410. doi: 10.3390/rs4051392
- UGarden. (2019). *History and Organization*. Retrieved Feb 2, 2019 from <https://ugarden.uga.edu/history-of-ugarden/>

- Underwood, J., Wendel, A., Schofield, B., McMurray, L., & Kimber, R. (2017). Efficient in-field plant phenomics for row-crops with an autonomous ground vehicle. *Journal of Field Robotics*, 34(6), 1061–1083. doi: 10.1002/rob.21728
- United States Department of Agriculture (USDA). (2016). *America's Diverse Family Farms*, Economic Information Bulletin, No. 164, Economic Research Service, U.S. Department of Agriculture (USDA), Washington, D.C., 16 p.
- United States Department of Agriculture (USDA). (2019). National Agricultural Statistics Service. *Georgia Agricultural Facts*. Retrieved from https://www.nass.usda.gov/Statistics_by_State/Georgia/Publications/More_Features/GA2018.pdf
- United States Department of Agriculture (USDA). (2020). *Local Food Directories: National Farmers Market Directory*. Retrieved Feb 1, 2020 <https://www.ams.usda.gov/local-food-directories/farmersmarkets>
- University of Georgia (2019). *Coastal Plain Station*. Retrieved Oct 31, 2019 from <https://www.caes.uga.edu/research/places/experiment-stations-rec/coastal-plain-station.html>
- USGS EROS Archive - Aerial Photography - National Agriculture Imagery Program (NAIP). (2019) USGS. Retrieved Oct 24, 2019 from https://www.usgs.gov/centers/eros/science/usgs-eros-archive-aerial-photography-national-agriculture-imagery-program-naip?qt-science_center_objects=0#qt-science_center_objects
- Westoby, M., Brasington, J., Glasser, N., Hambrey, M., & Reynolds, J. (2012). 'Structure-from-Motion' photogrammetry: A low-cost, effective tool for geoscience applications. *Geomorphology*, 179, 300–314. doi: 10.1016/j.geomorph.2012.08.021
- White, V. (1997) Farming with computers. *Journal of Soil & Water Conservation*. 52(6). 400-204
- Wolf, K. (2017). Importance of Agriculture in Georgia. *Small Business and Its Impact on Georgia*

2017. Small Business Development Center, University of Georgia. pp. 7-8. 2017.
Retrieved from https://issuu.com/ugasbdc/docs/small_business_impact_2016
- Wolf, P. R., & Dewitt B. A., (2000) *Elements of Photogrammetry with Applications in GIS*. 3rd ed., McGraw-Hill.
- Wormsloe Institute for Environmental History (n.d). *Research*. Retrieved Jan 1 2020 from <https://crew.uga.edu/research.html>.
- Xu, Y., Ou, J., He, H., Zhang, X., & Mills, J. (2016). Mosaicking of Unmanned Aerial Vehicle Imagery in the Absence of Camera Poses. *Remote Sensing*, 8(3), 204. doi: 10.3390/rs8030204
- Yastikli, N., (2007). Documentation of cultural heritage using digital photogrammetry and laser scanning. *Journal of Cultural Heritage* 8(4) 423 - 427 doi: doi.org/10.1016/j.culher.2007.06.003
- Yin, X., McClure, M. A., Jaja, N., Tyler, D. D., & Hayes, R. M. (2011). In-Season Prediction of \ Corn Yield Using Plant Height under Major Production Systems. *Agronomy Journal*, 103(3), 923–929. doi: 10.2134/agronj2010.0450
- Yuan, W., Li, J., Bhatta, M., Shi, Y., Baenziger, P., & Ge, Y. (2018). Wheat Height Estimation Using LiDAR in Comparison to Ultrasonic Sensor and UAS. *Sensors*, 18(11), 3731. doi: 10.3390/s18113731
- Zhang, N., Wang, M., & Wang, N. (2002). Precision agriculture—a worldwide overview. *Computers and Electronics in Agriculture*, 36(2-3), 113–132. doi: 10.1016/s0168-1699(02)00096-0
- Ziliani, M., Parkes, S., Hoteit, I., & McCabe, M. (2018). Intra-Season Crop Height Variability at Commercial Farm Scales Using a Fixed-Wing UAV. *Remote Sensing*, 10(12), 2007. doi: 10.3390/rs10122007

APPENDIX A

Overview of Results by Crop Type Over the Growing Season

3/19/2019

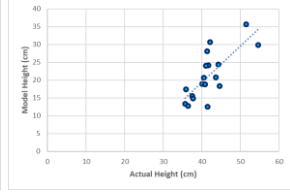
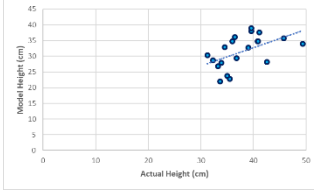
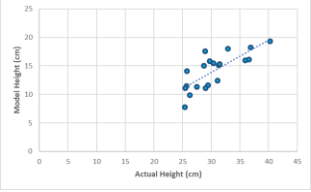
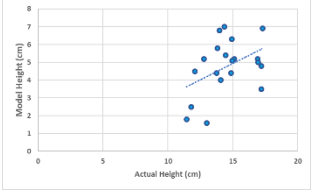
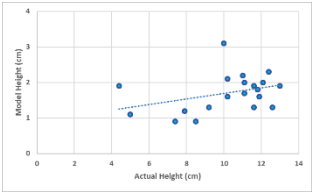
4/02/2019

4/16/2019

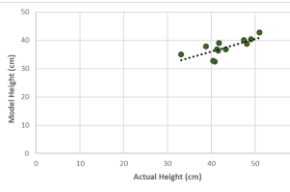
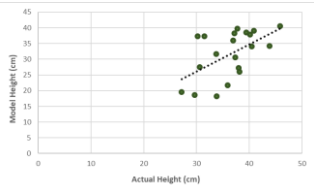
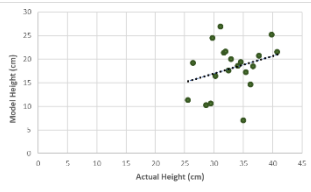
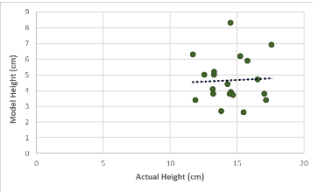
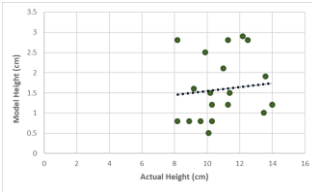
4/30/2019

5/14/2019

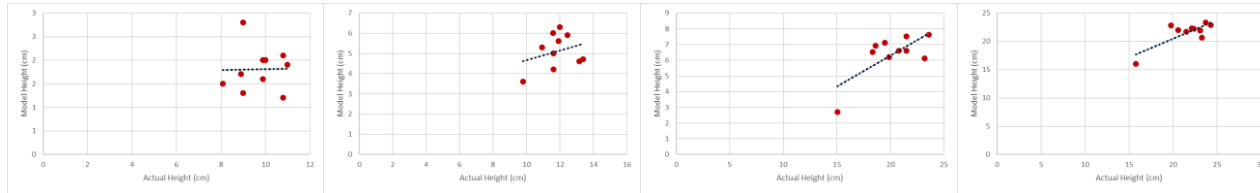
Collards



Kale



Cabbage



Peppers

